Palm Waste and Biomass Valorization

Editor-in-Chief: Ange Nzihou

Springer

Special Issue: Palm Waste and Biomass Valorization

Participating journal: Waste and Biomass Valorization

Palm plantations are common components of natural and cultivated flora around the world, and includes a wide variety of species (e.g. date palm, coconut, oil palm, sugar palm, doum palm, etc.). These plantations are the main source of livelihood for significant sectors of the world population, especially in the south. The main products of palm plantations (fruits) receive wide attention within the scientific and industrial community worldwide, whereas their biomass waste receive little attention. Despite that, palms generate a huge amount of biomass waste from pruning and fruit processing, which represent a burden on the palm growers and processors, and may cause fire accidents and infestation by dangerous insects. This biomass waste may represent a sustainable material base for a wide spectrum of industries ranging from compost, medium density fiber boards (MDF), block boards, and pulp, up to fiber reinforcements for advanced composites. Thus, there is a need to valorize palm biomass waste and maximize their added value via industrial technological advancement that can help in the sustainable development of vast rural areas around the world.

This Special Issue invites manuscripts that further our understanding of palm biomass and waste valorization in added value applications. Including, construction and building, pulp and paper, textiles and fibers, biocomposites, food products, lumber substitutes, organic fertilizers, natural fodder and silage, biofuel and biochar.

Participating journal

Journal

Waste and Biomass Valorization

Waste & Biomass Valorization is the first journal internationally dedicated solely to the valorization via chemical, thermal, biological or electrochemical treatment of waste and...

Publishing model	**Hybrid**
Journal Impact Factor	**2.8 (2024)**
Downloads	**836.3k (2024)**
Submission to first decision (median)	**22 days**

Editors

Othman Y. Alothman
Chemical Engineering Department, King Saud University, Riyadh, Saudi Arabia

Mohammad Jawaid
Laboratory of Biocomposite Technology, Institute of Tropical Forestry and Forest Products, Universiti Putra Malaysia, Selangor, Malaysia

Ramzi Khiari
1 University of Monastir, Faculty of Sciences of Monastir, Laboratory of Environmental Chemistry and Clean Process (LCE2P- LR21ES04), 5019 Monastir, Tunisia 2 Higher Institute of Technological Studies of Ksar Hellal...

Show more

Waste and Biomass Valorization (2024) 15:5833–5842
https://doi.org/10.1007/s12649-024-02665-3

ORIGINAL PAPER

Valorization of Date Molasses and Municipal Solid Waste for the Production of Cellulases by *Trichoderma reesei* Al-K1 149 in a Tray Reactor

Khaloud Mohammed Alarjani[1] · Mohamed S. Elshikh[1] · Mai Ahmad Alghmdi[1] · Selvaraj Arokiyaraj[2] · Vijayaraghavan Ponnuswamy[3]

Received: 17 December 2023 / Accepted: 17 July 2024 / Published online: 1 August 2024

Abstract
The main aim of this study is to utilize municipal solid waste (MSW) and date molasses as a culture medium to reduce the production cost of enzymes. A novel cellulase-producing fungus, *Trichoderma reesei* Al-K1 149, was isolated from the date molasses. MSW and date molasses were processed and used as the substrate (1:1 ratio) in solid-state fermentation. The proximate composition of the substrate revealed that the MSW was enriched with cellulostic material and contributed about 33% of the available biomass. Elements such as Ca, K, S, P, Mg, Fe, Cu, and Na were found in the MSW. Fungal cellulase production was at its maximum after 96 h of incubation with the yields of β-glucanase (98 ± 3.9 U/gds), carboxymethyl cellulase (CMCase) (241 ± 12.8 U/gds), and filter paperase (FPase) (31.2 ± 3.1 U/gds). The combination of municipal solid waste and date molasses was found to be the best source of nitrogen and carbon for the biosynthesis of cellulase by *T. reesei* Al-K1 149. The optimal temperature and moisture content of the medium for cellulase production by *T. reesei* Al-K1 149 were 40 °C and 60%, respectively. The optimal pH and inoculum were 6.0 and 8% (v/w), respectively. The optimized culture condition was used to produce cellulases in a laboratory-scale tray reactor, and enzyme production was enhanced twofold compared to the unoptimized medium. The cellulolytic ability was tested in biomass saccharification with various plant materials (palm sawdust, palm leaves, palm fruit waste, and filter paper) and saccharified plant materials effectively. These findings revealed that the enzymes secreted by strain Al-K1 149 may have significant value for the industrial saccharification process.

Keywords Municipal solid waste · Date molasses · Bio-waste · Solid-state fermentation · Optimization · Saccharification

Introduction

Municipal solid waste (MSW) bio-prospecting is one of the important subjects in environmental protection [1]. In England, more than 23 million tons of kitchen waste was generated in 2009–2010, which amounts to over 1000 Kg of kitchen waste per house [2]. The present methods for MSW management are landfill, incineration, anaerobic digestion, and composting. In recent years, the conversion of MSW into biogas by anaerobic conversion has attracted much more attention as a successful method to minimize environmental pollution and generate more renewable fuel. Interestingly, some MSW contain about 50% lignocellulosic material and anaerobic fermentation may not be effective in this process [3]. One of the important alternatives to methods is to hydrolyze the available lignocellulosic material into simple sugar. Then bioconversion of simple sugars into ethanol is a possible alternate of waste management. A ton of MSW generates about 150 L of ethanol after the fermentation of lignocellulosic from the waste [3]. Production of

✉ Khaloud Mohammed Alarjani
kalarjani@ksu.edu.sa; alarjanikm@gmail.com

[1] Department of Botany and Microbiology, College of Science, King Saud University, Riyadh 11451, Saudi Arabia

[2] Department of Food Science & Biotechnology, Sejong University, Seoul 05006, Korea

[3] Bioprocess Engineering Division, Smykon Biotech, Kanniyakumari, Tamilnadu, India

ethanol from MSW biomass is one of the viable technologies for renewable energy and the major constraints in cellulase production are low yield and the cost of cellulases [4]. In recent years, there has been an increasing interest in using various thermophilic fungi and bacteria for the production of cellulases, saccharification processes and fermentation of various lignocellulostic materials due to their broad substrate range and high operating temperature [5, 6]. Generally, the complete hydrolysis of cellulose substrate can be achieved by a combination of glucosidase, endoglucanases and exoglucanases [6]. Hence, it is desirable that the selected organism synthesize these types of enzymes. The Kingdom of Saudi Arabia shared more than 4 million tons of date's production and the contribution was about 72% of the Global share [7]. In KSA, palm trees cover about 162,000 hectares with about 23 million palm trees [8]. Other than fruits, leaves, trunks can be effectively used as raw materials for industrial processes. Date palm, *Phoenix dactylifera* is rich in lignin (25.82%), hemicelluloses (29.13%) and cellulose (45.3%) [9]. The lignocellulosic materials are processed through chemical, physical and mechanical pretreatments for saccharification by microbial cellulases [10].

Solid-state fermentation (SSF) is defined as the transformation of biomass in the near absence of free water or in the absence of water [6]. Recently, SSF has received more attention to explore the production of value-added products such as, biological lead molecules, biological control substances, enzymes and biopolymers [11]. Wilson [12] and Srivastava et al. [13] reported the optimization of hemicellulases, cellulase production and economic biofuel production. Both SSF and submerged fermentation have been widely used in the production of cellulases [14]. SSF required minimum equipment support was easy to operate, and was useful to handle large numbers of solid wastes, such as lignocellulose materials for enzyme production. Hence, SSF has been widely applied in the fermentation of food processing wastes and agricultural residues. The substrates, such as, oil palm biomass, sugar cane bagasse and wheat straw have been evaluated for cellulolytic enzyme production using *Trichoderma reesei* and *A. niger*. The fungus, *T. reesei* reportedly utilized water hyacinth, sugar cane bagasse, oil palm empty fruit branches, and rice bran substrates for cellulase production [15–17]. In a study, wheat straw was used as the substrate for cellulase production by *A. niger* [18]. Substrates such as, coconut coir pith, banana fruit stalk, rice husk, corn cob residue, rice straw, cow dung and banana peel have been utilized for cellulase production [14, 19, 20]. The Kingdom of Saudi Arabia is the second-largest producer of palm dates in the world. The annual production of dates was approximately 1.07 million tonnes [21]. In order to store the produced dates, date producers opted to store them as molasses. Date syrup or date molasses has a shelf life of about 24 months if stored under prescribed environmental conditions. After 24 months, it starts to crystallise and becomes inedible. It is rich in reducing sugars. In date molasses, fructose and glucose are the two major components [22]. The amount of these sugars varied based on the type of tree. For instance, glucose and fructose were determined to be the major sugar components and contributed 51.80% and 47.50%, respectively. The other components, such as fructose, sucrose, and galacturonic acid, were found in trace amounts [23]. Although date molasses and MSW contain large quantities of lignocellulosic material, there has been very limited work on the mixture of date molasses and MSW to produce cellulolytic enzyme using SSF. In this study, an attempt has been made to use the mixture of date molasses - MSW as the substrate for the production of cellulases.

Materials and Methods

Materials

The major chemicals, including, sodium hydroxide pellet, and glucose, were purchased from SigmaeAldrich, Co. USA. Carboxymethyl cellulose, acetic acid, and sodium acetate, methanol, and dichloromethane were purchased from Merck, Germany. The bacteriological culture medium was purchased from Himedia, India. The fungal DNA extraction kit (AllPrep DNA extraction kit) was purchased from Qiagen, Germany. Date molasses was purchased from the local market and municipal solid waste was collected in Chennai, India. Acetic acid, sodium acetate, citric acid, trisodium citrate, succinic acid, sodium succinate, disodium hydrogen phosphate, sodium dihydrogen phosphate, tris base, and hydrochloric acid were Analytical grade and these were used for the preparation of buffers between pH ranges 4.0 and 8.0.

Date Molasses and Municipal Solid Waste

Date molasses and MSW were used as substrates for cellulase production. The selection of these substrates was based on nutrient contents and availability. The MSW was autoclaved and an organic rich fraction was obtained after 30 min of incubation. Date molasses was directly used without filtration and MSW was sieved individually using a standard sieve (2 mm diameter). The sieved substrate was dried at 70 °C for 12 h. Date molasses and MSW were mixed at a 1:1 ratio and used as the substrate until otherwise stated.

Determination of Components MSW and Date Molasses

Hemicellulose and cellulose were tested using acid hydrolysis based on the methods suggested by the National Renewable Energy Laboratory (NREL/TP-500-42618). About 100 mg of sample was mixed with 1 mL of sulphuric acid (12 M) and incubated for 1 h at 37 °C. Then 10 mL of double distilled water was added, and the sample was incubated in a water bath for 2 h [24]. Finally, the hydrolyzed sugars were tested using a High Performance Liquid Chromatography (Shimadzu, Japan). (1100 series) equipped with a refractive index detector (RID) (Agilent, CA). A Shodex sugar SP0810 column was used for analysis. HPLC grade water was sterilized using 0.2 µm filter and degassed using a sonicator (Analab Scientific Instruments Private Limited, India) for 20 min. About 10 µL of sample was injected, and the flow rate was set to 0.5 mL/min. The lignin content of the sample was tested by the acetyl bromide method, as suggested by Sluiter et al. [24]. The absorbance of the sample was tested at 280 nm, and lignin was used as the standard [25]. The nitrogen content of the sample was tested using a nitrogen analyzer (G6 Leonardo, Bruker, Germany) [26]. The total lipid content of the sample was tested by the method of Folch with little modification [27]. MSW was extracted with methanol and dichloromethane at 1:2 (v/v) ratios and incubated for 3 h at 30 ± 2 °C. The trace element of MSW was tested after the extraction of the MSW sample with 20 mL of concentrated nitric acid. The available trace element was determined as described by Hokura et al. [28]. Proximate analysis of date molasses was carried out. The components, such as tannin, pectin, sugar, ash and protein content were analyzed from date molasses [29].

Pre-Treatment of Substrate by Alkali and Acid

About 1 kg of substrate was mixed with 2% sodium hydroxide (100 mL) or 1% sulphuric acid (100 mL) and kept in an autoclave for 15 min, 30 min, respectively. After 30 min, samples were neutralized using 1 M H_2SO_4 or 1 M NaOH. The solid fraction of the sample was retained, rinsed twice by adding double distilled water and centrifuged. Finally, the sample was dried at ambient temperature.

Isolation and Characterization of Fungus for Cellulolytic Enzyme Production

A total of 34 fungi were isolated from date molasses and cellulase screening was carried out. Date molasses was serially diluted and plated on potato dextrose agar plates. Then it was incubated at 28 ºC for five days. The isolated colonies were selected and further grown on potato dextrose agar. Based on productivity, one strain (Al-K1 149) was selected for characterization. A cellulase producing potent fungal strain was purified as described earlier [30]. 18 S rDNA was amplified and sequenced using a forward and a reverse primer [31]. The amplified PCR amplicon was purified and sequenced using Applied Biosystems (USA). The 18 S rDNA genes were sequenced at SciGenom Labs, Cochin, India.

Inoculum

Ten grams of substrate were transferred into 90 mL of double distilled water in a 250 mL Erlenmeyer flask. The medium was sterilized for 20 min at 121°C and incubated at 28 ± 2°C. In this culture medium, a plug (about 1×1 cm^2) of 8-day old mycelia was gently inoculated and incubated in a shaker incubator at 175 rpm for three days.

Production of Cellulases in SSF

Solid state fermentation was performed in a 250-mL Erlenmeyer containing 5.0 g of substrate. The dry substrate was moistened with sodium phosphate buffer (pH 6.5, 0.1 M) and the moisture content of the substrate was maintained at a ratio of 1:1.5. The culture medium was mixed, autoclaved at 121 °C for 30 min and inoculated with inoculum. Erlenmeyer flasks were incubated for 96 h under static culture conditions. After 96 h, cellulases were extracted by adding 50 mL of double distilled water and shaking the fermented medium on an orbital shaker for 30 min. The contents were filtered using a metallic sieve and further centrifuged (10,000 g, 4 °C). The clear supernatant was used as the crude enzyme [32].

Enzyme Assays

The crude enzyme was subjected to carboxymethyl cellulase (CMCase), β-glucosidase and filter paper activity (FPase) assay. A unit of b-glucosidase, FPase and CMCase was defined as being equivalent to the enzyme that liberates 1 µmole of glucose from salicin, Whatman filter paper, and carboxymethyl cellulose, respectively, in 0.05 M acetate buffer (pH 4.0) under standard assay conditions using dinitrosalicylic acid reagent method [33]. Enzyme activities were expressed as U/g dry substrate (U/gds) tested in the Erlenmeyer flask [34].

Optimization of Physical Factors for Cellulases Production in SSF

The mixture of MSW and date molasses is used as the substrate for enzyme production, unless otherwise stated. The

time course of cellulase synthesis was evaluated by preparing various sets of Erlenmeyer flasks (250 – mL) containing 5 g of substrate adjusted to 70% moisture content. The fermentation experiment was performed as described previously [35]. The Erlenmeyer flask was incubated for five days, and the production profile of cellulases was monitored every 24 h. The selected substrate (date molasses and MSW) is rich in carbon, nitrogen sources, and essential minerals. Hence, nutrient requirements were not considered for optimization studies, and only physical factors were optimized. The effect of different fermentation temperatures (25–50 °C), moisture content (40–80%), pH (4.0–8.0) and inoculum level (1–10%) on cellulase yield was analyzed. To adjust the pH, various buffers were used at a 0.1 M concentration (citrate buffer 4.0, acetate buffer 5.0, succinate buffer 6.0, phosphate buffer 7.0, and tris-buffer 8.0).

Fermentation of date molasses and MSW in a tray bioreactor

The optimized culture medium was selected, and the process parameters were validated using an open trays bioreactor. The open tray bioreactor consists of rectangular shaped stainless steel trays with a 4 cm depth and a 10×5 cm size. The tray reactor consists of three layers of trays, and the top of the tray was gently covered with a lid, and the bottom of the tray was arranged in such a way as to allow air inflow (Fig. 1). The solid medium was carefully mixed and transferred into a tray reactor. In all trays, solid substrate was filled, and the optimum level of inoculum was introduced. These stainless steel trays are autoclavable and compatible. After complete sterilization, 10% inoculums were introduced and incubated at 28 ± 2 ºC for four days. Enzyme was extracted as described previously, and CMCase, FPase and β-glucosidase activity were assayed.

Saccharification of Biomass

In this study, lignocellulosic materials such as palm sawdust, palm leaves, palm fruit waste and filter paper were used for saccharification process. The cellulolytic enzymes were obtained from lignocellulosic fermentation in tray bioreactor with *T. reesei* Al-K1 149. Commercial cellulase was used as the standard to validate the saccharification process. The saccharification process was performed at 45 °C at pH 5.0. The experiments were performed in a 250 mL Erlenmeyer flask containing various substrates (plam saw dust, palm leaves, palm fruit waste and filter paper), and 50 mL acetate buffer (pH 5.0, 50 mM). Then the Erlenmeyer flask was kept on a water bath for 5 min for constant heat transfer throughout the flask. To this end, cellulases obtained from the tray reactor were applied, and commercial enzymes were also added and validated. The saccharification process was continued for 24 h and the reducing sugar level was evaluated by the DNS method as suggested by Miller [33] using a UV-Visible spectrophotometer.

Results and Discussion

Composition of Substrates

In this study, the chemical composition of MSW was evaluated as suggested previously in materials and methods. In MSW, hydrocarbons contributed about 60%, showing that they were rich sources of carbon, which could be effectively applied as a novel medium for the production of biofuels. The co-fermentation of municipal sludge and date molasses was evaluated as a promising way to combine renewable energy production and waste management. The co-fermentation of food waste and municipal sludge [36], waste-activated sludge-distillation residue [37], green waste, and municipal solid waste [38] were used as culture media to improve productivity and yield of biomolecules. Kamyab et al. [39] used activated sludge and date syrup as inexpensive substrates for biohydrogen production. The stiff and loose properties of co-substrates led to improved fungal growth and product formation. The cellulose content of the MSW was about 33% which was similar to the results by Hussin et al. [40] and Barlaz et al. [41]. In some cases, the cellulose content in MSW was found to be high, where MSW obtained mainly from the milling, wood, and paper industries [42, 43]. In this study, the lignin content of the MSW sample was about 13% (Fig. 2), which was similar to the study of Hussin et al. [40]. The hemicellulose content of the MSW was determined to be 16%. However,

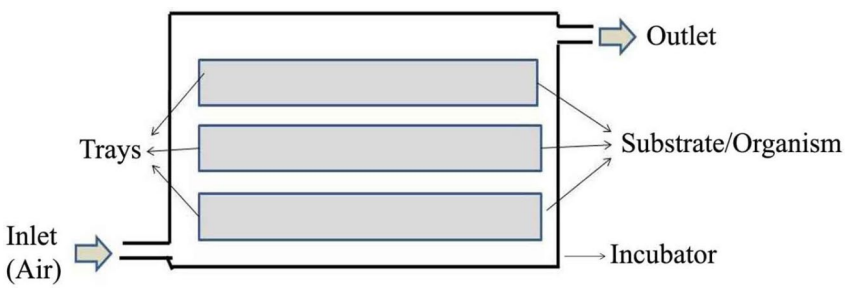

Fig. 1 Cellulases production in SSF using a tray bioreactor. The trays were filled with solid medium and culture was inoculated (10%)

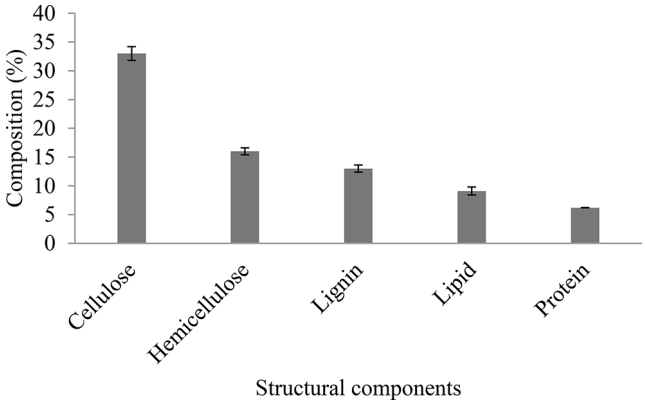

Fig. 2 Structural components of date molasses. The error bar represents the standard deviation

Table 1 Chemical composition of municipal solid waste. Mean ± SD ($n = 3$)

Metals	mg/kg
Ca	13,005 ± 198
K	1812 ± 21.4
S	4217 ± 13.2
P	912 ± 5.6
Mg	2115 ± 3.1
Na	1903 ± 21.3
Cu	412 ± 19.2
Fe	419 ± 12.6
Al	291 ± 10.2
Hg	41.5 ± 2.8
Au	0.2 ± 0.03
Cd	27 ± 1.31
Ag	1.2 ± 0.13

in some studies, a low level of hemicellulose availability was reported. For example, Ham et al. [44], and Price et al. [45] reported low availability of hemicellulose in the MSW. Moreover, lignocellulose accounts for more than 30% of municipal solid waste [46]. Lipid and total protein content contributed about 9.1%, 6.1%, respectively. di Bitonto et al. [47] reported low lipid content (4–10%) in MSW and it was higher (13%) in other MSW [48]. The chemical composition of the compost varied based on the source and country of origin [14]. The lipid content of the MSW was extremely low compared to previous reports. Generally, MSW derived from hotels, households, vegetable markets, fruit markets and juice processing units has a lower lipid content [36]. The contribution from total protein content was about 6.5%. This result was in accordance with the observations made previously by Ponsá et al. [49] and Hartmann and Ahring [50]. In this study, the composition of the trace element was described in (Table 1).

The elements such as Ca, K, S, P, Mg, Fe, Cu, and Na were determined from the MSW. The sulphur content was 4217 ± 13.2 mg/kg and the determined Ca level was 13,005 ± 198 mg/kg in MSW. The toxic metals such as Al, Hg, Au, Cd, and Ag were determined at a very low level which was similar to that of the previous study [51]. The date molasses was composed of tannin, pectin, sugar, ash and protein. The pH of the date molasses ranged between 4.7 and 5.4. Pectin content was about 0.32%, and tannin content was 0.45%. Reducing sugar contributed 69%, and the share of ash content was approximately 1.9%. The chemical and physical properties of the date molasses were described in (Table 2).

Table 2 Physical properties of date molasses

Physical properties	Composition (%)
Moisture	40–42
Protein	1.2–1.4
Total sugar	77.2–77.4
Ash	1.6–1.9
Tannin	0.3–0.4
Pectin	0.2–0.25
TDS	79–81
pH	4.4–5.1

Physico-Chemical Factors Affecting Cellulase Production

In the study, the influence of the fermentation period on cellulase production was optimized. In the case of fungi, the fermentation period is one of the important factors for the biosynthesis of enzymes. Cellulase production was at its maximum after 96 h of incubation with the yields of β-glucanase (98 ± 3.9 U/gds), CMCase (241 ± 12.8 U/gds) and FPase (31.2 ± 3.1 U/gds) as described in (Fig. 3). After four days of incubation, cellulase yield decreased gradually due to the drop in the medium pH and the release of proteolytic enzymes. In a study, Singhania et al. [15] also reported the maximum cellulase yield in *T. reesei* after 96 h incubation (102.65 U/gds). In another study, *Trichoderma* sp. was used for cellulase production on apple pomace as the substrate and showed a dramatic increase in the enzyme yield after 120 h of incubation (2.3 U/gds) [52]. The amount of cellulase production varied based on the substrate selected for fermentation. Campos et al. [53] used green coconut fibers for the production of carboxy methyl celluase (5.19 U/g) and filter paperase (1.19 U/g). Environmental factors affected enzyme production and the growth of microorganisms. In this study, enzyme production by *T. reesei* Al-K1 149 on biowaste was optimized with respect to moisture content, temperature, inoculum and pH of the substrate. In SSF, the optimum temperature range for enzyme production has been reported to be 25 to 30 °C [15]. Maximum yields of β-glucosidase (104 ± 3.2 U/gds), FPase (39.1 U/gds) and CMCase (264 U/gds) were found after 96 h at 40 °C, as described in (Fig. 4a). In *A. niger* YL128, the optimum

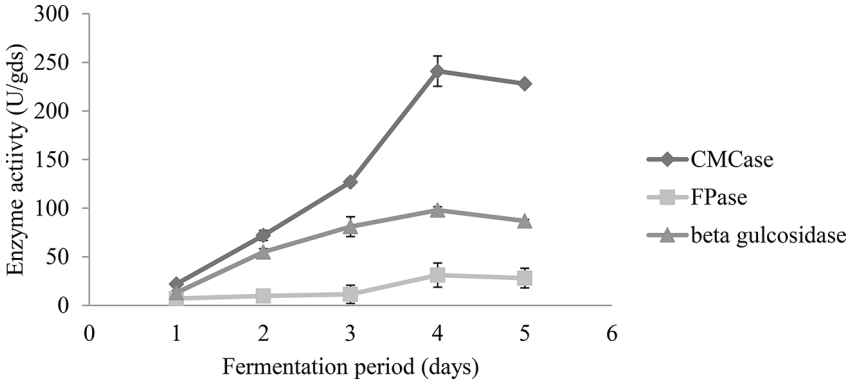

Fig. 3 Production of CMCase, β-glucosidase and FPase in solid state culture at various incubation times by *T. reesei* Al-K1-149 on MSW and date molasses

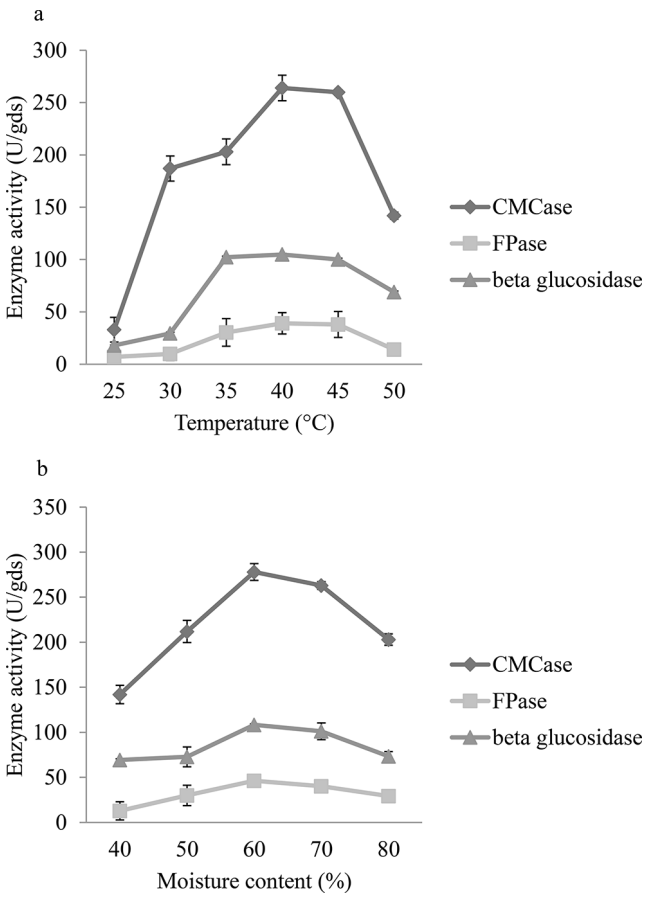

Fig. 4 Production of CMCase, β-glucosidase and FPase in solid state culture at various temperatures (**a**) and moisture levels (**b**) by *T. reesei* Al-K1-149 on MSW and date molasses

temperature was 30 °C for cellulase production [54]. In a study, saw dust was used as the substrate for cellulase production by *A. niger* and obtained the maximum yield at 28 °C. In *Trichoderma harzianum*, enzyme biosynthesis is enhanced with an increase in temperature up to optimum (35 °C) [55]. This incubation temperature was lower (32 °C) in *Aspergillus fumigates* for cellulase production [56]. Water is an important factor for microbial activity, and the depletion of available water affects functional changes in microorganisms. In SSF, both low and high moisture levels affected enzyme productivity. A lower moisture level causes a complete reduction in the solubility of available nutrients in the substrate, high water tension, and a higher moisture content of the solid substrate which decreased porosity, lowers oxygen transfer etc. [57]. The optimum moisture content was 60% and the enhanced yield was 108.4 ± 13.3 U/gds (β-glucosidase), 46.4 ± 11.4 U/gds (FPase) and 278 ± 10.5 U/gds (CMCase) as described in (Fig. 4b). In a study, 50% moisture content was reported as optimum for maximum FPase production in SSF [58] in the case of *A. niger* culture. In another study, moisture content ranging between 40 and 60% was optimum for CMCase and FPase yield for *Trichoderma koningii* in SSF [59]. In *Aspergillus* sp. S4B2F, cellulase yield was maximum when it was cultured at a 60% moisture level [60]. In this study, the pH of the substrate was adjusted between 4.0 and 8.0 using suitable buffers, and the results are depicted in (Fig. 5a). The highest enzyme yields were 117.4 ± 5.1 U/gds (β-glucosidase), 54.8 ± 8.2 U/gds (FPase) and 281 ± 10.8 U/gds (CMCase) at pH 6.0. At the acidic pH level (4.0), enzyme biosynthesis was decreased, and it gradually increased up to pH 6.0, then declined. The enzyme yields obtained in this study were highly consistent with previous studies on cellulase production by *Trichoderma* sp. and *Aspergillus niger* [61]. Likewise, the solid medium inoculated with 8% inoculum showed the highest enzyme yields of 120 ± 8.3 U/gds (β-glucosidase), 60.1 ± 13.2 U/gds (FPase) and 250 ± 10.3 U/gds (CMCase) which were decreased at the higher inoculum level (10%) as described in (Fig. 5b). Lower enzyme production at higher inoculum levels was mainly due to nutritional imbalance or an initial high concentration of conidial cells and anaerobic conditions in the medium, while the decreased yield at lower inoculum sizes was mainly due to the availability of fewer conidial cells, which are not enough to utilize the available fermentation medium [62]. In a study, Iqbal et al. [55] reported 10% inoculum as optimum carboxymethyl cellulase production from *T. harzianum*, and enzyme production was reduced above the optimum level.

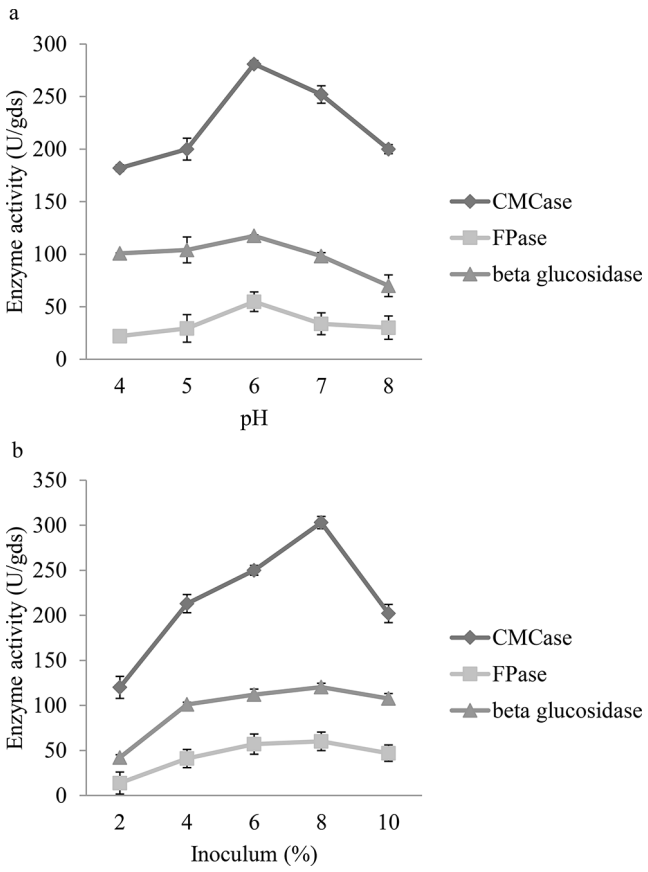

Fig. 5 Production of CMCase, β-glucosidase and FPase in solid state culture at various pHs (a) and inoculum levels (b) by *T. reesei* Al-K1-149 on MSW and date molasses

Production of Cellulases in a Tray Bioreactor

Tray bioreactors have been used for the production of various enzymes. In a study, Nahid et al. [63] extensively studied the application of tray bioreactors on enzyme production. Also, Mitra et al. [64] compared the yield of enzymes in different types of tray bioreactors. Gupta and Kar [65] analyzed the use of tray bioreactor on cellulolytic enzyme production. Also, Dhillon et al. [66] have used tray reactor for the production of xylanase and cellulase using co-cultured fungi. In this study, the tray reactor enhanced the production of cellulases over twofold than unoptimized conditions. Earlier, tray bioreactors were used for the production of fermented products such as, soy sauce, koji and tempeh, and various enzymes in SSF. Brijwani et al. [67] used *Aspergillus oryzae* and *Trichoderma reesei* for co-fermentation using agro industrial wastes. The combination of wheat bran and soybean has been utilized for cellulase production. And, the optimum composition of C: N ratio was obtained for the production of enzymes and the controlled release of nutrients. Dhillon et al. [66] recently used apple pomace as the substrate for the production of β-glucosidase and the process parameters were optimized by response surface methodology. Then, the optimized medium was applied for the production of enzymes in the tray bioreactor [68].

Saccharification of Agro-Wastes

Lignocellulosic materials such as palm sawdust, palm leaves, palm fruit waste, and filter paper were used for saccharification process. In this study, saccharification process was maximum up to 12 h of incubation and declined slowly (Fig. 6). In this case, until 12 h incubation reducing sugar level was found to be high, and about 89% saccharification

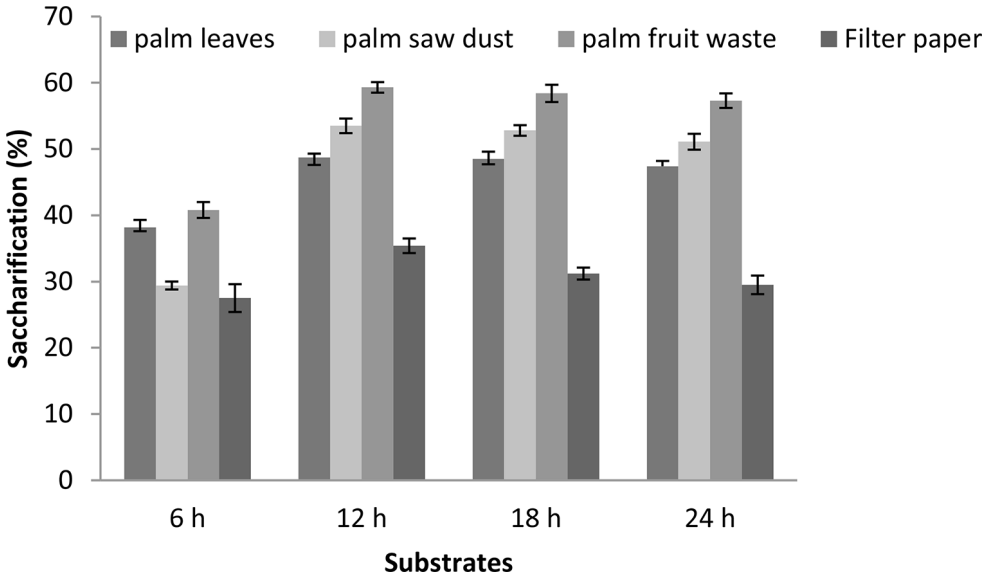

Fig. 6 Enzymatic saccharification at various incubation times with cellulases. The substrates (plam saw dust, palm leaves, palm fruit waste and filter paper) were treated with cellulases and the reducing sugar level was estimated

was obtained within the 12 h incubation time. Among the substrates used, cellulases released the maximum amount of reducing sugar in the reaction mixture containing palm fruit as the substrate. Also, enzyme activity in the reaction mixture was gradually declining up to 12 h of incubation. So, up to 12 h was optimum for saccharification process and later efficacy declined. In a study, Annamalai et al. [69] used pretreated rice straw for the saccharification process using cellulase obtained from *Bacillus carboniphilus* CAS 3. In another study, Gokhale et al. [70] reported that the enzymatic activity of cellulolytic enzymes increased to maximum up to 50 °C and decreased at higher temperatures, because of enzyme denaturation at higher temperatures. Also, Lan et al. [71] analyzed the saccharification process of cellulose wastes using cellulases from *Trichoderma viride* and the yield was compared with the control. Fungal cellulases and saccharification efficacy would help to reduce the use of various chemicals used in the enzyme industry in the saccharification process.

Conclusions

A hyperactive cellulolytic bacterial strain was isolated from date molasses and identified as *Trichoderma reesei* Al-K1 149. Municipal solid waste and date molasses (1:1 ratiowere used as substrates to improve enzyme production. The cellulase production was maximum after 96 h of incubation with the yields of β-glucanase (98 ± 3.9 U/gds), carboxymethyl cellulase (CMCase) (241 ± 12.8 U/gds) and filter paperase (FPase) (31.2 ± 3.1 U/gds). Optimum temperature (40 °C) and moisture content (60%) improved cellulase production. In the successive optimization trials, physical factors were optimized and over two fold enzyme yield was obtained in tray reactor. Subsequently, the enzymes used for saccharification of palm saw dust, palm leaves, palm fruit waste, and filter paper. The results indicated that the fungal strain can be considered for biomass saccharification and industrial applications.

Author Contributions Conceptualization: MSE, P.V; Writing review and editing: KMA; Methodology: S.A, VP; Resources: KMA, MAA; Data curation: S.A. VP; Writing original draft: VP; Investigation: VP, Supervision: SA.

Funding The authors extend their appreciation to the Researchers supporting project number (RSP2024R185), King Saud University, Riyadh, Saudi Arabia.

Data Availability Not applicable.

Declarations

Competing Interests The authors declare no competing interests.

References

1. Vergara, S.E., Tchobanoglous, G.: Municipal solid waste and the environment: A global perspective. Ann. Rev. Environ. Resour. **37**, 277–309 (2012)
2. Keeling, C.: Canterbury Region Waste Data Report 2009/2010. Environment Canterbury. (2011)
3. Li, S., Zhang, X., Andresen, J.M.: Production of fermentable sugars from enzymatic hydrolysis of pretreated municipal solid waste after autoclave process. Fuel. **92**(1), 84–88 (2012)
4. Shankar, A., Saini, S., Sharma, K.K.: Fungal-integrated second-generation lignocellulosic biorefinery: Utilization of agricultural biomass for co-production of lignocellulolytic enzymes, mushroom, fungal polysaccharides, and bioethanol. Biomass Conv Biorefin. **14**(1), 1117–1131 (2024)
5. Mansy, A.E., El-Desouky, E., El-Gendi, H., Abu-Saied, M.A., Taha, T.H., Amer, R.A.: Cellulosic fiber waste feedstock for bioethanol production via bioreactor-dependent fermentation. Fermentation. **9**(2), 176 (2023)
6. Chandel, H., Kumar, P., Chandel, A.K., Verma, M.L.: Biotechnological advances in biomass pretreatment for bio-renewable production through nanotechnological intervention. Biomass Con Biorefin. **14**(3), 2959–2981 (2024)
7. FAO.: Food and Agriculture Organization of the United Nations. Food and Agriculture Organization Statistical Databases (FAOSTAT); (2013)
8. El-Habba, M.S., Al-Mulhim, F.: The competitiveness of the Saudi Arabian date palm: An analytical study. Afr. J. Agric. **8**, 5260–5267 (2013)
9. Al-Mefarrej, H.A., Abdel-Aal, M.A., Nasser, R.A.: Chemical evaluation of some lignocellulosic residues for pulp and paper production. American-Eurasian J. Agric. Environ. Sci. **13**, 498–504 (2013)
10. Jahromi, M.F., Liang, J.B., Rosfarizan, M., Goh, Y.M., Shokryazdan, P., Ho, Y.W.: Effects of Aspergillus Niger (K8) on nutritive value of rice straw. Afr. J. Biotechnol. **9**(42), 7043–7047 (2010)
11. Lizardi-Jiménez, M.A., Hernández-Martínez, R.: Solid state fermentation (SSF): Diversity of applications to valorize waste and biomass. 3 Biotech. **7**(1), 44 (2017)
12. Wilson, D.B.: Cellulases and biofuels. Curr. Opin. Biotechnol. **20**, 295–299 (2009)
13. Srivastava, N., Srivastava, M., Mishra, P.K., Gupta, V.K., Molina, G., Rodriguez-Couto, S., Manikanta, A., Ramteke, P.W.: Applications of fungal cellulases in biofuel production: Advances and limitations. Ren. Sustain. Ener Rev. **82**, 2379–2386 (2018)
14. Vijayaraghavan, P., Arun, A., Al-Dhabi, N.A., Vincent, S.G.P., Arasu, M.V., Choi, K.C.: Novel *Bacillus subtilis* IND19 cell factory for the simultaneous production of carboxy methyl cellulase and protease using cow dung substrate in solid-substrate fermentation. Biotechnol. Biofuel. **9**, 1–13 (2016)
15. Singhania, R.R., Sukumaran, R.K., Pillai, A., Prema, P., Szakacs, G., Pandey, A.: Solid-state fermentation of lignocellulosic substrates for cellulase production by *Trichoderma Reesei* NRRL 11460. Ind. J. Biotechnol. **5**(3), 332–336 (2006)
16. Alam, M.Z., Mamun, A.A., Qudsieh, I.Y., Muyibi, S.A., Salleh, H.M., Omar, N.M.: Solid state bioconversion of oil palm empty fruit bunches for cellulase enzyme production using a rotary drum bioreactor. Biochem. Eng. J. **46**(1), 61–64 (2009)
17. Latifian, M., Hamidi-Esfahani, Z., Barzegar, M.: Evaluation of culture conditions for cellulase production by two *Trichoderma reesei* mutants under solid-state fermentation conditions. Bioresour Technol. **98**(18), 3634–3637 (2007)
18. Pensupa, N., Jin, M., Kokolski, M., Archer, D.B., Du, C.: A solid state fungal fermentation-based strategy for the hydrolysis of wheat straw. Bioresour Technol. **149**, 261–267 (2013)

19. Couto, S.R., Sanromán, M.A.: Application of solid-state fermentation to ligninolytic enzyme production. Biochem. Eng. J. **22**, 211–219 (2005)
20. Klein-Marcuschamer, D.: The challenge of enzyme cost in the production of lignocellulosic biofuels. Biotechnol. Bioeng. **109**, 1083–1087 (2012)
21. Taghizadeh-Alisaraei, A., Motevali, A., Ghobadian, B.: Ethanol production from date wastes: Adapted technologies, challenges, and global potential. Renew. Ener. **143**, 1094–1110 (2019)
22. El-Sharnouby, G.A., Aleid, S.M., Al-Otaibi, M.M.: Liquid sugar extraction from date palm (*Phoenix dactylifera* L.) fruits. Int. J. Food Process. Technol. **5**, 1–5 (2014)
23. Siddeeg, A., Zeng, X.A., Ammar, A.F., Han, Z.: Sugar profile, volatile compounds, composition and antioxidant activity of Sukkari date palm fruit. J. Food Sci. Technol. **56**, 754–762 (2019)
24. Sluiter, A., Hames, B., Ruiz, R., Scarlata, C., Sluiter, J., Templeton, D.: Determination of sugars, byproducts, and degradation products in liquid fraction process samples. Golden: Nat. Renew. Ener Lab. **11**, 65–71 (2006)
25. Sluiter, A., Hames, B., Ruiz, R., Scarlata, C., Sluiter, J., Templeton, D., Crocker, D.L.A.P.: Determination of structural carbohydrates and lignin in biomass. Lab. Anal. Proce. **1617**(1), 1–16 (2008)
26. Campbell, C.R., Plank, C.O.: Determination of total nitrogen in plant tissue by combustion. Plant Anal Ref Proc for S US Southern Coop. Ser. Bull. **368**, 20–22 (1992)
27. Cequier-Sánchez, E., RODRiguez, C.O., Zarate, R.: Dichloromethane as a solvent for lipid extraction and assessment of lipid classes and fatty acids from samples of different natures. J. Agric. Food Chem. **56**(12), 4297–4303 (2008)
28. Hokura, A., Matsuura, H., Katsuki, F., Haraguchi, H.: Multielement determination of major-to-ultratrace elements in plant reference materials by ICP-AES/ICP-MS and evaluation of their enrichment factors. Anal. Sci. **16**(11), 1161–1168 (2000)
29. Van Soest, P.V., Robertson, J.B., Lewis, B.A.: Methods for dietary fiber, neutral detergent fiber, and nonstarch polysaccharides in relation to animal nutrition. J. Dairy. Sci. **74**(10), 3583–3597 (1991)
30. Melo, S.C.O., Pungartnik, C., Cascardo, J.C.M., Brendel, M.: Rapid and efficient protocol for DNA extraction and molecular identification of the basidiomycete *Crinipellis Perniciosa*. Genet. Mol. Res. **5**(4), 851–855 (2006)
31. Kurtzman, C.P., Robnett, C.J.: Identification of clinically important ascomycetous yeasts based on nucleotide divergence in the 5'end of the large-subunit (26S) ribosomal DNA gene. J. Clin. Microbiol. **35**, 1216–1223 (1997)
32. Dhillon, G.S., Kaur, S., Brar, S.K., Verma, M.: Potential of apple pomace as a solid substrate for fungal cellulase and hemicellulase bioproduction through solid-state fermentation. Ind. Crop Prod. **38**, 6–13 (2012)
33. Miller, G.L.: Use of dinitrosalicylic acid reagent for determination of reducing sugar. Anal. Chem. **31**(3), 426–428 (1959)
34. Mandels, M., Andreotti, R., Roche, C.: January. Measurement of saccharifying cellulase. In *Biotechnol. Bioeng. Symp.;(United States)* (Vol. 6). Army Natick Development Center, MA.6, 21–23 (1976)
35. Kalaiyarasi, M., Vijayaraghavan, P., Raj, S.R.F., Vincent, S.G.P.: Statistical approach for the production of protease and cellulase from *Bacillus cereus* KA3. Bioprocess Eng. 1(4), 93–103 (2017)
36. Al-Dhabi, N.A., Esmail, G.A., Valan Arasu, M.: Co-fermentation of food waste and municipal sludge from the Saudi Arabian environment to improve lactic acid production by *Lactobacillus rhamnosus* AW3 isolated from date processing waste. Sustainability. **12**(17), 6899 (2020)
37. Wilinska-Lisowska, A., Ossowska, M., Czerwionka, K.: The influence of co-fermentation of agri-food waste with primary sludge on biogas production and composition of the liquid fraction of digestate. Energies. **14**(7), 1907 (2021)
38. Semeraro, B., Summa, D., Costa, S., Zappaterra, F., Tamburini, E.: Bio-delignification of green waste (GW) in co-digestion with the organic fraction of municipal solid waste (OFMSW) to enhance biogas production. Appl. Sci. **11**(13), 6061 (2021)
39. Kamyab, S., Ataei, S.A., Tabatabaee, M., Mirhosseinei, S.A.: Optimization of bio-hydrogen production in dark fermentation using activated sludge and date syrup as inexpensive substrate. Int. J. Green. Ener. **16**(10), 763–769 (2019)
40. Hussin, A.M., Collins, S.R.A., Merali, Z., Parker, M.L., Elliston, A., Wellner, N., Waldron, K.W.: Characterisation of lignocellulosic sugars from municipal solid waste residue. Biomass Bioen. **51**, 17–25 (2013)
41. Barlaz, M.A., Eleazer, W.E., Odle, W.S., Qian, X., Wang, Y.S.: Biodegradative Analysis of Municipal Solid Waste in laboratory-scale Landfills. United States Environmental Protection Agency (1997)
42. Wang, Y.S., Byrd, C.S., Barlaz, M.A.: Anaerobic biodegradability of cellulose and hemicellulose in excavated refuse samples using a biochemical methane potential assay. J. Ind. Microbiol. Biotechnol. **13**(3), 147–153 (1994)
43. Barlaz, M.A., Schaefer, D.M., Ham, R.: Bacterial population development and chemical characteristics of refuse decomposition in a simulated sanitary landfill. Appl. Environ. Microbiol. **55**(1), 55–65 (1989)
44. Ham, R.K., Norman, M.R., Fritschel, P.R.: Chemical characterization of fresh kills landfill refuse and extracts. J. Environ. Eng. **119**(6), 1176–1195 (1993)
45. Price, G.A., Barlaz, M.A., Hater, G.R.: Nitrogen management in bioreactor landfills. Waste Manage. **23**(7), 675–688 (2003). (1993)
46. Farmanbordar, S., Amiri, H., Karimi, K.: Synergy of municipal solid waste co-processing with lignocellulosic waste for improved biobutanol production. Waste Manage. **118**, 45–54 (2020)
47. di Bitonto, L., Antonopoulou, G., Braguglia, C., Campanale, C., Gallipoli, A., Lyberatos, G., Ntaikou, I., Pastore, C.: Lewis-Brønsted acid catalysed ethanolysis of the organic fraction of municipal solid waste for efficient production of biofuels. Bioresour Technol. **266**, 297–305 (2018)
48. Barampouti, E.M., Mai, S., Malamis, D., Moustakas, K., Loizidou, M.: Liquid biofuels from the organic fraction of municipal solid waste: A review. Renew. Sustain. Ener Rev. **110**, 298–314 (2019)
49. Ponsá, S., Gea, T., Sánchez, A.: Anaerobic co-digestion of the organic fraction of municipal solid waste with several pure organic co-substrates. Biosys Eng. **108**(4), 352–360 (2011)
50. Hartmann, H., Ahring, B.K.: Strategies for the anaerobic digestion of the organic fraction of municipal solid waste: An overview. Water Sci. Technol. **53**, 7–22 (2006)
51. Slack, R.J., Bonin, M., Gronow, J.R., Van Santen, A., Voulvoulis, N.: Household hazardous waste data for the UK by direct sampling. Environ. Sci. Technol. **41**(7), 2566–2571 (2007)
52. Sun, H., Ge, X., Hao, Z., Peng, M.: Cellulase production by Trichoderma sp. on apple pomace under solid state fermentation. Afr. J. Biotechnol. **9**, 163–166 (2010)
53. Campos, A.O., Asevedo, E.A., Souza Filho, P.F., Santos, E.S.D.: Extraction of Cellulases produced through solid-state fermentation by *Trichoderma reesei* CCT-2768 using green coconut fibers pretreated by Steam Explosion combined with Alkali. Biomass. **4**(1), 92–106 (2024)
54. Ja'afaru, M.I., Fagade, O.E.: Optimization studies on cellulase enzyme production by an isolated strain of *Aspergillus Niger* YL128. Afr. J. Microbiol. Res. **4**(24), 2635–2639 (2010)
55. Iqbal, H.M., Asgher, M., Ahmed, I., Hussain, S.: Media optimization for hyper-production of carboxymethyl cellulase using

proximally analyzed agroindustrial residue with *Trichoderma Harzianum* under SSF. IJAVMS. **4**, 47–55 (2010)
56. Gilna, V.V., Khaleel, K.M.: Biochemistry of cellulase enzyme activity of *aspergillus fumigatus* from mangrove soil on lignocellulosics substrate. Rec Res. Sci. Technol. **3**, 132–134 (2011)
57. Anto, H., Trivedi, U.B., Patel, K.C.: Glucoamylase production by solid-state fermentation using rice flake manufacturing waste products as substrate. Bioresour Technol. **97**(10), 1161–1166 (2006)
58. Chandra, M.S., Viswanath, B., Reddy, B.R.: Cellulolytic enzymes on lignocellulosic substrates in solid state fermentation by *Aspergillus Niger*. Indian J. Microbiol. **47**, 323–328 (2007)
59. Liu, J., Yang, J.: Cellulase production by *T. Koningii*. Food Technol. Biotechnol. **45**, 420–425 (2007)
60. Soni, S.K., Batra, N., Bansal, N., Soni, R.: Bioconversion of sugarcane bagasse into second generation bioethanol after enzymatic hydrolysis with in-house produced cellulases from aspergillus sp. S4B2F. BioRes. **5**(2), 741–757 (2010)
61. Gautam, S.P., Bundela, P.S., Pandey, A.K., Khan, J., Awasthi, M.K., Sarsaiya, S.: Optimization for the production of cellulase enzyme from municipal solid waste residue by two novel cellulolytic fungi. Biotechnol. Res. Int. **1**, 1–8 (2011)
62. Azzouz, Z., Bettache, A., Djinni, I., Boucherba, N., Benallaoua, S.: Biotechnological production and statistical optimization of fungal xylanase by bioconversion of the lignocellulosic biomass residues in solid-state fermentation. Biomass Con Biorefin 1–13 (2020)
63. Nahid, P., Vossoughi, M., Roostaazad, R., Ahmadi, M., Zarrabi, A., Hosseini, S.M.: Production of glucoamylase by *Aspergillus Niger* under solid state fermentation (research note). Int. J. Eng. **25**(1), 11–17 (2012)
64. Mitra, R.D., Silva, C.M., Youvan, D.C.: Fluorescence resonance energy transfer between blue-emitting and red-shifted excitation derivatives of the green fluorescent protein. Gene. **173**(1), 13–17 (1996)
65. Gupta, U., Kar, R.: Optimization and scale up of cellulase free endo xylanase production by solid state fermentation on corn cob and by immobilized cells of a thermotolerant bacterial isolate. Jordon J. Biol. Sci. **1**(3), 129–134 (2008)
66. Dhillon, G.S., Brar, S.K., Valero, J.R., Verma, M.: Bioproduction of hydrolytic enzymes using apple pomace waste by *A. Niger*: Applications in biocontrol formulations and hydrolysis of chitin/chitosan. Bioprocess. Biosyst Eng. **34**, 1017–1026 (2011a)
67. Brijwani, K., Oberoi, H.S., Vadlani, P.V.: Production of a cellulolytic enzyme system in mixed-culture solid-state fermentation of soybean hulls supplemented with wheat bran. Process. Biochem. **45**, 120–128 (2010)
68. Khanahmadi, M., Arezi, I., Amiri, M.S., Miranzadeh, M.: Bioprocessing of agro-industrial residues for optimization of xylanase production by solid-state fermentation in flask and tray bioreactor. Biocat Agric. Biotechnol. **13**, 272–282 (2018)
69. Annamalai, N., Rajeswari, M.V., Balasubramanian, T.: Enzymatic saccharification of pretreated rice straw by cellulase produced from *Bacillus carboniphilus* CAS 3 utilizing lignocellulosic wastes through statistical optimization. Biomass Bioen. 68, 151–160 (2011b) (2014)
70. Gokhale, A.A., Lu, J., Lee, I.: Immobilization of cellulase on magnetoresponsive graphene nano-supports. J. Mol. Cat B: Enzy. **90**, 76–86 (2013)
71. Lan, T.Q., Wei, D., Yang, S.T., Liu, X.: Enhanced cellulase production by *Trichoderma viride* in a rotating fibrous bed bioreactor. Bioresour Technol. **133**, 175–182 (2013)

Waste and Biomass Valorization (2024) 15:5819–5831
https://doi.org/10.1007/s12649-024-02618-w

ORIGINAL PAPER

Investigation of Water Turbulence Effects on Microalgal Cell Wall Damage in Thin-Layer Cascade Systems: A Fluid–Structure Interaction Approach

Shehnaz Akhtar[1,2] · Sadia Siddiqa[2] · Maqusud Alam[1] · Prosun Roy[3] · Sang-Wook Lee[2] · Cheol Woo Park[1]

Received: 7 November 2023 / Accepted: 11 June 2024 / Published online: 21 June 2024

Abstract

Turbulent flow mixing plays a critical role in optimising microalgal cultivation in thin-layer cascade (TLC) systems. However, the small size of microalgal cells makes them highly susceptible to hydrodynamic stresses generated by turbulent mixing. The mechanical properties of microalgal cell walls under turbulent conditions and their implications on cell viability and biofuel production in TLC systems remain largely unexplored. In this study, a novel fluid–structure interaction-based numerical model was developed to investigate the effects of turbulent mixing on microalgal cell wall damage in TLC systems. This study focused on assessing cell wall damage at various locations within the TLC system, considering the hydrodynamic and geometric characteristics of the system. It examined parameters such as aspect ratio, flow depth and mass flow rate to analyse cell wall shear stress, deformation and von Misses stress. Results demonstrated that appropriate turbulent mixing conditions are crucial in TLC systems to mitigate the risk of microalgal cell wall damage. Specifically, shallow and narrow TLC systems with high mixing intensities were found to pose a great risk to cell wall integrity. This study provides valuable insights into optimising turbulent mixing in TLC systems, enabling enhanced microalgal cultivation and improved biofuel production. By understanding and managing the impact of turbulent flow on microalgal cell wall integrity, this research contributes to the development of efficient and sustainable TLC systems for microalgae-based applications.

Keywords Thin-layer cascade reactor · Microalgal cell wall deformation · FSI · Von mises stress

Nomenclature

d	Water depth [m]
D_h	Hydraulic diameter [m]
W	Channel width [m]
L	Channel length [m]
f	Body force [N/m³]
I	Identity matrix
K	Turbulent kinetic energy [m²/s²]
p	Pressure [Pa]
Re	Reynolds number [1]
St	Stokes number [1]
U	Time-averaged velocity [m/s]
U_{max}	Maximum velocity [m/s]
u′	Fluctuating component of velocity [m/s
u_f	fluid velocity vector [m/s]
u_s	Solid displacement [m]
W	Strain energy density function
d_p	Algal cell diameter [m]

Greek symbols

v_T	Kinematic eddy viscosity [Pa.s]
μ	Dynamic viscosity [Pa.s]
ρ	Water density [kg/m³]
ρ_p	algal cell density [kg/m³]
u_p	Chlorella cell velocity [m/s]
τ_p	Relaxation time [s]

✉ Cheol Woo Park
chwoopark@knu.ac.kr

[1] School of Mechanical Engineering, Kyungpook National University, 80 Daehakro, Bukgu, Daegu 41566, Korea

[2] School of Mechanical Engineering, University of Ulsan, Ulsan 44610, Korea

[3] Department of Mechanical and Industrial Engineering, University of Wisconsin Platteville, 1 University Plaza, Platteville, WI 53818, USA

σ_{ij} Stress tensor in a solid [N/m²]
σ_k Prandtl number for kinetic energy
σ_ω Prandtl number for dissipation rate
ω Dissipation rate [1/s]

Subscript

s Solid
f Fluid

Introduction

Turbulent flow mixing plays a crucial role in thin-layer cascade (TLC) reactors because it prevents the sedimentation of microalgal cells. By keeping the cells suspended in water, turbulent flow facilitates the removal of oxygen and enhances the interaction between microalgal cells, sunlight and carbon dioxide. Additionally, turbulence reduces the thickness of the boundary layer surrounding the microalgal cells [1–3]. This reduction in the boundary layer thickness leads to an increased diffusion rate of nutrients to the cell surface. As a result, turbulent flow promotes nutrient uptake by microalgal cells, aiding their growth and productivity in the reactor. Furthermore, in the absence of mixing, uppermost cells become saturated with light, limiting light availability to lower cells, and hindering overall growth. However, mixing at an appropriate frequency offers a solution to this challenge. By promoting vertical movement within the water column, mixing ensures that all cells receive adequate exposure to light. This improved light distribution throughout the reactor enhances photosynthetic activity and biomass production [4–6]. Increasing the mass flow rate can enhance turbulent mixing in the reactor. However, the sensitivity of microalgal cells to fluid stresses due to their small size should be considered. High turbulence magnitudes can lead to damage in their cell walls [7–9]. Despite this, there are few quantitative studies characterizing the stress sensitivity of algal cells, and existing research varies greatly in strains, methodology, and reactor configurations [10–12]. Consequently, there is limited data on cell wall damage, making it challenging to determine the stress levels to which cells are exposed and their response to it.

Increasing the water depth in a reactor result in a larger water volume, which in turn leads to a reduction in water circulation velocity. Consequently, turbulent mixing becomes less effective. This reduction in turbulent mixing can have negative implications because it limits the interaction of microalgal cells with sunlight, carbon dioxide and nutrients [13]. Carefully balancing water depth and circulation velocity is therefore necessary to ensure efficient turbulent mixing and maximise the benefits of sunlight, carbon dioxide and nutrient availability for microalgal growth [14]. Increasing the water velocity in a deep reactor can enhance turbulent mixing, but it also increases the power consumption [15]. Meanwhile, reducing the water depth of the reactor can lead to more effective turbulent mixing, resulting in an increase in algal productivity [16]. Turbulent mixing plays a crucial role during sunrise and sunset hours, when the level of oxygen in the reactor increases. The removal of excess oxygen through turbulence during these critical time periods can double the algal productivity compared with that under nonturbulent conditions [17].

Different studies have provided conflicting data on the impact of water turbulence on algal productivity. Some studies have shown that increasing water turbulence negatively affects algal productivity, whilst others have reported insignificant change. Previous research by Weissman et al. and Drapcho suggested that algal productivity increases within a certain turbulence range, beyond which further increases in turbulence have negligible effects on microalgal growth [18, 19]. Therefore, the reduced productivity observed in some studies may be attributed to microalgal cell wall damage resulting from the use of high-magnitude turbulence [15, 18]. A cell wall is a structural layer that surrounds microalgal cells and offers the cytoplasm, nucleus and other cell parts structural support and defence against the outside environment. Owing to its high tensile strength (elastic modulus = 8.5 MPa), the cell wall has a mechanical structure [20]. Large hydrodynamic stresses, however, cause damage to the cell wall, leaving the internal parts of the cell exposed to the outside world. The microalgal cell is destroyed by this cell wall damage, which reduces the algal productivity.

Investigating the impact of turbulence on microalgal cell damage has gained significant interest amongst researchers. Previous studies have examined the effects of turbulence on microalgal species through fluid mechanical properties, such as dissipation rate, microeddy length and shear stress in the TLC reactor and raceway ponds [18, 21]. In a prior study, computational fluid dynamic (CFD) particle tracing was employed by the authors to investigate the mixing of microalgal cells in a TLC reactor [13]. However, these earlier studies primarily concentrated on the examination of mixing phenomena and did not consider the effects of turbulence on microalgal cell wall damage [22, 23]. Limited attention has been given to the mechanical structure of the microalgal cell wall and its susceptibility to damage. As mentioned earlier, the cell wall plays a crucial role in providing structural support and protection to the cell components, and damage to it can lead to reduced algal productivity. Hence, the assessment of the mechanical characteristics of the cell wall, including wall deformation and von Mises stress, becomes crucial to comprehend the effect of turbulence on microalgal cell damage [24]. Turbulence varies in different sections of the reactor, resulting in varying flow

stresses experienced by the algal cells in each Sect. [13]. Turbulence in the reactor depends on the mass flow rate and geometric features of the reactor (culture depth and channel width), so the mechanical properties of the algal cell are also affected by these parameters. Therefore, a comprehensive study that models the mechanical structure of microalgal cell walls in a TLC reactor, considering the effects of water turbulence, is needed to effectively estimate cell damage and improve microalgal productivity.

The objective of this study is to develop a novel numerical model based on fluid–structure interaction (FSI) for investigating the impact of water turbulence on microalgal cell wall damage in a TLC reactor. Specifically, the focus is on predicting the influence of turbulence on the cell wall structure of *Chlorella*, a unicellular and spherical algal species. This study employs the arbitrary Lagrangian–Eulerian (ALE) method to simulate the effects of water turbulence on microalgal cell walls. The investigation includes estimating cell wall damage at four key locations within the reactor, considering the hydrodynamic and geometric properties of the reactor. The accuracy of the CFD model is verified by comparing the simulated water velocity with the experimental data available in the literature. Various reactor configurations, including aspect ratio (AR), water depth and mass flow rate, are examined to assess their impact on cell wall shear stress, wall deformation and von Misses stress at different reactor locations. The findings of this study contribute to optimising the mass flow rate to achieve the desired turbulence in the flow whilst minimising the impact on microalgal cell wall integrity.

Physical Model

The simulations were performed using a TLC reactor developed by Apel et al. [25]. The reactor comprised four major components, namely, an intake module, an upper platform, a flow reversal module and a lower platform, as shown in Fig. 1. The upper and lower platforms of the reactor are the major cultivation units, which are oriented in opposing directions. Both channels are 4 m long and 1 m wide. The intake module, which distributes water across the top channel, is the reactor's initial module. It forms a 55° angle with the top plate. A drip edge at the upper platform's end allows the fluid to flow smoothly into the reversal module (length: 5 cm, angle to vertical: 10°), which redirects the

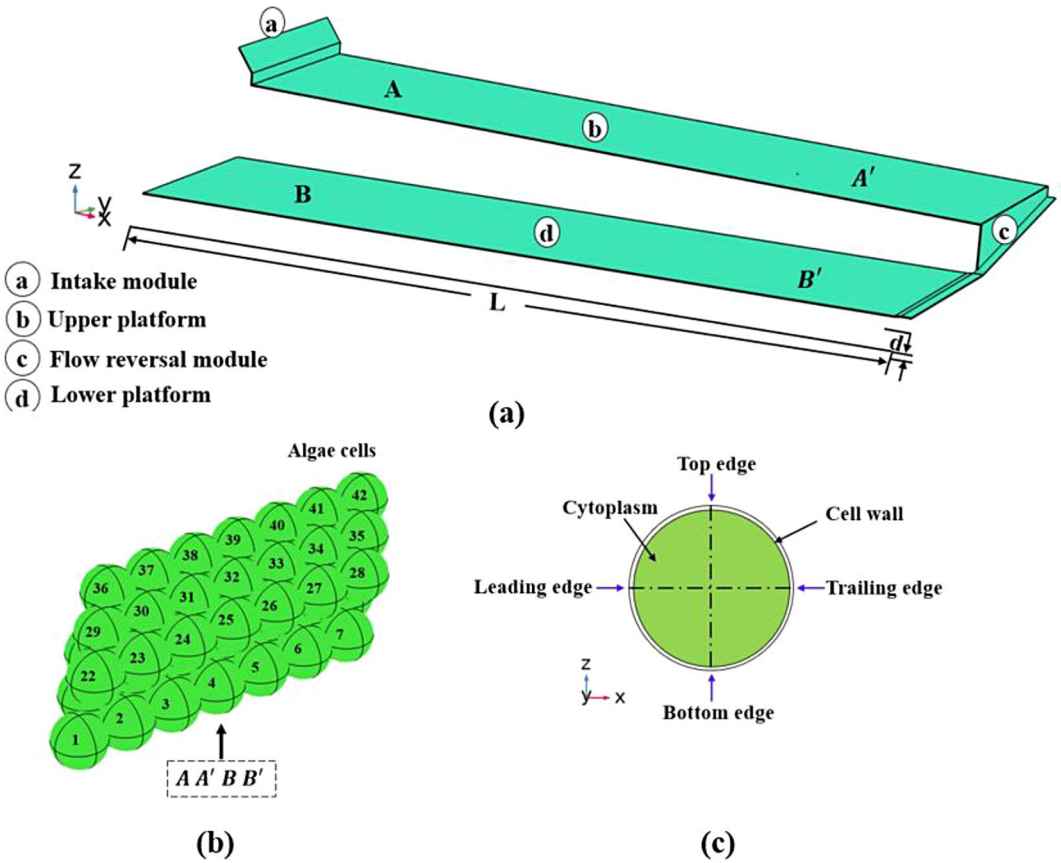

Fig. 1 (**a**) Computational model of the TLC reactor, (**b**) the position and arrangement of microalgal cells within the reactor, and (c) structure of a single algal cell, including its surfaces, cell wall, and cytoplasm

Table 1 Summary of key parameters used in the study

Parameters	Value
AR	{180, 260, 340}
Water depth	{5.6 mm, 7.5 mm, 10 mm}
Mass flow rate	(2.8–3.6) kg/s
Slope angle	{1°}

Table 2 Properties of microalgal cells used in the study

Microalgal Cell	Diameter (µm)	Thickness (µm)	Density (kg/m^3)	Viscosity (Pa. s)	Elastic Modulus (MPa)
Cell Wall	–	0.285	1060	–	8.5
Cytoplasm	6.93	–	864	0.0052	–

fluid onto the lower platform. The reversal module's bottom is inclined in the flow direction to facilitate gravity-driven flow to the lower platform. Table 1 shows the numerical values for the reactor's key geometric characteristics.

The effects of water turbulence on the cell wall structure were extensively investigated by examining four major locations (A, A', B and B') of microalgal cells in the reactor (Fig. 1). In real conditions, a commercial reactor employed for biomass production has millions of microalgal cells. From the perspective of CFD modelling, a major difference exists in the dimensions or size of the reactor (metres) and the microalgal cells (micrometres), which necessitates extensive computational meshing and time. It becomes much more complicated when implementing the multiphysics (fluid domain = water flow and cell cytoplasm, solid domain = cell wall) involved in this problem. The investigation of the effect of turbulent water flow on millions of microalgal cells requires a complicated and time-consuming three-dimensional CFD FSI model that considers multidimensional and multiphysics issues. Accordingly, a reactor containing a total of 174 spherical microalgal cells (*Chlorella*) with a distinct cell wall and cytoplasm domains was numerically simulated.

Only 42 cells are displayed in Fig. 1 to visualise the position and arrangement of microalgal cells. The cytoplasm of a *Chlorella* cell measures 6.93 µm in diameter, whilst the cell wall measures 0.285 µm in thickness. To simulate the effect of water turbulence on the microalgal cell wall, this study has to consider a number of *Chlorella* cell parameters, including cell size, density, viscosity and elastic modulus. Because this study did not culture the microalgae (*Chlorella* cells), these characteristics could not be assessed. Previous experimental research by [24, 26–28] provided the necessary *Chlorella* cell characteristics. Table 2 lists the physical, hydrodynamic and structural characteristics of spherical microalgal cells (*Chlorella*) [20, 26, 28]. For a more comprehensive understanding of microalgal cell damage within the reactor, four edges (leading, trailing, top and bottom) of the microalgal cells are defined with respect to the flow direction (Fig. 1). The cell wall damage was examined when the microalgal cells reached certain points in the reactor (A, A', B and B'). The microalgal cells must follow the water flow to effectively interact with nutrients and CO_2 before reaching the reactor outlet. The Stokes number (St) is a dimensionless value commonly used to predict whether a relative velocity will exist between a fluid and a particle [24, 29, 30]. The governing equation of *St* is expressed as follows:

$$S_t = \frac{\tau_p U}{D_h} \tag{1}$$

$$\tau_p = \frac{\rho_p {d_p}^2}{18\mu} \tag{2}$$

where d_p denotes the microalgal cell diameter (m), ρ_p denotes the microalgal cell density (kg/m^3), and τ_p denotes the relaxation time of the microalgal cell (s). *Chlorella* microalgal cells with the condition ($St << 1$) successfully followed the water flow and reached the reactor outlet [13, 31]. Aspect ratio is a key parameter in open channel flow systems because it significantly affects the flow characteristics of reactor [32]. Therefore, this study used the non-dimensional aspect ratio (AR) to investigate the effects of reactor geometry on microalgal cell wall damage in TLC reactor.

AR = Channel width (m) /Channel depth (m) = W/d.

Three different values of ARs (180, 260 and 340) were utilised with different water depths to examine their effects on microalgal cell wall deformation and von Mises stresses at different position in the reactor.

Mathematical Modelling

Hydraulic diameter (Dh) and the Reynolds number were used to evaluate the open-channel flow behaviour, as given below:

$$D_h = \frac{4dW}{W + 2d} \tag{3}$$

$$Re = \frac{\rho D_h U}{\mu} \tag{4}$$

where W stands for the channel's width (m), d for the water's depth (m) and U for the average water velocity (m/s). With a density of (ρ) 1000 (kg/m^3) and a viscosity (µ) of 0.001 (Pa. s), water was chosen as the working fluid. Reynolds numbers in the range of 10,200 to 14,200 were used to describe the flow behaviour in the TLC reactor [33,

34]. For turbulent flows in an open channel with relatively high Reynolds numbers, the k-turbulence model is a suitable option [35, 36]. Therefore, this model was selected to simulate the hydrodynamics of this study. To assess the validity of using a coupled FSI approach versus treating cells as point particles, an analysis was performed comparing the size of the microalgal cells to relevant turbulence scales. Their size was compared to the Kolmogorov length scale (η), a characteristic length scale in turbulent flows. The Kolmogorov length scale was found to be in the range of 1.07×10^{-5} m to 8.42×10^{-6} m. The total diameter of the Chlorella cells, including the cell wall, is 7.5×10^{-6} m. This suggests that the Chlorella cell diameter is comparable to the Kolmogorov length scale, indicating that cells are not negligible in size relative to the smallest turbulence eddies. Therefore, a point particle approximation may not be completely accurate, and a coupled FSI model is more suitable to simulate the effect of turbulence on the cells [37].

Fluid Flow Modelling

This study integrated two different approaches for modelling: solid mechanics, which focused on the microalgal cell wall by using a Lagrangian description in a material frame, and fluid flow, which considered water and cytoplasm by using a Eulerian description in a spatial frame. This integration was achieved through the ALE technique to characterise the fluid flow and derive the velocity field of the water and cytoplasm within the microalgal cell, Reynolds-averaged Navier–Stokes (RANS) equations were employed. For computational efficiency and simplification, the intercellular fluid within the microalgal cell was disregarded, and the cytoplasm was modelled as a Newtonian viscous fluid [26]. Table 2 lists the cytoplasm's fluid properties adopted in this study [26]. RANS simulations were chosen due to computational constraints. RANS primarily captures mean flow characteristics and may not fully represent the high-frequency, local turbulence fluctuations that contribute to cell damage. However, it's important to note that the fluid velocity was not simply imposed on cell boundaries; rather, flow around each cell was simulated. This approach aids computational efficiency while still capturing the essential fluid-cell interactions. The current study serves as a foundation for identifying regions that may require more detailed analysis using high-fidelity simulations in future.

Governing Equations

The RANS equations for Newtonian and incompressible fluid flows are as follows:

- Continuity Eq.

$$(\nabla.\mathbf{u}_f) = 0, \tag{5}$$

where ρ_f is the fluid density (kg/m³), and $\mathbf{u}_f$ is the fluid velocity vector (m/s).

- Momentum Eq.

$$\rho_f\frac{\partial \mathbf{u}_f}{\partial t} + \rho_f(\mathbf{u}_f\cdot\nabla)\mathbf{u}_f + \nabla\cdot\left[-p\mathbf{I} + \mu\left(\nabla\mathbf{u}_f + (\nabla\mathbf{u}_f)^T\right)\right] + \mathbf{f}_f, \tag{6}$$

where p is the fluid pressure (Pa), I is the identity matrix, and $\mathbf{f}_f$ is the body force per unit volume (N/m³). These equations provide a time evolution of the flow. RANS equations are obtained by manipulating these equations. The velocity vector $\mathbf{u}_f$ in Eqs. (5) and (6) will be replaced with $\mathbf{U}+\mathbf{u}'$, where $\mathbf{U}$ is the time-averaged velocity field (m/s), and $\mathbf{u}'$ is the fluctuating component of velocity (m/s). The k–ω turbulence model is based on two equations: turbulent kinetic energy and specific dissipation rate. The governing equation of the turbulent kinetic energy (k) is as follows:

$$\frac{\partial k}{\partial t} + u_j\frac{\partial k}{\partial x_j} = \tau_{ij}\frac{\partial u_i}{\partial x_j} - \beta^* k\omega + \frac{\partial}{\partial x_j}\left[(\nu + \sigma_k\nu_T)\frac{\partial k}{\partial x_j}\right] \tag{7}$$

,where σ_k and σ_ω are the turbulent Prandtl numbers for kinetic energy and dissipation rate, respectively; k is the turbulent kinetic energy (m²/s²); ω is the dissipation rate (1/s); and ν_T is the kinematic eddy viscosity (Pa.s); constants $\sigma_\omega = 0.5$ and $\beta^* = 0.09$ [38]. The turbulent dissipation rate (ω) for the k–ω turbulence model is as follows:

$$\frac{\partial \omega}{\partial t} + u_j\frac{\partial \omega}{\partial x_j} = \alpha\frac{\omega}{k}\tau_{ij}\frac{\partial u_i}{\partial x_j} - \beta^*\omega^2 + \frac{\partial}{\partial x_j}\left[(\nu + \sigma_\omega\nu_T)\frac{\partial k}{\partial x_j}\right], \tag{8}$$

The kinematic eddy viscosity (ν_T) described by the k–ω turbulence model is as follows:

$$\nu_T = \frac{k}{\omega}, \tag{9}$$

Algal Cell Wall Modelling

Large hydrodynamic stresses caused by a high turbulence magnitude induce damage to the cell wall and other mechanical components of microalgal cells [17, 35]. Therefore, the cell wall of a spherical microalgal cell *(Chlorella)* was modelled as an elastic structure filled with cytoplasm [31, 36].

Governing Equations

The governing equation for calculating the solid displacement for the microalgal cell wall is given below:

$$\rho_s \frac{\partial^2 \mathbf{u}_s}{\partial t^2} = \frac{\partial \sigma_{ij}}{\partial x_j} + \rho_s \mathbf{f}_s, \tag{10}$$

where $\mathbf{u}_s$ denotes the solid displacement (m), σ_{ij} represents the component of the stress tensor in a solid (N/m²), ρ_s denotes the solid density (kg/m³) and f_s is the body force component acting on the solid (N/m³). The determination of σ_{ij} emanates from the application of the constitutive equation of a Newtonian fluid. The cumulative force imparted onto the microalgal cell wall by the fluid corresponds to the negative of the reactive force upon the fluid, as expressed by the following equation [39]:

$$\mathbf{f}_s = n \cdot \{-p\mathbf{I} + \left(\mu \left(\nabla \mathbf{u}_f + (\nabla \mathbf{u}_f)^T\right)\right)\}, \tag{11}$$

where $\mathbf{I}$ is the identity matrix, $\mathbf{f}_s$ is the body force on the solid (N/m³), n is the outward normal to the boundary, and $\mathbf{u}_f$ is the fluid velocity vector (m/s). The microalgal cell wall stores energy when structural deformation occurs. The strain energy density function W was used to measure this energy.

$$s_{ij} = \frac{\partial W}{\partial \epsilon_{ij}} \text{where} i, j \, \epsilon \{1,2,3\}, \tag{12}$$

where s_{ij} and ϵ_{ij} are the Green–Lagrange strain tensor and second Piola–Kirchhoff stress components, respectively [40, 41]. A transformation of the force between the two coordinate systems was necessary because the Navier–Stokes equations were solved in the spatial (deformed) frame, whilst the solid mechanic interfaces were described in the material (undeformed) frame. Hence, a coordinate transformation was performed in the ALE model as follows:

$$\mathbf{f}_f = \mathbf{f}_s \frac{dv}{dV}, \tag{13}$$

where dv and dV are the mesh element scale factors for the spatial and material (reference) frames, respectively; and $\mathbf{f}_f$ and $\mathbf{f}_s$ are the forces acting on the fluid and algal cell walls (N/m³), respectively.

Table 3 Mesh elements of the TLC reactor and algal cells

Geometries	Elements	Extremely fine	Extra fine	Finer
Microalgal cells and TLC reactor	Domain	(5,361,121)	(2,706,637)	(1,325,990)
	Boundary	(1,444,820)	(1,002,290)	(229,608)
	Edge	(25,976)	(20,364)	(15,487)

Numerical Simulations and Mesh Generation

In this study, the commercial software COMSOL Multiphysics was utilised to investigate the impact of fluid turbulence on the damage to microalgal cell walls in a TLC reactor. The ALE method was employed through the FSI interface of COMSOL Multiphysics to model the interaction between water turbulence and the microalgal cell wall structure. A total of 172 spherical microalgal cells, each characterised by distinct cell wall and cytoplasm domains, were introduced into the reactor at four specified locations denoted as points A, A', B and B' in Fig. 1. The fluid and structural properties of these microalgal cells were calculated as they reached these predetermined locations within the reactor. The reactor and microalgal cells were discretised using a free tetrahedral mesh. To ensure precise flow field calculations at the FSI boundaries of the microalgal cells, a boundary layer mesh with a dense element distribution was employed. Three different mesh sizes, fine, extra fine and extremely fine, were utilised in this study, with variations by a factor of five. Detailed information regarding the mesh elements can be found in Table 3. A grid independency test was conducted to assess the accuracy of the ALE methodology used in this study. The wall shear stress and algal cell wall deformation were estimated at location B within the reactor, as illustrated in Fig. 2. These properties are plotted on the FSI interface (bottom, top, leading, and trailing edges) of microalgal cell 15 (Fig. 1b&c). Minimal differences were observed between the results of shear stress and cell wall deformation. Consequently, all simulations in this study were conducted using the extra-fine mesh element size.

Methodology Verification

To verify the accuracy of the applied model, the findings of this investigation were compared with the numerical results of [22] in Fig. 3. The numerical findings matched the measured water velocity in the reactor, thereby verifying that the proposed methodology can be applied to the model turbulence effect on the microalgal cell wall damage in TLC reactors.

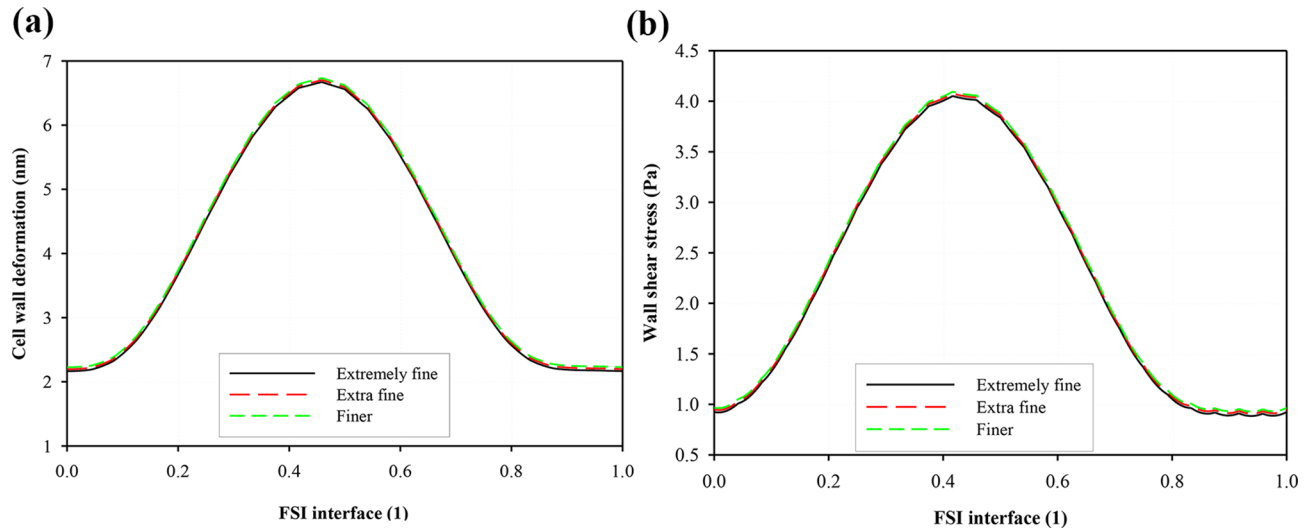

Fig. 2 Mesh independence test for (**a**) cell wall deformation (nm) and (**b**) wall shear stress (Pa) at a mass flow rate of 2.8 kg/s for a TLC reactor with AR = 180 and a water depth of 5.6 mm

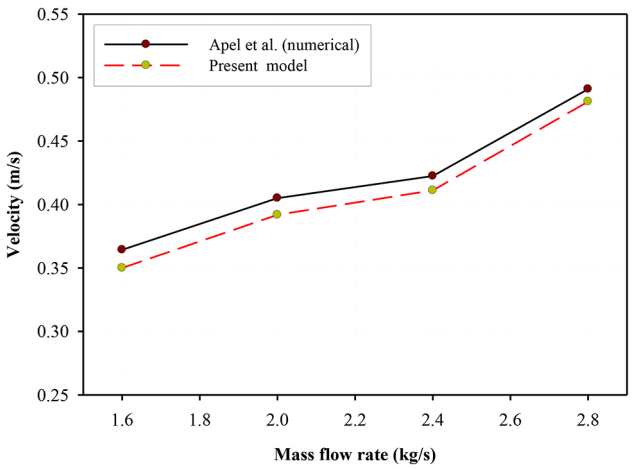

Fig. 3 Comparison of the average water velocity in the reactor with the numerical results of Apel et al. [22]

Results and Discussion

The mechanical properties of algal cell walls were computed at four different locations (A, A', B and B') in the reactor to estimate the effects of the hydrodynamics and geometric properties (water depth and channel width) of the reactor on algal cell wall damage. The results are plotted in terms of cell wall deformation, von Mises stress and wall shear stress.

Effect of Microalgal Cell Location

The microalgal cell wall mechanical properties are plotted at four reactor locations. Two distinct locations were chosen at the upper channel (locations A and A′) and two at the lower channel (locations B and B′) of the TLC reactor (Fig. 1). Figure 4 depicts the effect of different microalgal cell locations on cell wall deformation and von Mises stress. The results are plotted for a reactor with a water culture depth of 5.6 mm, AR = 180 and a mass flow rate of 2.8 kg/s. These properties are plotted on the FSI interface (bottom, top and leading edges) of microalgal cell 15.

The top and leading regions of the microalgal cell wall deformed more than the bottom edge area (Fig. 4a). The low deformation at the bottom edges indicated that the contact of microalgal cells with one another helped reduce the effect of flow stresses on the cell walls. The maximum deformation in the cell wall was recorded at location B′ because of the highly turbulent flow in this region of the reactor. When the microalgal cells were at locations B and A', the cell wall deformation was minimal.

Figure 4b depicts an inverse correlation between cell wall deformation and von Mises stress. The top edge of the microalgal cells showed the lowest von Mises stress, whereas the bottom and trailing edges showed the highest because the high fluid forces induced high stresses on the cell wall. The microalgal cells exhibited high resistance to cell wall deformation at location A, as shown by the maximum von Mises stress, whereas minimal resistance to wall deformation was suggested by the smallest von Mises stress at locations A′, B and B′. These findings implied that the microalgal cells' top and leading edges were very fragile, particularly when they were in the reactor's lower channel (location B'), which could influence the production of the algae.

Figure 5 displays the contour plots of the cell wall deformation (nm) of four different cells at two locations (B and B') in the reactor. The contour plots exhibit similar trend, but with variations in magnitude. Owing to the adequate

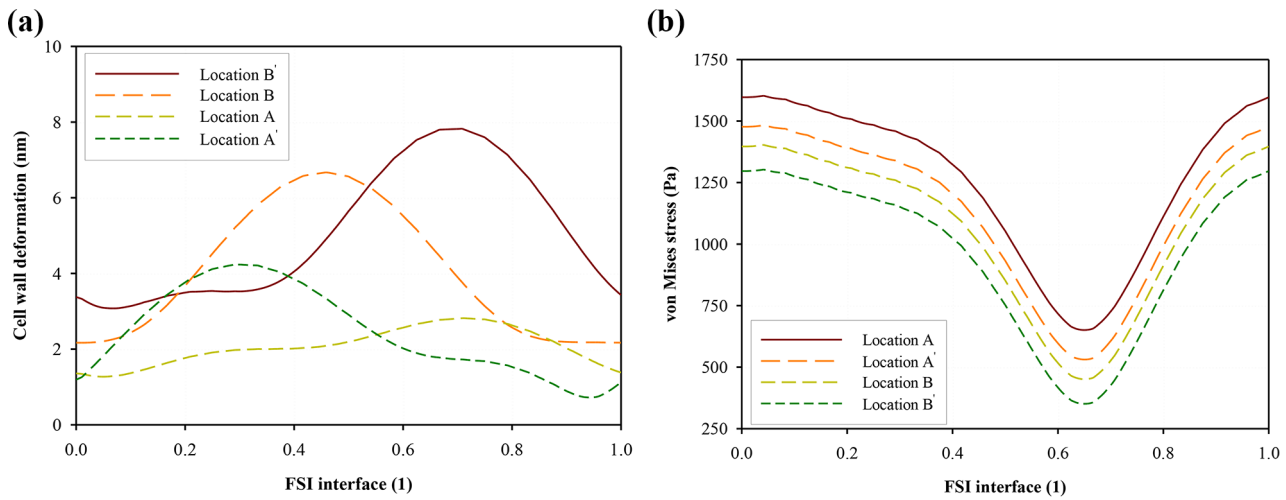

Fig. 4 Effect of microalgal cell wall location on (**a**) cell wall deformation (nm) and (**b**) von Mises stress (Pa) for a reactor with AR = 180 at a water depth of 5.6 mm and a mass flow rate of 2.8 kg/s

contact with surrounding microalgal cells, the deformation of the middle microalgal cells (30 and 41) was minimal. The microalgal cells near the corners, or 1 and 15, on the contrary, had significant wall deformation as a result of little contact with the surrounding cells. Turbulent mixing was increased in the lower channel of the reactor (location B′) because of the velocity increase here due to the geometric shape of the reactor. Therefore, cell wall deformation was at the highest when the microalgal cells moved to location B′ of the reactor, as depicted in Fig. 5b. The microalgal cells could be destroyed by excessive algal cell wall deformation because it damages the cells' internal components, such as the nucleus and chloroplast. These findings suggested that position B' is crucial for microalgal production because microalgal cell damage is likely to happen in this region of the reactor [16, 18]. This study thus employed microalgal cell 15 at position B' to further investigate the impact of the reactor's geometric and hydrodynamic characteristics on microalgal cell damage.

To analyse nutrient diffusivity, the wall shear stress on the microalgal cell's surface was estimated. As illustrated in Fig. 6, the microalgal cell's lower and trailing edges displayed minimal cell wall shear stress, whereas the leading edge and upper regions experienced significant shear stress levels. A pronounced increase in wall shear stress occurred at location B' because of the presence of intense turbulent mixing. This observation suggested that nutrient diffusivity was enhanced at locations B' and A. This enhancement could be attributed to the reduction in boundary layers around the cell surface, which was a consequence of the elevated shear stress levels in these specific areas. However, it's important to consider the stress tolerance in macroalgae, which varies depending on factors such as species, habitat, and environmental conditions. Generally, macroalgae can withstand stresses caused by hydrodynamic forces if they are lower than the mechanical strength. However, specific values for stress tolerance typically range from approximately 0.2 to 1.0 MPa for mechanical strength of wall and 5 to 50 Pa for wall shear stress [42–44].

Effect of Mass Flow Rate

Turbulent mixing in a reactor is directly related to the mass flow rate or water velocity, and increasing the mass flow rate can enhance turbulent mixing. Thus, the impact of mass flow rate on the radial wall deformation (nm) and von Mises stress (Pa) of microalgal cells in a reactor with an AR of 180 and a water depth of 5.6 mm is plotted in Fig. 7.

Cell wall deformation was directly proportional to the mass flow rate. An increase in mass flow rate led to greater turbulent mixing, resulting in increased cell wall deformation due to higher hydrodynamic stresses (Fig. 7a).

Specifically, as the mass flow rate increased from 2.8 kg/s to 3.2 kg/s, the wall deformation increased by nearly 20%. Further increasing the mass flow rate from 3.2 kg/s to 3.6 kg/s resulted in a maximum augmentation of 25% in cell deformation (Fig. 7a). A higher mass flow rate may reduce the boundary layer around microalgal cells, thereby enhancing nutrient diffusivity. However, the substantial fluid stresses generated at high mass flow rates significantly compromised the integrity of the microalgal cell wall.

Figure 7b shows the effect of mass flow rate on the radial von Mises stress (Pa) of microalgal cells. The von Mises stress increased with an increase in the mass flow rate because of the large hydrodynamic stresses on the microalgal cells. An approximate increase of 21% in von Mises stress occurred when the mass flow rate increased from 2.8 kg/s to 3.2 kg/s, and an increase of 24% was observed

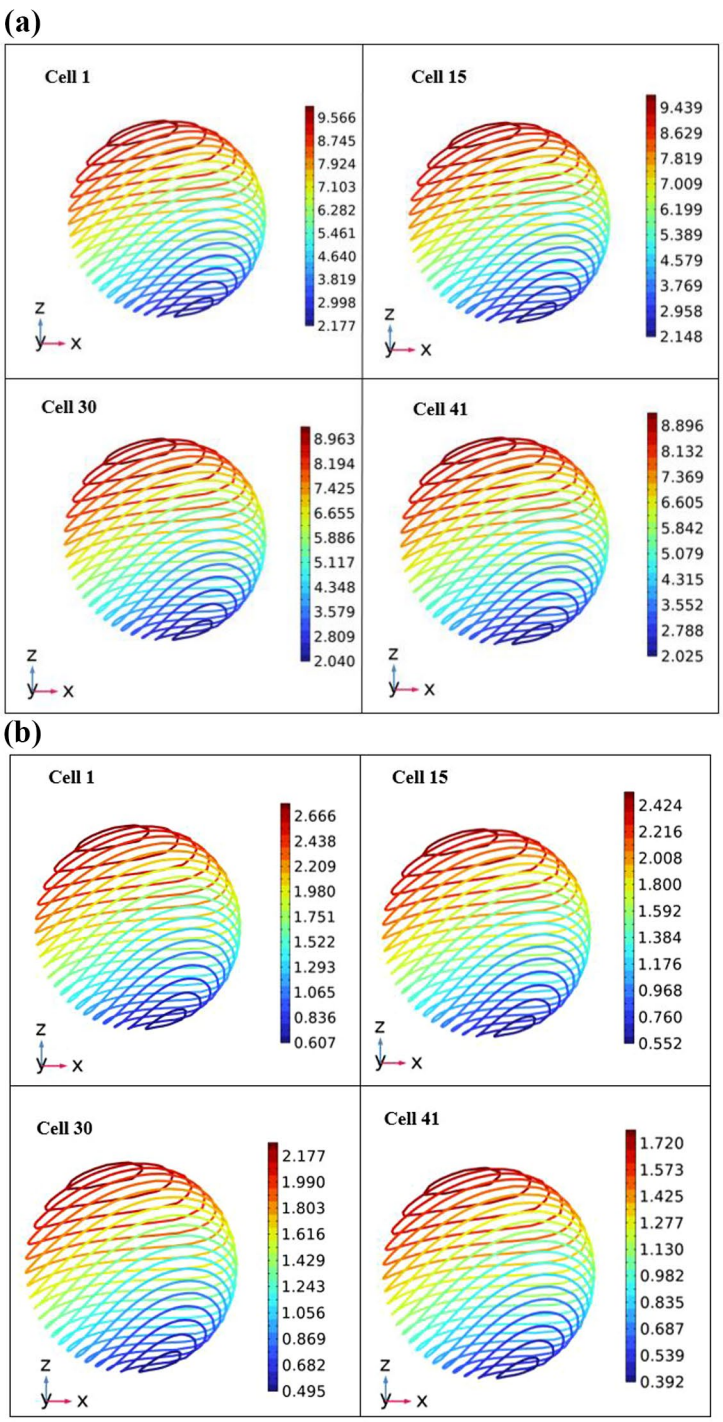

Fig. 5 Contour plots of cell wall deformation (nm) for a TLC reactor with AR = 180 at a depth of 5.6 mm and a mass flow rate of 2.8 kg/s at (**a**) location B′ and (**b**) location B

when the mass flow rate increased from 3.2 kg/s to 3.6 kg/s. Accordingly, elevated mass flow rates are unfavourable for microalgal cultivation within the TLC reactor due to the considerable deformation of microalgal cell walls and the associated high-power requirements [16, 17].

Effect of AR

Figure 8 depicts the effect of AR on the radial wall deformation (nm) and von Mises stress (Pa) of microalgal cells in a reactor with a culture depth of 5.6 mm and a mass flow rate of 2.8 kg/s. Figure 8a demonstrates that as AR increased, a reduction in microalgal cell wall deformation occurred, which could be attributed to the decrease in turbulent mixing

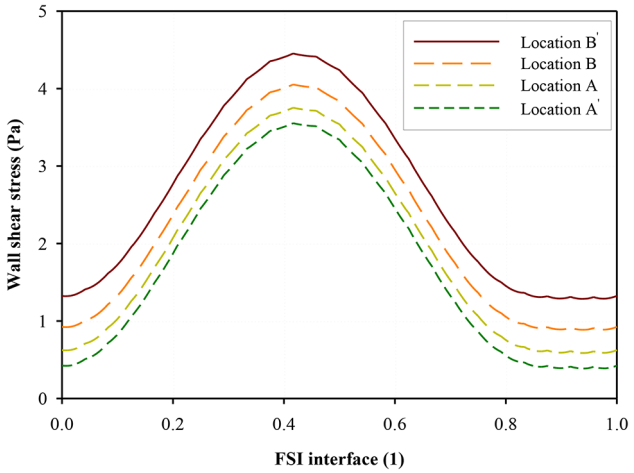

Fig. 6 Effect of microalgal cell wall location on wall shear stress (Pa) for a TLC reactor with AR = 180 at a depth of 5.6 mm and a mass flow rate of 2.8 kg/s

resulting from the higher AR values. With an increase in AR, the water velocity within the reactor decreased, subsequently leading to reduced turbulent mixing. TLC reactors characterised by larger AR values experience lower water velocities, which in turn contribute to the decreased cell wall deformation due to the small applied fluid forces [24, 37]. A maximum reduction of approximately 10% in cell wall deformation was observed as the AR increased from 180 to 260. By contrast, an increase in AR from 260 to 340 led to a 17% decrease in cell wall deformation.

Figure 8b depicts the effect of AR on the radial von Mises stress (Pa) of the microalgal cells in the reactor. This study employed the radial von Mises stress to assess if the microalgal cell wall could sustain the applied turbulence flow forces. The von Mises stress exhibited a significant decrease as the AR of the reactor increased. Specifically, increasing the AR from 180 to 260 resulted in a reduction of approximately 16% in von Mises stress. Similarly, a decrease of approximately 12% in von Mises stress was observed as the AR increased from 240 to 360. These observations suggested that turbulent mixing is particularly effective in reactors with smaller ARs. It enhances the distribution of sunlight and facilitates nutrient transport to the surface of microalgal cells. However, reactors with narrow channels (characterised by smaller ARs) result in substantial cell wall deformations, indicating a higher likelihood of significant damage to microalgal cells and consequently reduced cell productivity [15, 17, 19, 20].

Effect of Water Depth

Water depth has a considerable impact on microalgal cell wall damage because of its direct influence on turbulent mixing in the reactor. Figure 9 shows the estimation of the effect of water depth on the wall deformation (nm) and von Mises stress (Pa) of microalgal cells in a reactor with AR = 180 and a mass flow rate of 2.8 kg/s. In Fig. 9a, the deformation of the microalgal cell wall exhibited an inverse relationship with water depth. When the water depth increased from 5.6 mm to 7.5 mm, the cell wall deformation decreased by approximately 18%. Likewise, an increase in water depth from 7.5 mm to 10 mm resulted in a 20% reduction in microalgal cell wall deformation. These findings emphasised that reactors with shallower culture depths enable sunlight to penetrate to the reactor's bottom, promoting uniform mixing of microalgal cells, which in turn enhances effective light utilisation within the system [2–4].

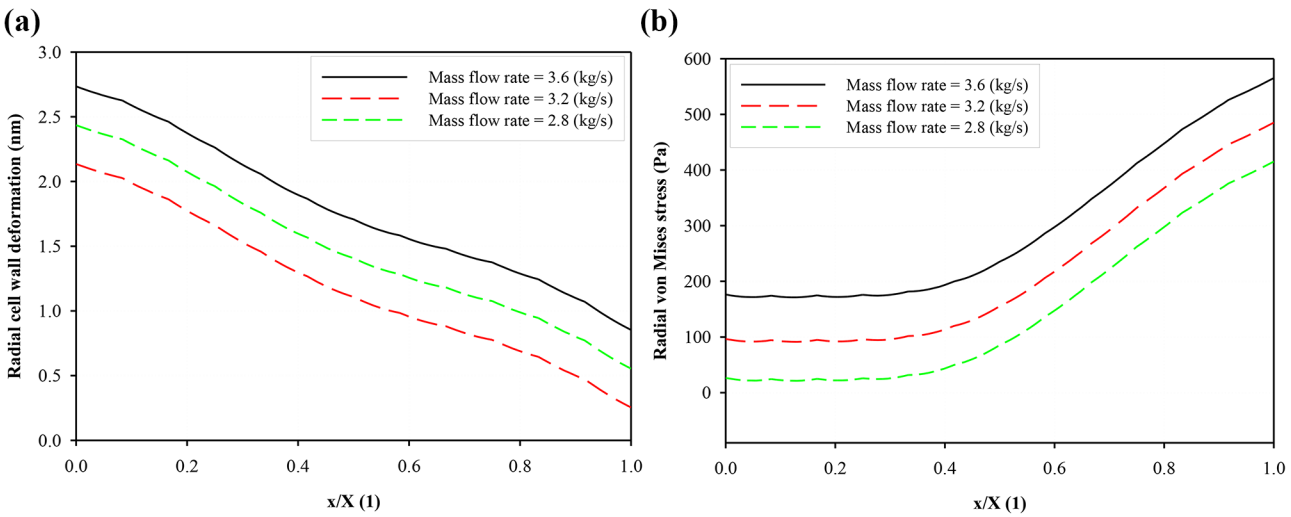

Fig. 7 Effect of mass flow rate on (**a**) radial cell wall deformation (nm) and (**b**) von Mises stress (Pa) for a TLC reactor with a water depth of 5.6 mm and AR = 180

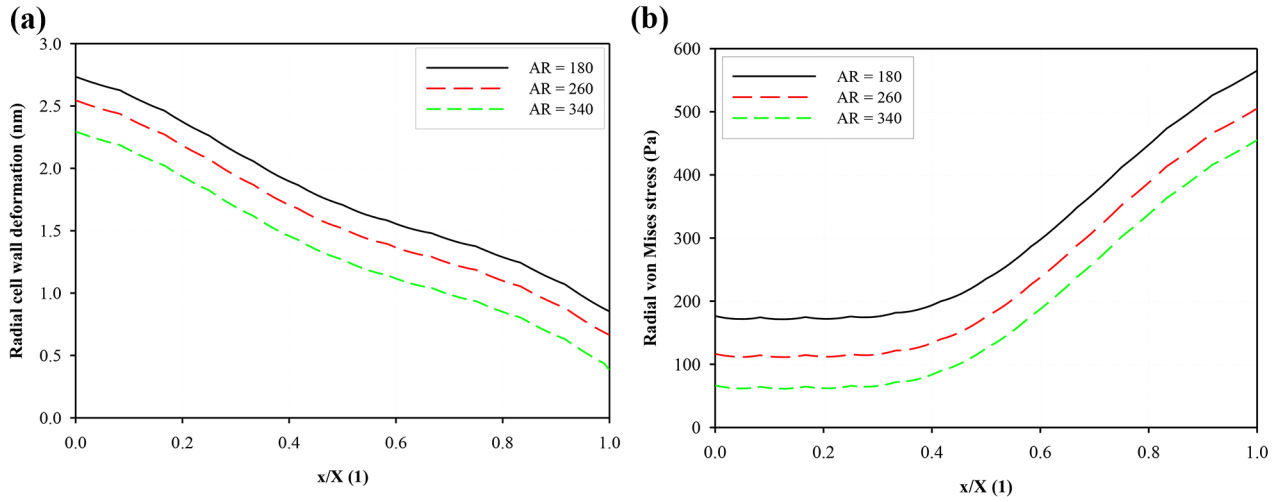

Fig. 8 Effect of AR on (**a**) radial cell wall deformation (nm) and (**b**) von Mises stress (Pa) for a TLC reactor with a water depth of 5.6 mm and a mass flow rate of 2.8 kg/s

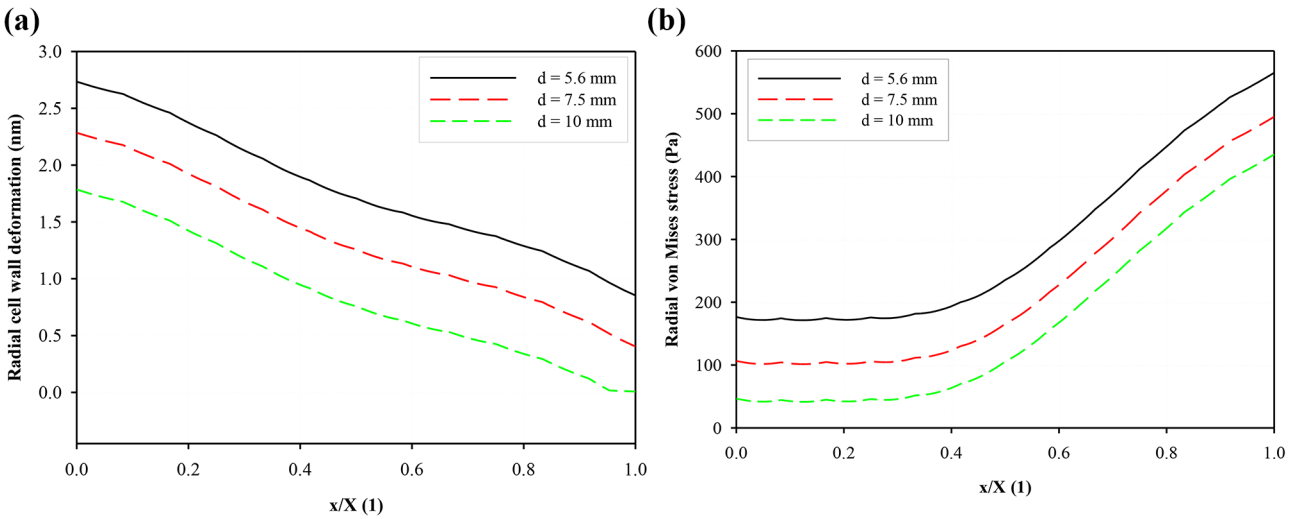

Fig. 9 Effect of water depth on (**a**) radial cell wall deformation (nm) and (**b**) von Mises stress (Pa) for a TLC reactor with AR = 180 and a mass flow rate of 2.8 kg/s

Figure 9b depicts the effect of water depth on the von Mises stress (Pa) of microalgal cells. The von Mises stress magnitudes were significantly influenced by the culture depth. Increasing the water depth resulted in a decrease in von Mises stress because of small hydrodynamic fluid forces. Specifically, when the water depth increased from 5.6 mm to 7.5 mm, the von Mises stress decreased by approximately 25%. Conversely, when the water depth decreased from 7.5 mm to 10 mm, the von Mises stress decreased by approximately 33%. These findings suggested that microalgal cells in shallow reactors are more susceptible to damage due to significant cell wall deformations, which can adversely affect the microalgal culture and subsequently reduce biomass productivity [16–18].

Conclusion

A numerical model based on FSI was employed to investigate the effect of turbulence on microalgal cell wall damage in a TLC reactor. The influence of water turbulence was simulated using the ALE numerical approach. This study examined how the hydrodynamic and geometric characteristics of the reactor, such as channel width and depth, affect microalgal cell wall damage at four distinct locations within the reactor. Furthermore, it explored the impact of ARs and water depth mass flow rate on microalgal cell walls in terms of parameters such as wall shear stress, cell wall deformation and von Mises stress at the same four reactor locations.

- The high cell wall shear stresses at locations B' and A led to a decrease in the boundary layer around the cell surface, which increased the nutrient diffusivity rates to the microalgal cells at these locations.
- Microalgal cells that encountered the water flow were considerably deformed, and their particle–particle interactions reduced the impact of flow stresses on their cell wall structure. Von Mises stress exhibited an inverse relationship with cell wall deformation, whilst cell wall shear stress showed a direct correlation with cell wall deformation.
- Microalgal cell wall deformation was important at locations B' and A, indicating that algal production might be considerably reduced/affected in these reactor zones. The increase in AR reduced the microalgal cell wall deformation and von Mises stresses. TLC reactors with wide channels are thus suitable for algal cultivation due to minimum cell wall damage.
- Increasing water depth led to a decrease in cell wall deformation and von Mises stresses, whereas shallow water depths resulted in increased microalgal cell wall damage. Meanwhile, increasing the mass flow rate considerably increased the cell wall deformation and von Mises stress. To maximise algal production, the appropriate hydrodynamic and geometric parameters should be chosen to ensure effective turbulent mixing with minimal damage to the microalgal cell wall.

Acknowledgements This work was supported by the National Research Foundation of Korea grant funded by the Korean government (MSIT) (No. RS-2023-00208673).

Declarations

Conflict of Interest The authors declare no conflict of interest.

References

1. Grobbelaar, J.U., Kroon, B.M.A., Burger-Wiersma, T., Mur, L.R.: Influence of medium frequency light/dark cycles of equal duration on the photosynthesis and respiration of Chlorella pyrenoidosa. Hydrobiologia. **238**(1), 53–62 (1992). https://doi.org/10.1007/BF00048773
2. Marshall, J.S., Huang, Y.: Simulation of light-limited algae growth in homogeneous turbulence. Chem. Eng. Sci. **65**(12), 3865–3875 (2010). https://doi.org/10.1016/j.ces.2010.03.036
3. Schapira, M., Seuront, L., Gentilhomme, V.: Effects of small-scale turbulence on Phaeocystis globosa (Prymnesiophyceae) growth and life cycle. J. Exp. Mar. Biol. Ecol. **335**(1), 27–38 (2006). https://doi.org/10.1016/j.jembe.2006.02.018
4. Doucha, J., Livansky, K.: Novel outdoor thin-layer high density micro-algal culture system: Productivity and operational parameters. ARCHIV FUR HYDROBIOLOGIE-SUPPLEMENT-. **106**, 129 (1995)
5. Chiarini, A., Quadrio, M.: The light/dark cycle of microalgae in a thin-layer photobioreactor. J. Appl. Phycol., pp. 1–13, (2020)
6. Grobbelaar, J.U.: Factors governing algal growth in photobioreactors: The 'open' versus 'closed' debate. J. Appl. Phycol. **21**, 489–492 (2009)
7. Bałdyga, J., Pohorecki, R.: Influence of turbulent mechanical stresses on microorganisms. Appl. Mech. Rev. **51**(1), 121–140 (1998). https://doi.org/10.1115/1.3098987
8. Blersch, D.M., Kangas, P.C., Mulbry, W.W.: Turbulence and nutrient interactions that control benthic algal production in an engineered cultivation raceway. Algal Res. **2**(2), 107–112 (2013). https://doi.org/10.1016/j.algal.2013.01.001
9. Barbosa, M.J., Albrecht, M., Wijffels, R.H.: Hydrodynamic stress and lethal events in sparged microalgae cultures. Biotechnol. Bioeng. **83**(1), 112–120 (2003). https://doi.org/10.1002/bit.10657
10. Barbosa, M.J., Albrecht, M., Wijffels, R.H.: Hydrodynamic stress and lethal events in sparged microalgae cultures. Biotechnol. Bioeng. **83**(1), 112–120 (2003)
11. Gudin, C., Chaumont, D.: Cell fragility—the key problem of microalgae mass production in closed photobioreactors. Bioresour Technol. **38**, 2–3 (1991)
12. Märkl, H., Bronnenmeier, R., Wittek, B.: The resistance of microorganisms to hydrodynamic stress. Int. Chem. Eng. **31**(2), 185–196 (1991)
13. Akhtar, S., Ali, H., Park, C.W.: Complete evaluation of cell mixing and hydrodynamic performance of thin-layer cascade reactor. Appl. Sci. (Switzerland). **10**(3) (2020). https://doi.org/10.3390/app10030746
14. Akhtar, S., Ali, H., Park, C.W.: Effective Prediction of Monthly Heat Transfer Characteristics in a Thin-Layer Cascade Reactor Subjected to Outdoor Conditions, vol. 2022. (2022)
15. Weissman, J.C., Goebel, R.P., Benemann, J.R.: Photobioreactor design: Mixing, carbon utilization, and oxygen accumulation. Biotechnol. Bioeng. **31**(4), 336–344 (1988). https://doi.org/10.1002/bit.260310409
16. Bosca, C., Dauta, A., Marvalin, O.: Intensive outdoor algal cultures: How mixing enhances the photosynthetic production rate. Bioresour Technol. **38**(2), 185–188 (1991). https://doi.org/10.1016/0960-8524(91)90152-A
17. Chisti, Y.: Biodiesel from microalgae. Biotechnol. Adv. **25**(3), 294–306 (2007). https://doi.org/10.1016/j.biotechadv.2007.02.001
18. Drapcho, C.M., Brune, D.E.: The partitioned aquaculture system: Impact of design and environmental parameters on algal productivity and photosynthetic oxygen production. Aquac Eng. **21**(3), 151–168 (2000). https://doi.org/10.1016/S0144-8609(99)00028-X
19. Grobbelaar, J.U.: The influence of light/dark cycles in mixed algal cultures on their productivity. Bioresour Technol. **38**(2), 189–194 (1991). https://doi.org/10.1016/0960-8524(91)90153-B
20. MUNNS, R., GREENWAY, H., SETTER, T.L., KUO, J.: Turgor Pressure, Volumetric Elastic Modulus, Osmotic Volume and Ultrastructure of Chlorella emersonii Grown at High and Low External NaCl, *J Exp Bot*, vol. 34, no. 2, pp. 144–155, Feb. (1983). https://doi.org/10.1093/jxb/34.2.144
21. Akhtar, S., Park, C.W.: Investigation on Hydrodynamics of Thin-layer Cascade System, Proc. KSVI Conference. 31–32, (2019)
22. Severin, T.S., Apel, A.C., Brück, T., Weuster-Botz, D.: Investigation of vertical mixing in thin-layer cascade reactors using computational fluid dynamics. Chem. Eng. Res. Des. **132**, 436–444 (2018). https://doi.org/10.1016/j.cherd.2018.01.036
23. Carvalho, A.P., Meireles, L.A., Malcata, F.X.: Microalgal reactors: A review of enclosed system designs and performances. Biotechnol. Prog. **22**(6), 1490–1506 (2006). https://doi.org/10.1021/bp060065r
24. Secomb, T.W., Hsu, R., Pries, A.R.: Blood flow and red blood cell deformation in nonuniform capillaries: Effects of the endothelial

surface layer. Microcirculation. **9**(3), 189–196 (2002). https://doi.org/10.1038/sj.mn.7800132
25. Apel, A.C., et al.: Open thin-layer cascade reactors for saline microalgae production evaluated in a physically simulated Mediterranean summer climate, *Algal Res*, vol. 25, no. March, pp. 381–390, (2017). https://doi.org/10.1016/j.algal.2017.06.004
26. Williams, P.J.L.B., Laurens, L.M.L.: Microalgae as biodiesel & biomass feedstocks: Review & analysis of the biochemistry, energetics & economics. Energy Environ. Sci. **3**(5), 554–590 (2010). https://doi.org/10.1039/b924978h
27. Wijaya, F.B., Mohapatra, A.R., Sepehrirahnama, S., Lim, K.M.: Coupled acoustic-shell model for experimental study of cell stiffness under acoustophoresis. Microfluid Nanofluidics. **20**(5), 1–15 (2016). https://doi.org/10.1007/s10404-016-1734-1
28. Jia, F., Ben Amar, M., Billoud, B., Charrier, B.: Morphoelasticity in the development of brown alga Ectocarpus siliculosus: From cell rounding to branching. J. R Soc. Interface. **14**(127) (2017). https://doi.org/10.1098/rsif.2016.0596
29. Brennen, C.E.: Fundamentals of Multiphase Flow. Cambridge University Press, Cambridge (2005). https://doi.org/10.1017/CBO9780511807169
30. Lucci, F., Ferrante, A., Elghobashi, S.: Is Stokes number an appropriate indicator for turbulence modulation by particles of Taylor-length-scale size?, **025101**, (2011). https://doi.org/10.1063/1.3553279
31. Ali, H., Cheema, T.A., Yoon, H.S., Do, Y., Park, C.W.: Numerical prediction of algae cell mixing feature in raceway ponds using particle tracing methods. Biotechnol. Bioeng. **112**(2), 297–307 (2015). https://doi.org/10.1002/bit.25443
32. Auel, C., Albayrak, I., Boes, R.M.: Turbulence characteristics in supercritical open channel flows: Effects of Froude number and aspect ratio. J. Hydraul. Eng. **140**(4), 04014004 (2014)
33. Savat, J.: The hydraulics of sheet flow on a smooth surface and the effect of simulated rainfall. Earth Surf. Processes. **2**, 2–3 (1977)
34. Chow, V.T.: Open-channel Hydraulics. in In: Open-channel Hydraulics. McGraw-Hill (1959)
35. Wilcox, D.C.: Reassessment of the scale-determining equation for advanced turbulence models. AIAA J. **26**(11), 1299–1310 (1988)
36. Wilcox, D.C.: Simulation of transition with a two-equation turbulence model. AIAA J. **32**(2), 247–255 (1994)
37. Elghobashi, S.: On Predicting Particle-Laden Turbulent Flows*, (1994)
38. Wilcox, D.C.: Turbulence Modeling for CFD, vol. 2. DCW industries La Canada, CA (1998)
39. Zienkiewicz, O.C., Taylor, R.L.: The Finite Element Method for Solid and Structural Mechanics. Elsevier (2005)
40. Ciarlet, P.G.: *Mathematical Elasticity I*. (1988)
41. Zhang, Q., Song, C.: *Multiphysics Modeling - Numerical Methods and Engineering Applications*. (2016)
42. Burnett, N.P., Koehl, M.A.R.: Ecological biomechanics of damage to macroalgae. Front. Plant Sci. **13** (2022). Frontiers Media S.A.https://doi.org/10.3389/fpls.2022.981904
43. Schutten, J.: Biomechanical Limitations on Macrophytes in Shallow Lakes. Instituut voor Biodiversiteit en Ecosysteemdynamica (IBED) (2005)
44. Koehl, M.A.R.: Ecological biomechanics of marine macrophytes, *Journal of Experimental Botany*, vol. 73, no. 4. Oxford University Press, pp. 1104–1121, Feb. 24, (2022). https://doi.org/10.1093/jxb/erab536

Waste and Biomass Valorization (2024) 15:5805–5817
https://doi.org/10.1007/s12649-024-02550-z

ORIGINAL PAPER

Valorisation of Agricultural Residue Bio-Mass Date Palm Fibre in Dry-Blended Polycaprolactone (PCL) Bio-Composites for Sustainable Packaging Applications

Abu Saifullah[1] · Nirmal George Chacko[1] · Hom Nath Dhakal[1] · Sakib Hossain Khan[1] · Forkan Sarker[2] · Zhongyi Zhang[1]

Received: 31 January 2024 / Accepted: 17 April 2024 / Published online: 13 May 2024

Abstract

Purpose This study experimentally developed and characterised dry-blended Polycaprolactone (PCL)/date palm fibre biodegradable composites for sustainable packaging applications. Date palm fibres are collected from date palm trees as by-products or waste materials. They will be valorised in bio-composite application to promote fibre-based sustainable packaging items over their non-biodegradable synthetic polymer based conventional packaging products. In the dry-blending process, fibre and polymer are mixed with a shear mixer, while, in a melt-blending process, an extruder is used to extrude fibre/polymer blends after applying heating and high shear pressure to melt and mix polymer with fibres. Dry-blending process offers many comparative advantages, such as less equipment, steps, cost, process degradation, energy consumption and hence, lower harmful environmental emissions; while, a proper fibre/polymer mixing is a challenge and it needs to be achieved properly in this process. Therefore, it is important to understand the effects of dry-blending process on manufacturing of PCL/date palm fibre bio-composites for packaging applications, before promoting the dry-blending as a suitable alternative to the melt-blending process.

Methods Short chopped fibres were grinded as powders and dry-blended at a ratio of $(0-10\%)$ (w/w) with PCL polymer using hand and a shear mixer for 30 min, following a compression moulding process to produce bio-composite samples. Tensile, water contact angle, SEM, TGA, DSC and DMA tests and analysis were conducted. The dry-blended PCL/date palm fibre composites' properties were compared with reported melt-blended samples' results found in literature.

Results Dry-blended samples showed an increase in tensile modulus values (up-to 20%) with fibre inclusion and these values were found close to the melt-blended samples in the literature. Tensile strength and strain values were reduced which could be related to the poor fibre/polymer interface. Fibre addition affected the thermal, thermo-mechanical and crystallisation processes in PCL polymer matrix.

Conclusion Dry-blending is capable of producing bio-composites with a very comparable properties to melt-blended counterparts, although a more details study is needed to conduct in future. The results of this study, could be used carefully to design dry-blended PCL/date palm fibre bio-composites for possible packaging applications. The irregular fibre distribution in dry-blended samples could be improved in different ways which should be investigated in future.

✉ Abu Saifullah
abu.saifullah@port.ac.uk

[1] Advanced Polymers and Composites (APC) Research Group, School of Mechanical and Design Engineering, University of Portsmouth, Anglesea Road, Anglesea Building, Portsmouth PO1 3DJ, UK

[2] Department of Textile Engineering, Dhaka University of Engineering & Technology (DUET), Gazipur, Bangladesh

Graphical Abstract

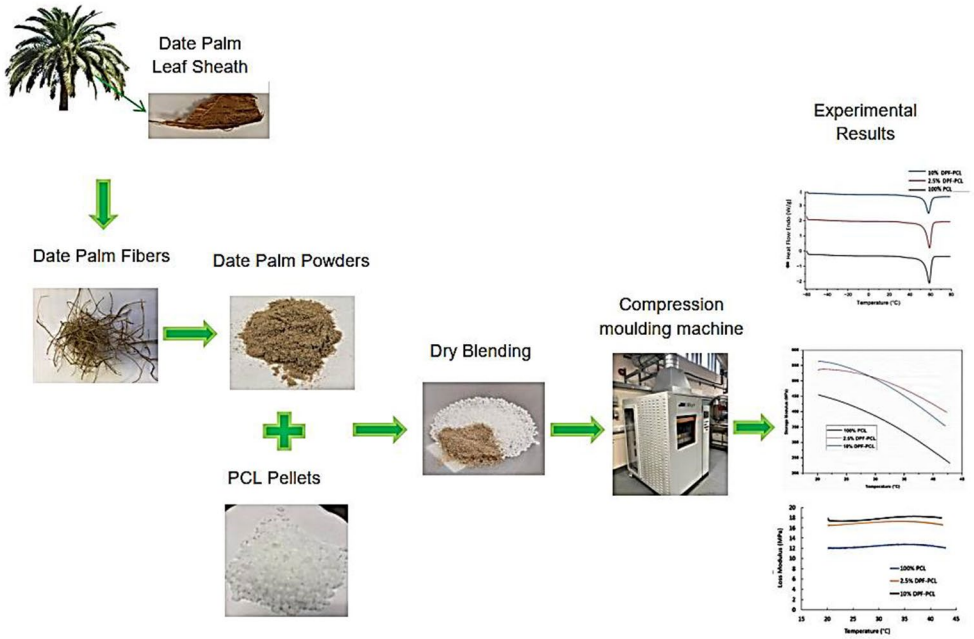

Keywords Date palm fibre · Valorisation · Dry-blending · Melt-blending · Sustainable packaging · Polycaprolactone (PCL)

Introduction

Synthetic fibres are typically derived from petroleum-based sources, which contribute to negative environmental impact and deplete non-renewable resources. In contrast, natural fibres a competitive alternative, especially those derived from plants (flax, hemp, jute, date palm fibre), are renewable and biodegradable [1]. The processing of natural fibres has less impact on the environment compared to synthetic fibres [2]. Natural fibres may require a higher percentage in fibre reinforced composite applications compared to glass fibres, but this leads to a reduction in resin percentage, resulting in pollution reductions caused by non-biodegradable polymers [3]. The low density of natural fibres leads to better specific efficiency, resulting in fewer emissions during service life such as automotive applications [4]. Lower energy consumption in processing of natural fibre contributes to overall environmental sustainability and the natural fibres show superior environmental performance in various aspects when compared to synthetic fibres, such as glass fibres [3]. Natural fibres have additional advantages, including low cost, good thermal and acoustical insulation characteristics, energy recovery, reduced tool wear in machining operations, degradability, and reduced dermal and respiratory irritation. Despite these benefits, challenges hinder the widespread adoption of natural fibres in polymer matrix composites. High moisture absorption and poor adhesion present obstacles, limiting applications and requiring strategies such as coupling agents, fibre property enhancement through various chemical treatments, and careful production method selection [5]. Additionally, the irregularity in natural fibre shape poses difficulties in predicting mechanical properties.

Composite materials have evolved by incorporating synthetic fillers like carbon and glass fibres and into thermosets or thermoplastic polymer matrices such as epoxy, polyester, vinyl ester, polyethylene, polypropylene, polyethylene terephthalate and polyamide. Nevertheless, the increasing need for environmentally-friendly products has led to a transition towards the creation of composites produced from biological sources and are also capable of decomposing naturally [6]. Lignocellulosic fibres derived from plants have become increasingly popular as organic fillers in developing composites. These fillers are commonly combined with biodegradable polymer matrices like polylactic acid (PLA), thermoplastic starch (TPS) and polycaprolactone (PCL), which can be produced from biomass or synthesized from petroleum [7]. These materials have the qualities of being biodegradable and/or recyclable, and in numerous instances, they are completely produced from biological sources. Furthermore, these materials exhibit non-toxic characteristics, high tensile and flexural modulus, the ability to be processed

at lower temperatures, and adjustable properties for specific uses.

The increasing awareness of the need to conserve non-renewable natural resources has led to the advancement of environmentally friendly applications of advanced polymeric materials, specifically bio-based composites derived from agricultural and industrial waste products. This movement corresponds to the wider transition towards sustainable practices, propelled by environmental concerns and efforts to mitigate climate change. Agro-industrial wastes, which are produced during agricultural processes, and by-products, which are generated from industrial activities, are acknowledged as inexpensive raw resources that have considerable promise to be valorised for the development of advanced sustainable materials. Various literature recognizes the economic and environmental benefits of using renewable sources, highlighting their ability to break down naturally and reduce waste [8]. Bio-based composites offer a viable alternative to conventional polymeric materials due to their renewable source and frequently biodegradable properties. This strategy not only helps conserve resources but also tackles concerns regarding trash disposal and environmental effect. While biopolymers possess renewability and biodegradability, they frequently demonstrate diminished mechanical strength, permeability, and thermal stability, restricting their applicability in certain contexts [9]. A prevalent approach to augment their overall performance and enhance commercial feasibility entails introducing reinforcing agents [10]. These additives, alternatively termed fillers or reinforcements, are integrated into biopolymers to enhance particular properties like strength, resilience, and thermal resistance. The potential of agricultural bio-waste as effective reinforcements in composite manufacture reported in various literatures [11]. Furthermore, bio-waste can be valorised and utilized in many formats to produce composite materials and their wide-ranging uses. The adaptability of bio-waste can be used at many stages and processes, leading to enhanced characteristics of composite materials.

Date palm fibres are sourced from date palm trees, mainly cultivated in hot and humid regions, such as Arab and North African countries. Although date palm trees are cultivated mainly for fruits, date palm fibres are collected as by-products or agricultural waste materials from yearly fruit harvesting activities, or maintenance and pruning actions of these tress to encourage their good growth. The production of date palm fruit on a global scale has consistently shown a steady increase, highlighting the growing significance of date palm trees. It is estimated that currently near about 100 million date palm trees are present worldwide [18]. A single date palm tree produces at-least 26 Kg/year of agricultural waste materials from different parts of its structure [12, 13] and from this, it can be easily understood the amount and availability of date palm fibre agricultural waste bio-mass across the world. It has been reported that only in MENA (Middle east and North Africa) regions, this agricultural waste materials production can be varied from 2.6 to 2.8 million tonnes annually [12].

Presently, a significant portion of date palm fibres is directed towards low-value products. Thus, finding sensible and innovative methods to utilize agricultural residues like date palm fibres is gaining attention from both researchers and industry. The goal is to move away from traditional low-value applications and explore new ways of incorporating these fibres into polymer composite reinforcements or other advanced applications, which could lead to enhanced resource utilization and value creation. This approach not only aligns with sustainability goals but also has the potential to offer economic benefits. Various research has been carried out using recyclable or virgin thermoplastics like High Density Polyethylene (HDPE) and polypropylene (PP) with virgin or recycled natural fibres [14] with keeping the sustainability goal in mind. Date palm wood flour mixed with recycled polypropylene exhibited increased tensile strength [15] and similar results are reported by reinforcing recycled high density polyethylene with date palm fillers [16].

Date palm fibres can be turned into as foam materials and utilised them for heat and sound insulation properties. Chemical blowing agents [17] can be mixed with fibres in a polymer matrix, which can be melted and create foaming bubbles in mixed fibre-polymer phases during the manufacturing process of fibre/polymer-based foam. For date palm fibre in polymer composites, Mousa et al. reported the date palm agricultural biomass mixed with PLA using melt blending technique showed higher elongation at break with the addition of plasticizer and shows potential in semi-structural packaging applications [18]. Films of PLA reinforced with date palm leaves fillers manufactured using extrusion blowing techniques are also reported to show enhanced tensile properties [19]. The incorporation of date palm midrib powder as a reinforcing filler in the biodegradable polyvinyl alcohol (PVA) matrix led to a significant improvement in tensile strength [20]. Dhakal and co-authors [21] studied the mechanical properties of date palm fibre leaf sheath powders with biodegradable polycaprolactone (PCL) as matrix and reported that the tensile strength is highest at 20%wt and is comparable with other agricultural waste biomass like wheat bran [22]. Dhakal et al. further reported that using PCL as a matrix in date palm composites in comparison with other polymers like TPU, PLA and phenolic resin showed higher tensile strength and the plausible explanation of this is higher affinity of PCL at the interface of the lignocellulose fibres.

Conventional packaging derived from petroleum is widely utilized in various applications owing to its notable features such as impressive specific strength, durability, ease of processing, and cost-effectiveness. However, despite these merits, this type of packaging comes with a substantial environmental downside as it requires several centuries to undergo complete decomposition [23]. The protracted decomposition period gives rise to significant environmental concerns, creating difficulties in waste management and sustainability efforts. Natural fibre based sustainable packaging are gaining upmost importance in the recent time in order to limit the production of conventional petroleum-based packaging materials. Utilizing composite materials composed of natural fibres is highly advantageous in packaging applications, particularly as an alternative to synthetic materials derived from petroleum. A noteworthy example is - a company specializing in packaging material crafted from coconut fibre, and there are several attempts being made to produce food packaging utilizing cereal waste, such as straw [24, 25]. The utilization of date palm fibres and agricultural waste biomass in powdered form presents a substantial merit as a filler material in food packaging. From an environmental perspective, these materials pose no complications in terms of recycling or disposal after use.

Polycaprolactone (PCL) is a potential fossil-based biodegradable material for sustainable packaging applications and its various properties such as hydrophobicity, moisture or oxygen barrier performances, mechanical properties etc. are engineered and tailored through blending with other bio-polymers, such as PLA [26]. PCL is reported to exhibit lower tensile strength but when blended with another biodegradable polymer PLA, showed higher stiffness. In this regard, valorisation of agricultural biomass (date palm fibres) as reinforcing agents in different bio-degradable polymers like PCL, has the potential to enhance the overall mechanical behaviour of fibre/polymer bio-composites for semi-structural or non-load bearing packaging applications [27]. There are two ways date palm fibres can be used in a polymer matrix – (1) for fibre reinforced composites, date palm fibres (long, short, chopped etc.) can be placed as layer by layer with polymer matrix, followed by a compression moulding or other fibre reinforced composite manufacturing technique and (2) fibres at a particular size can be blended with polymers and use this fibre/polymer blend in different plastic moulding processes, such as injection, compression etc. to produce ultimate products. The fibre/polymer blending process can be done in two different ways- (1) melt blending through an extrusion process and (2) dry-blending process.

In an extrusion melt blending process, heating and higher shear force are used to melt polymer, so that the melted polymer can be mixed with fibres properly. This is an established industrial process to mix fibres in the polymer effectively and properly. In contrast, an extrusion process requires expensive equipment, initial investment in any industry, highly skilled manpower to operate the equipment, large space to accommodate equipment and the whole manufacturing process and the most importantly, the extrusion process itself requires an extensive amount of energy consumption for material processing. In addition, it has been reported that in the melt blending process, date palm fibre/PP bio-composites face thermal degradation [17] which could be harmful for ultimate composites performances in a real-life environment. Unlike the melt extrusion process, in a dry-blending process, fibres are mixed with polymer by manually and/or with a high-speed shear mixer without applying any heating for the polymer melting. Although, a dry-blending is an easy process, requires no special equipment/initial business investment/significant fibre and polymer degradations, less process energy consumption and cost, this process has a lacking of proper fibre distribution in the polymer matrix. Considering the advantageous characteristics of a dry-blending process, it is possible to use the dry-blending as an alternative to the melt blending process and this needs an in-depth study on the performance analysis of any dry blended fibre/polymer bio-composites. The process optimisation and the removal of the extrusion process for the blending of fibre and polymers, will allow the cleaner production concept in this field, which will ultimately reduce process waste, energy and resource consumption for the manufacturing of bio-composites, promote workers safety work environment and a quicker process leading to a lower production cost.

In this work, we added date palm fibre in PCL polymer matrix through a dry-blending process and the dry-blended fibre-polymers were used in a compression moulding technique to manufacture PCL/date palm fibre bio-composites for sustainable packaging applications. PCL is a cheap, hydrophobic, fossil-based biodegradable polymer, abundantly available in the current market and low melting polymer which have made the bio-composite manufacturing process easier in terms of energy and resource consumption. Date palm fibres were grinded into powder so that they could be mixed in a better way with PCL polymer pellet during the dry-blending process. The objectives of this study were to develop dry-blended PCL/date palm fibre bio-degradable composites at different fibre/polymer weight ratios and characterise their mechanical, water contact angle, thermal and thermo-mechanical properties. Also, these properties of dry-blended bio-composites were compared with melt blended PCL/date palm fibre samples, reported in literature so far, in order to understand the effects of dry-blending on PCL/date palm fibre composites' properties so that they can be applied in sustainable packaging applications.

Table 1 Date palm fibre details

Fibres	Density (g/cm^3)	Breaking tensile strength (MPa)	Tensile modulus (GPa)	Elongation (%)
Date palm fibres	0.9–1.2 [1, 28, 29]	170–275 [1]	5–12 [1]	5–10 [1]

Materials and Methods

Materials

PCL polymer was purchased from Easy Composites, UK as the Mouldphorm grade with a molecular weight (M_w) of 55,000 g/mol, MFI of 9 g/10 min (80° C, 2.16 Kg) and density of 1.145 ($^{g}/_{cm^3}$). Leaf sheath date palm fibres were collected from Saudi Arabia (Al-Ahsa, Eastern Province) as long fibres in bundles. Date palm fibre physical and mechanical properties are given in Table 1 [1, 28, 29].

Date Palm Fibre Grinding Process

Long fibres were cleaned in hot water, dried in an open environment for 72 h, then chopped into 1 cm long fibres, followed by a further drying operation in an oven for two hours at 80 °C. The dried chopped fibres were grinded into powders using a powerful laboratory scale bench-top RETSCH Ultra Centrifugal Mill ZM 300 in a cryogenic grinding mode to avoid any fibre degradation during the grinding operation (Fig. 1). The grinding speed was up-to 18,000 rpm and a stainless-steel ring sieve of 350 µm was used to produce the fibre powder with a range of particle size of 350–500 µm. In this mill the grinding operation is happened by impact and shearing effects between the rotor and the fixed ring sieve (Fig. 1).

Table 2 PCL/date palm fibre bio-composite samples details

Samples	PCL (w/w %)	Date palm fibre powder (w/w %)
100% PCL	100	---
2.5% DPF-PCL	97.5	2.5
5% DPF-PCL	95	5
7.5% DPF-PCL	92.5	7.5
10% DPF-PCL	90	10

Dry-Blending and Compression Moulding for PCL/Date Palm Fibre Bio-Composite Manufacturing

Date palm fibre powders were blended with PCL polymer pellets at different ratios (Table 2) by the dry-blending process using hand mixing followed by a shear mixing process. The dry blended PCL/date palm fibre mixtures were compression moulded into 160 mm (l) × 160 mm (w) × 2 mm (t) moulded plaques using an electrically heated hydraulic press. The compression moulding process involved the heating of empty mould (both upper and lower parts of the mould) at 120° C for 20 min, the subsequent placing of polymer and fibre mixtures evenly on the lower part of the mould very quickly and closing the mould, followed by a heating stage of the mould with fibre/polymer mixture for 10 min at 120° C without any pressure. After that, a 5 MPa pressure was used on the mould for 8 min at the same temperature. with the following pressure release and normal air-cooling stages for the temperature down to 20° C before the de-moulding of moulded bio-composites was taken place.

Tensile Testing

Tensile test was conducted on PCL/date palm fibre bio-composite samples according to ISO 527 -2 test standard using a Universal testing equipment (Zwick/Roell Z010) with a load cell of 10 kN. ISO 527-2 5 A type test specimens were cut from moulded bio-composite panels with a cutting puncher and they were tested at a displacement rate of 50 mm/min

Fig. 1 Date palm fibres and PCL polymer pellets – (**a**) original long fibres, (**b**) fibres grinded as powder, (**c**) fibre powder and polymer pellet are placed side by side, just before the dry-blending process

until they became broken in tensile tests. Five specimens of each type of bio-composite samples were tested.

SEM Characterisation

Scanning Electron Microscopy (SEM) images of PCL/date palm fibre bio-composites' broken surfaces with a 5 mm × 5 mm dimension were taken using a Zeiss Evo ma10 equipment at different magnification scales. A thin layer gold coating was applied for 40 s with a Quorum Q150R Plus sputter coater on specimens before taking SEM images. The images were investigated to understand the distribution of fibres within PCL polymer matrix.

Water Contact Angle Measurements

A KSV CAM-101 machine equipped with a CAM 2008 software was used to measure the water contact angle of bio-composites' surfaces for revealing information about their surface wettability. Water droplets were placed at different positions of the same sample and 10 measurements were taken for calculating an average water contact angle value of each sample.

Differential Scanning Calorimetry (DSC)

DSC analysis of manufacture PCL/date palm fibre bio-composites were carried out in a TA Q 100 DSC equipment, using a heat-cool-heat method, wherein, the first heating cycle was started from − 60 °C to 80 °C, followed by a cooling cycle from 80 °C to -60 °C with a subsequent second heating cycle up-to 80 °C. For both heating and cooling cycles, the same heating or cooling rate of 10° C/min was used. The degree of crystallinity of samples was measured with the following equation, wherein, ΔH_f and ΔH_{f° are the heat of fusion per gm of bio-composite samples and 100% PCL crystalline samples respectively. ΔH_{f° was considered as 135.31 J/g for the degree of crystallinity calculation.

Degree of crystallinity,

$$Xc\,(\%) = \frac{\Delta H_f}{\Delta H_{f^0}} \times 100\%$$

Thermogravimetric Analysis (TGA)

A TA Q 50 TGA equipment was used to investigate the Thermal stability and degradation behaviours of bio-composites in an air atmosphere in the temperature range from 30 °C to 700 °C at a heating rate of 20 °C/min.

Thermo-mechanical Analysis (DMA)

The thermo-mechanical properties of bio-composites were determined from 20° C to 45° C at a heating rate of 2° C/min, a 1 Hz oscillation frequency and a 20 µm strain amplitude, in a nitrogen gas atmosphere using a double cantilever mode DMA TA Q 800 equipment. From DMA experiments, both storage modulus (E_o) and loss factor (tanδ) were measured.

Results and Discussion

Tensile Properties Analysis of Dry-Blended PCL/Date Palm Fibre Bio-Composites

Figure 2a provides typical tensile stress-strain curve up-to breaking points of dry-blended PCL/date palm fibre bio-composites, while, Fig. 2b shows the tensile curves up-to 20% strain of all tested bio-composites, so that the initial tensile test response of PCL/date palm fibre composites can be seen clearly. Average tensile properties data are presented in Table 3. From them, it can be seen that 100% PCL plastic samples have high strain value which was found to decrease significantly with the addition of date palm fibres in its matrix. Only a 2.5% (w/w) date palm fibre addition into the PCL matrix made a huge decline in the strain (%) values compared to the 100% PCL samples. A further continuous decrease was also noticed with the increase of date palm fibre percentage in the main polymer matrix; between them,

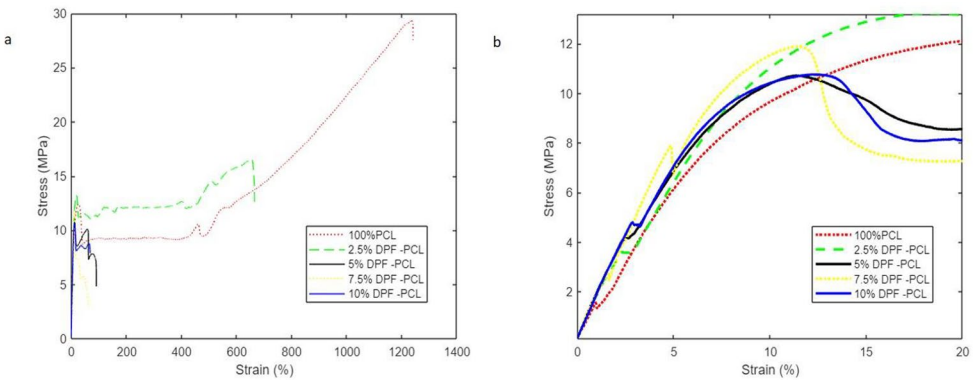

Fig. 2 (**a**) Tensile stress-strain curves of dry blended PCL/date palm fibre bio-composites (**b**) Tensile stress-strain curves up-to 20% strain for all bio-composites

Table 3 Tensile properties of dry blended PCL/date palm fibre bio-composites

Sample types	Tensile maximum strength (MPa)	Tensile strain at break (%)	Tensile modulus (MPa)
100% PCL	14.431 (±2.897)	1400 (±244.644)	148.975 (±0.487)
2.5% DPF-PCL	12.318 (±1.593)	346.674 (±336.644)	176.372 (±12.668)
5% DPF-PCL	9.164 (±1.819)	74.135 (±43.663)	183.25 (±20.179)
7.5% DPF-PCL	9.757 (±2.316)	46.836 (±15.026)	196.086 (±20.466)
10% DPF-PCL	9.649 (±0.917)	48.836 (±14.409)	198.005 (±19.630)

the higher fibre percentage – 7.5% and 10% fibres (w/w) showed very similar strain values of dry-blended PCL/date palm fibre bio-composites. Based on this observation, it can be said that perhaps a further increase of fibre contents into the polymer matrix might not reduce the strain values very sharply, which needs to be confirmed with experimental work in a future research.

The observed strain value decrease is not unexpected, since the fibre addition in the polymer matrix creates inhomogeneous structure and a poor adhesion at fibre-polymer interfaces which brings brittleness or reduction in the strain values. In opposite, tensile modulus was seen to increase with the increase of fibre addition percentages. In this work, the 100% PCL sample modulus was found within the expected range. The 2.5% DPF-PCL bio-composites showed a tensile modulus of 176 MPa which was almost a 20% increase compared to only PCL samples. The highest modulus (198 MPa) was found for the 10% DPF-PCL bio-composites and this was very close to the modulus value of the 7.5% DPF-PCL bio-composites. For maximum strength data, a decline of strength values up-to 33% was determined for the 10% DPF-PCL samples compared to their 100% PCL bio-composite counterparts. From these tensile data, it is obvious that the fibre increases the resistance to tensile force in the PCL matrix at the start of tensile loading, resulting in an increase in the dry-blended composites' modulus values, which was not continued for long to support an increase in the maximum strength values, because of the significant drop in the ductility properties of the PCL matrix as found in strain data of tested bio-composites.

SEM Images of Dry-Blended PCL/Date Palm Fibre Bio-Composites' Fractured Surfaces

SEM image analysis was employed to understand the fracture surface morphology under tensile loading and fibre distribution in the dry blended PCL/date palm fibre bio-composites. All composite types were investigated, although images from only 2.5% DPF-PCL and 7.5% DPF-PCL bio-composites are included in Fig. 3, since all bio-composite types showed a similar result. Fracture surface features support the findings of tensile tests of bio-composites in this work. From SEM, it is obvious that 2.5% DPF-PCL bio-composite has less fibre contents compared to 7.5% DPF-PCL samples, as expected. Fibre content has a direct impact on tensile properties [30], as observed in this work. Fibre powders were not found distributed throughout the PCL matrix, instead, a fibre rich and fibre less areas were identified due to the agglomeration of fibre powders and this effect was more obvious with 7.5% DPF-PCL specimens. The irregular distribution of fibre powders created a less adhesion at fibre powder-polymer interfaces [1, 31, 32]. Also, their hydrophilic (fibres) – hydrophobic (PCL polymer) polarities were responsible for their less adhesion.

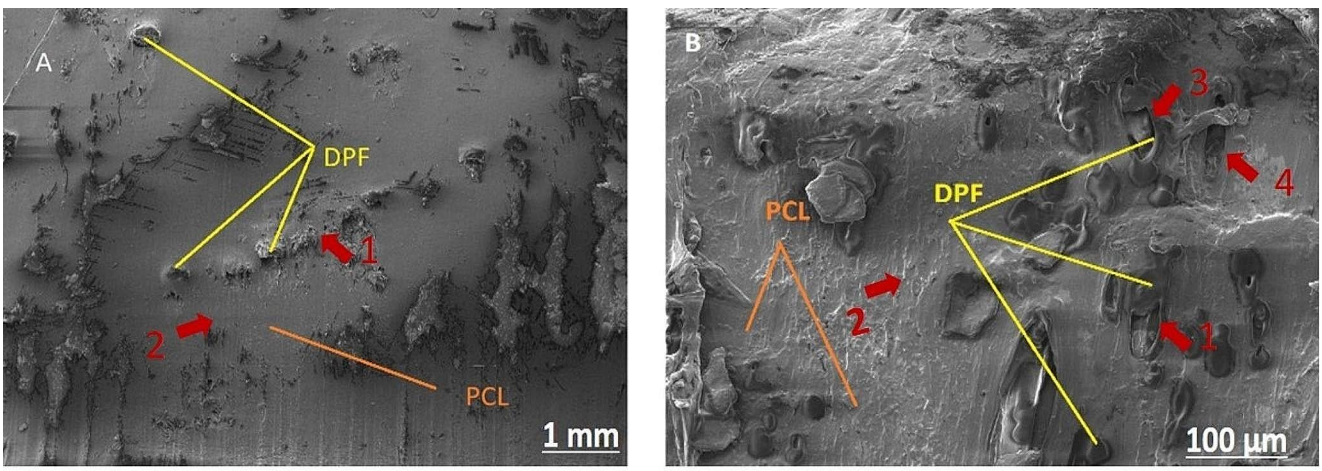

Fig. 3 SEM images of (**A**) 2.5% DPF-PCL and (**B**) 7.5% DPF-PCL bio-composites' fracture surfaces. DPF and PCL matrix are shown where they are abundantly seen in images. (1–4) number markings provide different information, 1 = DPF fibre rich area; 2 = PCL matrix rich area; 3 = debonding of fibre/matrix interface; 4 = fibre pull out

Brittle failure feature was seen in both Fig. 3 (a, b), since the fibres were found broken clearly and the PCL matrix surface showed very close to smooth failure surface. In Fig. 3b, the debonding between the fibre-polymer interface was noticed and also, fibre pull out was occurred under tensile loading scenario. Based on these fracture surface features, it is clear that fibres provided some support to the PCL matrix to increase the mechanical properties, such as tensile modulus with an increasing fibre content, but due to a poor fibre-matrix adhesion interface the brittleness was increased of produced bio-composites. This observation supports the determined tensile properties in the earlier section.

Water Contact Angle of PCL/Date Palm Fibre Bio-Composites

Water contact angle measurements provide information on hydrophilic or hydrophobic nature of polymer material surfaces linking to the relative wettability of materials [33, 34]. In our work, this was measured through placing water droplets on bio-composite surfaces and capturing the angle between water droplets and bio-composite surfaces.

From Fig. 4, it can be seen that only PCL moulded samples have 77° water contact angle which is found very similar, but slightly lower, to the values reported in literature [35] This could be due to the manufacturing of PCL based substrate through different manufacturing processes, such as compression moulding vs. solvent casting. Differences in manufacturing processes may increase surface roughness and this might have decreased the water contact angle values of compression moulded 100% PCL samples in this work. The date palm fibre incorporation reduced contact angles proportionally with their relative contents in PCL matrix bi-composites. Date palm fibres are hydrophilic and it is expected that their addition in PCL matrix had increased the composite surface roughness and these reasons were responsible to reduce the water contact angle of date palm fibre/PCL bio-composites. For 2.5% and 5% date palm fibre-based composites, similar contact angles were measured to only date palm fibre contact angle, reported at 66°±3° [36] in other works in the literature. The lowest water contact angle was noticed for the 10% DPF-PCL composites wherein the highest fibre content was used.

Analysis of DSC Results

Figure 5 (a - b) shows heating and cooling cycles of DSC analysis for providing information on melting and non-isothermal crystallisation behaviours of PCL/date palm fibre bio-composites respectively. The melting temperature of only PCL and 2.5% DPF-PCL composites were found very close to each other, while, 10% DPF-PCL samples showed a slightly lower melting temperature. This could be related to the significant reduction in the crystallinity percentage of 10% DPF-PCL sample. The crystallinity was also found to reduce for the 2.5% DPF-PCL bio-composites compared

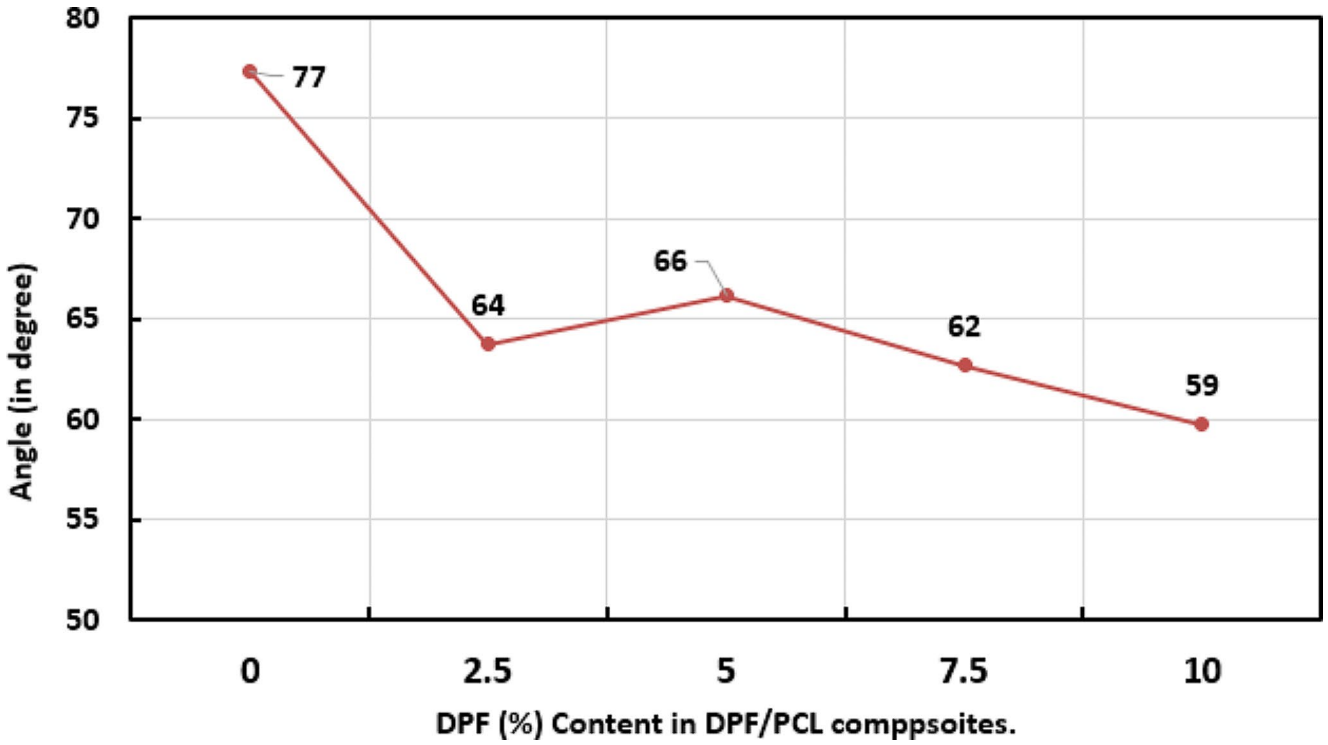

Fig. 4 Water contact angles of PCL/date palm fibre (DPF) bio-composites

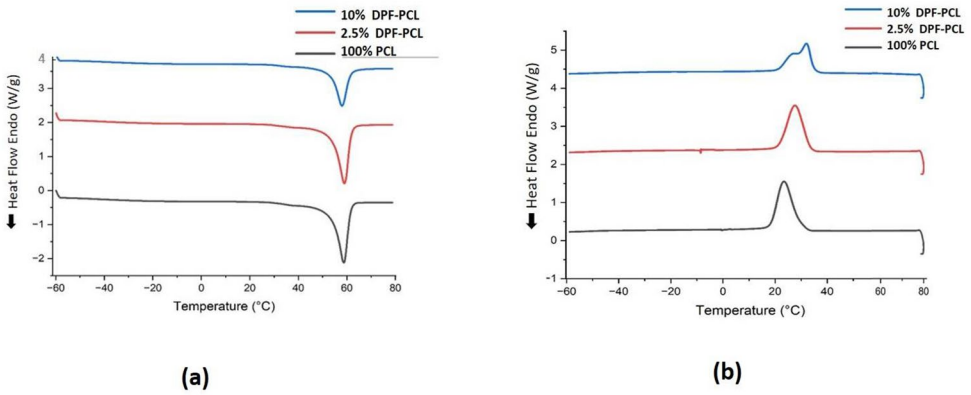

Fig. 5 DSC analysis of bio-composites –heating cycle (**a**) and cooling cycle (crystallisation) (**b**)

Table 4 DSC analysis data for melting and crystallisation behaviour of PCL/date palm fibre bio-composites

Samples	Melting		Crystallisation			
	Melting temperature (T_m, °C)	Crystallinity (%)	On-set temperature (T_0, °C)	Peak temperature (T_c, °C)	Crystallisation time (s)	
					Half time ($t_{1/2}$)	Full time
100% PCL	58.86	55.40	33.82	23.46	62.16	104.34
2.5% DPF-PCL	59.01	53.75	36.46	27.69	52.62	108.30
10% DPF-PCL	57.96	33.08	38.60	31.95	39.90	118.08

to 100% PCL samples, but not as significant as 10% DPF-PCL samples. Non-isothermal crystallisation analysis was carried out at only 10° C/min cooling rate to understand the crystallisation behaviour of developed bio-composites in this work. It is very obvious that the crystallisation on-set shifted towards higher temperatures with increasing fibre contents in PCL-DPF composites compared to only PCL samples. The crystallisation rate was also faster due to the incorporation of fibres into PCL matrix, which can be found from crystallisation half-time data (Table 4).

In this work, the crystallisation half-time was measured based on the time taken from the on-set of crystallisations to the peak of crystallisation of samples. The faster crystallisation half-time, higher crystallisation on-set and peak temperatures were also found for other natural fibres, such as flax [37] or sisal fibre [38] based polymer bio-composites in previous works reported in the literature. Date palm fibre surfaces acts as nucleating sites in PCL matrix that accelerates the crystalline growth, although date palm fibre incorporation didn't increase the overall crystallinity compared to 100% PCL samples. Because, the fibre surface also complicates the crystallization process at the same time with the promotion of a slow additional secondary crystallisation process [39], which was quite obvious for 10% DPF-PCL bio-composites from their second shoulder in the crystallisation peak temperature. Moreover, the overall crystallisation time was found higher for date palm fibre composites because of this secondary crystallisation, which basically was occurred to improve the crystalline order of bio-composites.

TGA Results Analysis

TGA curves show that the degradation in DPF-PCL bio-composites starts earlier unlike only PCL samples. This was occurred due to the fibre incorporation in PCL matrix. The similar finding was also reported for flax fibre-based bio-composites [37] Date palm fibre generally shows thermal degradation in three stages [40, 41] - the first stage is between room temperature to 110 °C relating to the moisture loss within the fibre structure; the second stage happens at 280 °C linking to the low molecular weight hemicellulose degradation and finally, the third stage is for the cellulose degradation at 360 °C. In our work, 2.5% and 10% DPF-PCL bio-composites showed similar degradation behaviours at 280° C and 360 °C for hemicellulose and cellulose degradation respectively, while, the moisture evaporation at around 100 °C was not found very obvious. Degradations at 280° C and 360 °C are also very vivid in DTG curves, wherein, at 280° C almost 10% weight loss or degradation was identified and at 360° the main degradation was occurred. 100% PCL samples showed only one degradation step at near about 360° C- 400° C (Fig. 6).

Dynamic Mechanical Thermal (DMA) Analysis

DMA graphs provide good information on stiffness and fibre-matrix interfacial adhesion of bio-composites [42, 43]. In Fig. 7 (a), date palm fibre addition in the PCL matrix increased the storage modulus according to their relative contents in both 2.5% and 10% DPF-PCL samples. This result also supports the tensile modulus increase of PCL/

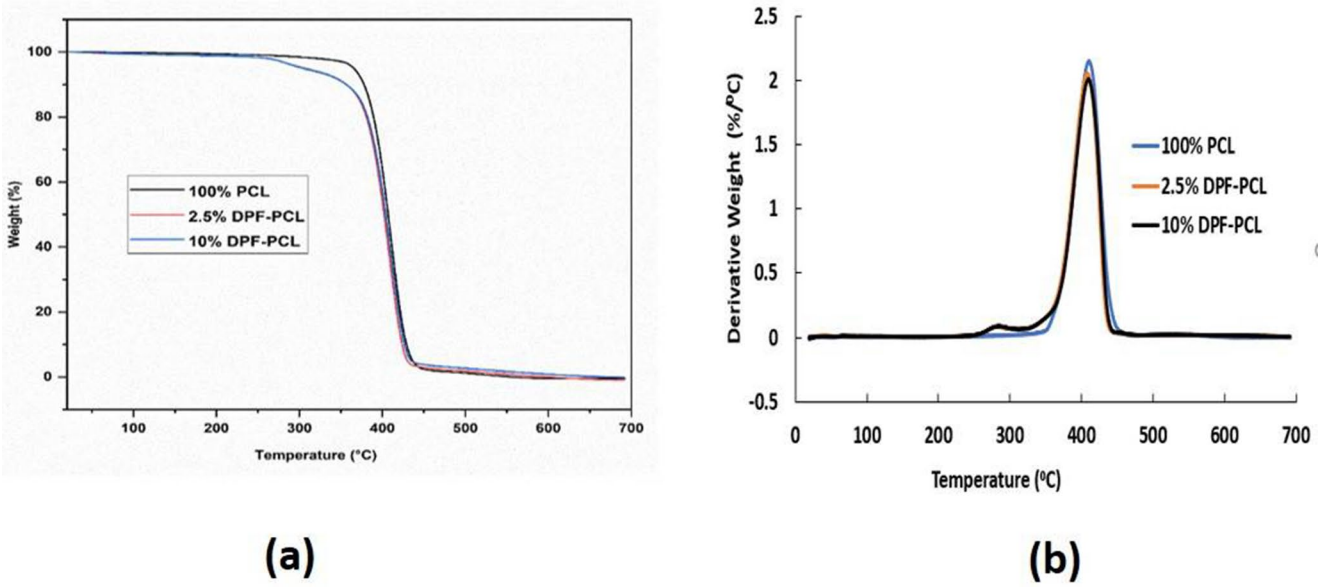

Fig. 6 Thermogravimetric analysis of – (**a**) TGA and (**b**) DTG curves of DPF-PCL bio-composites

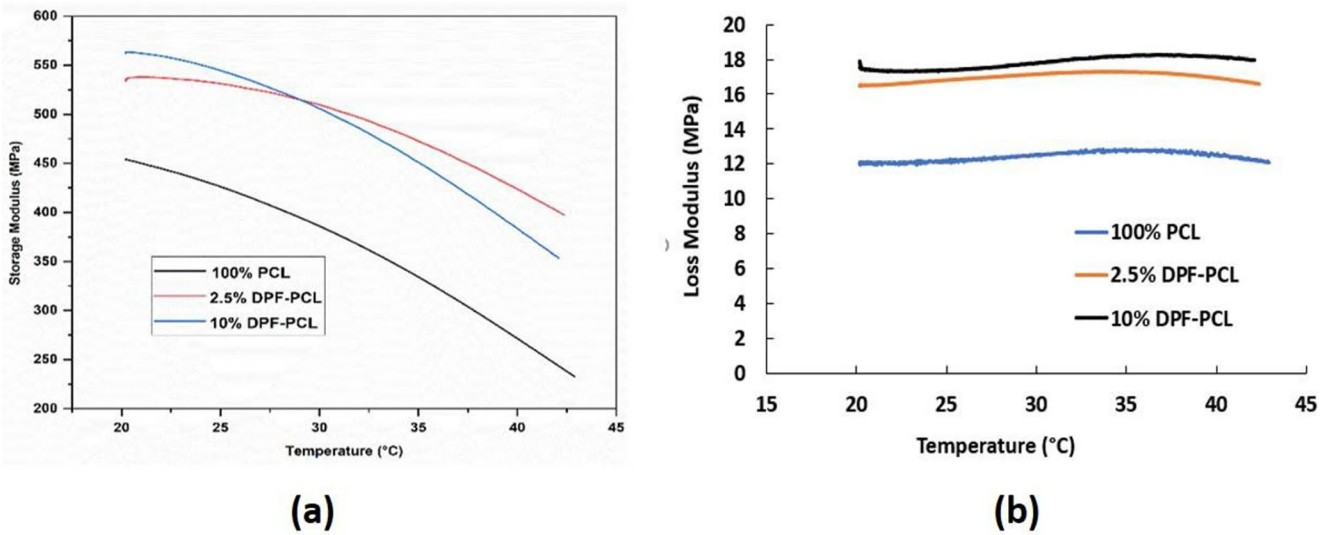

Fig. 7 DMA graphs of DPF-PCL bio-composites – (**a**) storage modulus and (**b**) loss modulus

date palm fibre bio-composite, described earlier. Although 10% DPF-PCL samples showed a higher storage modulus up-to 30 °C, they showed an opposite trend in the storage modulus value after 30° C compared to 2.5% DPF-PCL composites. In DSC results analysis, it was seen that the 10% date fibre contents promoted the secondary crystallisation in PCL matrix very obviously, which ultimately reduced the degree of crystallinity significantly compared to other date palm fibre-PCL bio-composites.

A higher fibre content in 10% DPF-PCL composites resisted more mechanical force initially and increased their elastic responses and hence, showed a higher storage modulus. But, with the increase of heating temperature, the molecular mobility of less crystalline PCL polymer in 10% DPF-PCL bio-composites also started to increase more, leading to a reduction in the storage modulus after 30 °C. Based on storage modulus curves, it was expected that only PCL samples would exhibit higher loss modulus values compared to fibre incorporated composites which was found totally opposite in DMA tests. 10% DPF-PCL composites had higher loss modulus compared to 2.5% DPF-PCL or 100% PCL samples. The observed higher loss modulus in bio-composites could be due to the fibre incorporation in polymer matrix which has better capability to dissipate energy in irregular fibre distribution and weak fibre-polymer interface in bio-composites.

Effects of Dry-Blending on Manufacturing of PCL/Date Palm Fibre Bio-Composites and a Literature-Based Comparison with Melt Blended PCL/Date Palm Fibre Bio-Composites

As discussed earlier, the dry-blending process removes an extra melt extrusion process from the compression moulding or other moulding based bio-composite manufacturing process. In our work, despite of having irregular fibre powders distribution in the polymer matrix due to the dry-blending process, the manufactured PCL/date palm fibre bio-composites demonstrated a very comparable tensile properties to melt-blended PCL/date palm fibre counterparts, reported in the literature. Dhakal et al. manufactured date palm fibre /PCL bio-composites and characterised their tensile and low velocity impact properties [21]. For a 20% date palm fibre in PCL matrix, they reported a tensile modulus of 284 MPa, strain of 21% and tensile strength of 24 MPa. In this work, tensile modulus, strain and tensile strength values were achieved as 198 MPa, 48% strain and 9.6 MPa respectively with a 10% fibre-based PCL bio-composites. Although, it is very difficult to compare directly these two different studies on PCL/DPF composites, it is expected that with the increase of date palm fibres up-to 20% in the current dry-blended composites, the modulus values will be increased and could be comparable to a value of 284 MPa. The reduced tensile strength in this work compared to the literature could be due to the differences in PCL polymer grade differences, since we used a very flexible PCL polymer grade for the bio-composite manufacturing. Therefore, based on this literature comparison, it can be said that the dry-blending process is capable of producing date palm fibre-PCL bio-composites with good mechanical properties through using less processing steps during blending and compression moulding processes. A further dry-blended compression moulding process optimisation could be investigated in future to improve a regular fibre distribution in polymer matrix by employing- (1) both polymer and fibres as powder materials at similar powder particle sizes for better mixing and (2) placing the dry-blended powdered fibre and polymer on compression moulding moulds using a distribution tool to evenly distribute the dry-blend throughout the whole moulds. In these ways fibre distribution regularities could be achieved, leading to an improvement in ultimate composites' mechanical performances. Dry-blending of date palm fibre in the polymer matrix showed similar thermal performances to melt blended natural fibres into different polymers (flax fibre in PCL, bamboo fibre in PCL and sisal fibre in PP), such as an insignificant reduction in thermal degradation resistance of bio-composites with reduced degree of crystallinity and the promotion of a slow secondary crystallisation in PCL polymer.

Design Implications for Sustainable Packaging Applications

It is hoped that the findings of this work will be helpful to promote the use of dry-blending process as an alternative to melt-blending process for manufacturing of PCL/date palm fibre bio-composites with good mechanical and thermal performances. The observed mechanical properties might be enough and could be used to carefully design PCL/date palm fibre bio-composites for sustainable packaging applications, wherein, mechanical load bearing demand is not a likely scenario and also the ductility property of packaging products is not the utmost priority. The thermal properties analysis also indicates that PCL/date palm fibre-based bio-composites can be easily used from a normal temperature to 40–45 °C. Considering both mechanical and thermal properties, some potential sustainable applications could be - disposable cutlery items, disposable plates, food container or tray mainly for cold, normal or slightly warm foods, packaging box for gift items or carrying vegetables/fruits/chocolates, small to medium size packaging trolleys or bags for storing or transferring components (electrical or DIY tools etc.) carrying very small amount of mechanical loads etc. For sustainable packaging products, barrier properties to moisture, oxygen and other gases with required functionalities are very important. In this regard, the observed less water contact angle of dry-blended PCL/date palm fibre composites is an indication of hydrophilicity with increasing surface roughnesses which might affect the deposition of barrier coating layer on surfaces positively [33] and hence, influence ultimate barrier properties of bio-composite packaging products. This warrants a detail investigation in future.

Conclusions

Dry-blended PCL/date palm fibre bio-composites were manufactured and their mechanical and thermal properties were investigated. Key findings are summarised as below-.

- Tensile modulus values showed an increase up-to 20% for the 10% DPF-PCL bio-composites, while, tensile strength and strain values were reduced compared to 100% PCL samples. The lower mechanical properties could be related to an irregular fibre distribution in dry-blended composite samples.
- The inclusion of date palm fibre affected the crystallisation in PCL polymer matrix, reduced the degree of crystallinity and promoted a secondary crystallisation process.

- TGA analysis showed a slight reduced thermal degradation performance for the fibre addition in polymer compared to only PCL samples. DMA results also supported tensile and thermal analysis findings.
- Dry-blended PCL/date palm fibre composites showed a comparable tensile and thermal properties with the melt blended PCL/date palm fibre bio-composites reported in the literature. A further dry-blending process optimisation should be carried out in future to improve a regular fibre distribution in polymer matrix leading to an improvement in their ultimate mechanical properties.
- Current findings and properties of dry-blended PCL/date palm fibre bio-composites could be carefully designed for various low mechanical load bearing or non-mechanical load carrying sustainable packaging applications.

Acknowledgements Not applicable.

Author Contributions Abu Saifullah: conceptualization, experimental design, supervision, methodology investigation, sample manufacturing, data analysis, writing and revision. Nirmal George Chacko: literature search and review, experimental works, sample manufacturing, tests, results and data analysis, first draft writing. Hom Nath Dhakal: conceptualisation, experimental design, supervision, fibre collection, data analysis, writing and revision. Sakib Hossain Khan: literature review, data analysis and presentation, writing and revision, sample manufacturing and experimental works. Forkan Sarker: methodology and experimental design, data analysis, writing and correction, sample manufacturing. Zhongyi Zhang: experimental design, supervision, results analysis, writing and corrections.

Funding We are declaring that no funds, grants, or other supports were received during the experimental work and preparation of this manuscript.

Data Availability Data will be made available upon any reasonable request to the corresponding author.

Declarations

Competing Interests Authors are declaring that there are no relevant financial or non-financial interests to disclose.

References

1. Yamini Jhanji, D.: *Natural Fibers: The Sustainable Alternatives for Textile and Non-Textile Applications*, in *Natural Fiber*, J. Han-Yong, Editor. IntechOpen: Rijeka. p. Ch. 1. (2022)
2. Gonzalez, V., Lou, X., Chi, T.: Evaluating environmental impact of natural and synthetic fibers: A Life Cycle Assessment Approach. Sustainability. **15**(9), 7670 (2023)
3. Al-Oqla, F.M., Salit, M.S.: *2 - Natural fiber composites*, in *Materials Selection for Natural Fiber Composites*, F.M. Al-Oqla and M.S. Salit, Editors. Woodhead Publishing. pp. 23–48. (2017)
4. Mohammed, L., et al.: A review on Natural Fiber Reinforced Polymer Composite and its applications. Int. J. Polym. Sci. **2015**, 243947 (2015)
5. Khan, S.H., et al.: *Characterization and Comparative Evaluation of Structural, Chemical, Thermal, Mechanical, and Morphological Properties of Plant Fibers*, in *Annual Plant: Sources of Fibres, Nanocellulose and Cellulosic Derivatives: Processing, Properties and Applications*, R. Khiari, M. Jawaid, and M.N. Belgacem, Editors. Springer Nature Singapore: Singapore. pp. 1–45. (2023)
6. Cheung, H., et al.: Natural fibre-reinforced composites for bioengineering and environmental engineering applications. Compos. Part. B: Eng. **40**(7), 655–663 (2009)
7. Shaikh, S., Yaqoob, M., Aggarwal, P.: An overview of biodegradable packaging in food industry. Curr. Res. Food Sci. **4**, 503–520 (2021)
8. Kumar, S., Darshna, A., Ranjan, D.: A review of literature on the integration of green energy and circular economy. Heliyon. **9**(11), e21091 (2023)
9. Das, A., et al.: A comprehensive review on recent advances in preparation, physicochemical characterization, and bioengineering applications of biopolymers. Polym. Bull. (Berl). **80**(7), 7247–7312 (2023)
10. Aaliya, B., Sunooj, K.V., Lackner, M.: Biopolymer composites: A review. Int. J. Biobased Plast. **3**(1), 40–84 (2021)
11. Fayomi, O.S.I., et al.: *Potential of bio-wastes in the development of composites for manufacturing application* Materials Today: Proceedings, 38: pp. 2353–2357. (2021)
12. Awad, S., et al.: A critical review on date Palm Tree (Phoenix dactylifera L.) Fibres and their uses in bio-composites. Waste Biomass Valoriz. **12**(6), 2853–2887 (2021)
13. Nasser, R.A., et al.: Chemical Analysis of different parts of date palm (Phoenix dactylifera L.) using Ultimate, Proximate and Thermo-Gravimetric techniques for Energy Production. Energies. **9**(5), 374 (2016)
14. Khandaker, S., et al.: From industrial jute fibre spinning wastes to biofibre-reinforced plastics. Mater. Chem. Phys. **313**, 128586 (2024)
15. AlMaadeed, M.A., et al.: Date palm wood flour/glass fibre reinforced hybrid composites of recycled polypropylene: Mechanical and thermal properties. Mater. Design. **42**, 289–294 (2012)
16. Augustia, V., et al.: Effect of date palm Fiber loadings on the Mechanical properties of High Density Polyethylene/Date Palm Fiber composites. Key Eng. Mater. **773**, 94–99 (2018)
17. Saifullah, A., et al.: Low velocity impact (LVI) and flexure-after-impact (FAI) behaviours of rotationally moulded sandwich structures. J. Mater. Res. Technol. **15**, 3915–3927 (2021)
18. Mousa, N., et al.: A New Green Composite based on plasticized polylactic acid mixed with date Palm Waste for single-use plastics applications. Polymers. **14**(3), 574 (2022)
19. Kharrat, F., et al.: *Extrusion blowing of composite films from poly(lactic acid) / date palm leaf filler for packaging applications: Preparation and Characterization*. (2021)

20. Umar, Y., et al.: Development and characterization of polyvinyl alcohol filled with date palm midrib powder. J. Thermoplast. Compos. Mater. **36**(4), 1437–1449 (2021)
21. Dhakal, H., et al.: Mechanical properties of leaf sheath date palm fibre waste biomass reinforced polycaprolactone (PCL) biocomposites. Ind. Crops Prod. **126**, 394–402 (2018)
22. Hejna, A., et al.: On the Correlation of Lignocellulosic Filler Composition with the Performance properties of Poly(ε-Caprolactone) based biocomposites. Waste Biomass Valoriz. **11**(4), 1467–1479 (2020)
23. Chiellini, E., et al.: Composite films based on Biorelated Agroindustrial Waste and Poly(vinyl alcohol). Preparation and Mechanical properties characterization. Biomacromolecules. **2**(3), 1029–1037 (2001)
24. Dev, B., et al.: Mapping the progress in natural fiber reinforced composites: Preparation, mechanical properties, and applications. Polym. Compos. **44**(7), 3748–3788 (2023)
25. Curling, S.F., et al.: Feasibility of using straw in a strong, thin, pulp moulded packaging material. Ind. Crops Prod. **97**, 395–400 (2017)
26. Sarasam, A.R., Krishnaswamy, R.K., Madihally, S.V.: Blending chitosan with polycaprolactone: Effects on physicochemical and antibacterial properties. Biomacromolecules. **7**(4), 1131–1138 (2006)
27. Urquijo, J., Guerrica-Echevarría, G., Eguiazábal, J.I.: Melt processed PLA/PCL blends: Effect of processing method on phase structure, morphology, and mechanical properties. J. Appl. Polym. Sci., **132**(41). (2015)
28. Abdellah, M.Y., et al.: Characteristic properties of date-palm fibre/sheep wool reinforced polyester composites. J. Bioresources Bioprod. **8**(4), 430–443 (2023)
29. Bourmaud, A., et al.: Exploring the potential of waste leaf sheath date palm fibres for composite reinforcement through a structural and mechanical analysis. Compos. Part A: Appl. Sci. Manufac. **103**, 292–303 (2017)
30. Saada, K., et al.: Exploring tensile properties of bio composites reinforced date palm fibers using experimental and modelling approaches. Mater. Chem. Phys. **314**, 128810 (2024)
31. Asim, M., et al.: Effect of surface modified date palm fibre loading on mechanical, thermal properties of date palm reinforced phenolic composites. Compos. Struct. **267**, 113913 (2021)
32. Ghori, S.W., Rao, G.S., Rajhi, A.A.: Investigation of Physical, Mechanical Properties of Treated Date Palm Fibre and Kenaf Fibre Reinforced Epoxy Hybrid composites. J. Nat. Fibers. **20**(1), 2145406 (2023)
33. Yorseng, K., et al.: Influence of Accelerated Weathering on the mechanical, fracture morphology, Thermal Stability, Contact Angle, and water absorption properties of Natural Fiber Fabric-based Epoxy Hybrid composites. Polymers. **12**(10), 2254 (2020)
34. Stark, N.M., Matuana, L.M.: Characterization of weathered wood–plastic composite surfaces using FTIR spectroscopy, contact angle, and XPS. Polym. Degrad. Stab. **92**(10), 1883–1890 (2007)
35. Li, T.-T., et al.: Preparation and property evaluations of PCL/PLA composite films. J. Polym. Res. **28**(5), 156 (2021)
36. Perera, H.J., Goyal, A., Alhassan, S.M.: Surface properties of alkylsilane treated date palm fiber. Sci. Rep. **12**(1), 9760 (2022)
37. Arbelaiz, A., et al.: Thermal and crystallization studies of short flax fibre reinforced polypropylene matrix composites: Effect of treatments. Thermochim. Acta. **440**(2), 111–121 (2006)
38. Joseph, P.V., et al.: The thermal and crystallisation studies of short sisal fibre reinforced polypropylene composites. Compos. Part A: Appl. Sci. Manufac. **34**(3), 253–266 (2003)
39. Huang, Y., et al.: Nonisothermal Crystallization Kinetics of Modified Bamboo Fiber/PCL composites. J. Appl. Polym. Sci. - J. APPL. POLYM. SCI., 116. (2010)
40. Bezazi, A., et al.: Investigation of the date palm fiber for green composites reinforcement: Quasi-static and fatigue characterization of the fiber. Ind. Crops Prod. **146**, 112135 (2020)
41. Al-Oqla, F., Hayajneh, M., Al-Shrida, M.: Mechanical performance, thermal stability and morphological analysis of date palm fiber reinforced polypropylene composites toward functional bioproducts. Cellulose. **29**, 1–17 (2022)
42. Ahamed, B., et al.: High performance short jute fibre preforms for thermoset composite applications. Compos. Part. C: Open. Access. **9**, 100318 (2022)
43. Hasan, M., et al.: Improved mechanical performances of unidirectional jute fibre composites developed with new fibre architectures. RSC Adv. **11**(37), 23010–23022 (2021)

Waste and Biomass Valorization (2024) 15:5771–5784
https://doi.org/10.1007/s12649-024-02500-9

ORIGINAL PAPER

Enhanced Production of Levulinic Acid from Oil Palm Empty Fruit Bunch

Litavadee Chuaboon[1,2] · Chatcha Saengsen[1] · Orawan Sookbampen[1] · Euntae Yang[3] · Hafiza Shukor[4] · Yusuf Chisti[5] · Wichitpan Rongwong[1,6]

Received: 5 December 2023 / Accepted: 17 March 2024 / Published online: 13 April 2024

Abstract

Levulinic acid (LA) was produced from oil palm empty fruit bunch (OPEFB) pretreated in two different ways: (1) a two-step treatment with peracetic acid (PA) and alkaline peroxide (AP); and (2) an ammonia soak pretreatment. The pretreated material was subjected to acid hydrolysis (5% w/v sulfuric acid, 125 °C to 175 °C, 120 min) to produce LA. Compared to the ammonia treatment, the two-step PA–AP pretreatment was better in removing lignin from OPEFB, and resulted in a higher LA yield based on the mass of the pretreated OPEFB. On a mass basis, the LA yield was 31.1% on pretreated OPEFB, that had been pretreated using the PA–AP process, but only 16.7% from the biomass treated using the ammonia process. The kinetics of acid-catalyzed production of LA from the pretreated OPEFB were investigated to develop a mathematical model for predicting the conversion of cellulose to the intermediates (glucose, 5-hydroxymethylfurfural), and the final product, LA. The hydrolysis of cellulose to glucose was found to be the rate-controlling step in acid-catalyzed production of LA, confirming the importance of the delignification pretreatment in making cellulose more amenable to hydrolysis. During the two-stage acid hydrolysis, the reaction at 175 °C for 15 min in the first stage, followed by 125 °C for 105 min in the second stage, resulted in LA molar yield (based on cellulose) of ~40%. This was comparable to the yield obtained if both steps were performed at 150 °C for a total of 120 min.

Keywords Levulinic acid · Oil palm Empty Fruit Bunch · Cellulose Conversion · Lignocellulose

Introduction

Levulinic acid (LA; 4-oxopentanoic acid, $CH_3C(O)CH_2CH_2CO_2H$) is among the top 12 biomass-derived platform chemicals [1]. Its ketone carbonyl and carboxyl functional groups can be used for transforming it into other valuable products. LA-derived products include methyltetrahydrofuran (an industrial solvent), ethyl levulinate (a fuel oxygenate and lubricity enhancer), succinic acid, and many other useful chemicals [2–5]. LA can be made via acid-catalyzed hydrolysis of cellulose recovered from the inexpensive and plentiful lignocellulosic biomass, including agroindustrial wastes [5–10] such as oil palm empty fruit bunch (OPEFB).

Oil palm empty fruit bunch (OPEFB) is an unwanted byproduct of the palm oil industry, a major commercial sector in parts of southeast Asia, as palm oil is the most widely used plant oil worldwide. In southern Thailand alone nearly 5000 tons of crude palm oil is produced daily [11]. Typically, palm oil factories buy the entire oil palm fruit bunch

✉ Wichitpan Rongwong
wichitpan.ro@wu.ac.th

1 Biomass and Oil Palm Center of Excellence, Walailak University, Nakhon Si Thammarat 80160, Thailand

2 School of Pharmacy, Walailak University, Nakhon Si Thammarat 80160, Thailand

3 Department of Marine Environmental Engineering, Gyeongsang National University, Gyeongsangnam-do 53064, Republic of Korea

4 Centre of Excellence for Biomass Utilization (CoEBU), Faculty of Chemical Engineering & Technology, Universiti Malaysia Perlis (UniMAP), Arau, Perlis 02600, Malaysia

5 Institute of Tropical Aquaculture and Fisheries, Universiti Malaysia Terengganu, Kuala Nerus, Terengganu 21030, Malaysia

6 School of Engineering and Technology, Walailak University, Nakhon Si Thammarat 80160, Thailand

from the farmer for extracting the oil, and the empty fruit bunch is discarded. OPEFB makes up nearly 25% of the oil palm fruit bunch. Absent other uses, OPEFB is often burnt for energy [11]. OPEFB contains cellulose (20–50%), hemicellulose (23–36%), and lignin and other residues (22–51%) [12]. Cellulose and hemicellulose are natural polymers of sugars, and may be hydrolyzed to simple sugars such as glucose and fructose, to serve as precursors for diverse high-value chemicals including LA.

For producing LA from OPEFB, the lignocellulosic biomass must first be delignified to recover relatively pure cellulose for subsequent acid-catalyzed hydrolysis to LA. The processing scheme used is depicted in Fig. 1, although the specific delignification pretreatment and the conditions of subsequent acid-hydrolysis vary depending on the use and the nature of the biomass involved. During acid-catalyzed hydrolysis, the cellulose is first broken down to its monomeric sugar, glucose, and the latter isomerizes to fructose and further hydrolyzes to the major intermediate 5-hydroxymethylfurfural (HMF) that is rapidly transformed to LA [13], as illustrated in Fig. 1.

Many different physical, chemical, and combined physicals–chemical pretreatments have been developed for delignification of the diverse kinds of lignocellulosic biomass [14–17] for producing LA. The choice of pretreatment depends on its efficacy for the type of biomass being treated and the cost of processing. Pretreatments generally seek to delignify the biomass to make cellulose more readily accessible for hydrolysis to sugars for conversion to products such as LA. Pretreatments also open-up the tightly packed structure of the cellulose itself, to make it more susceptible to subsequent treatments. A prior delignification greatly enhances the yield of LA from the biomass compared to if no delignification was used [6, 18, 19]. The yield enhancing effect of a pretreatment is proportional to its delignification efficacy. For example, compared to untreated rice straw, a 5-fold higher concentration of LA was obtained in the reaction mixture by using rice straw that had been pretreated [6]. Similarly, a 20% higher yield of LA was obtained from cellulose that had been pretreated with a combination of phosphoric acid and hydrochloric acid [18].

Often multiple pretreatments may be used in combination for effective delignification. For example, depending on the biomass, an alkaline pretreatment alone may achieve 20–80% delignification [20]. A particularly effective pretreatment developed specifically for OPEFB involved the use of peracetic acid (PA) in the first step and then further treatment with alkaline peroxide (AP) [21]. This PA–AP pretreatment achieved 98% delignification of OPEFB at room temperature and atmospheric pressure. Importantly, although nearly all lignin was removed, more than 85% of the cellulose originally present in the OPEFB was retained in the pretreated solids. A high retention of cellulose is important as this is the substrate wanted for subsequent conversion to LA. Although the PA–AP pretreatment has not been evaluated in the context of producing LA, in principle it has the potential to enhance the yield of LA from the pretreated OPEFB.

In view of the demonstrated delignification efficacy of the PA–AP pretreatment for OPEFB, this treatment was compared in the present study with the alternative of simple soaking of OPEFB in aqueous ammonia at room temperature for delignification (Fig. 1). The aqueous ammonia pretreatment was used for comparison because of its simplicity, low cost, and widespread acceptance [22]. The delignified OPEFB from these two pretreatments was subsequently subjected to acid-catalyzed hydrolysis to produce LA. The reaction kinetics of production of LA from the pretreated OPEFB were examined. Different temperature–time regimens were evaluated during acid-catalyzed hydrolysis of the pretreated biomass, in attempts to enhance the yield of LA as this strategy had been shown to be useful in producing LA from some types of lignocellulosic biomass [8, 23]. A higher temperature early during the acid-catalyzed hydrolysis had increased the yield of hydroxymethylfurfural (HMF), an intermediate that was rapidly converted to LA even if the reaction temperature in later stages of hydrolysis was reduced [10].

Materials and methods

OPEFB Composition and Morphology

OPEFB was obtained from Taksin Palm Co., Ltd (2521), Surat Thani province, Thailand. As received OPEFB was washed and dried to constant weight in an oven at 105 °C. The dried OPEFB was ground using a hammer mill (PX-MFC 90D; Kinematica AG, Malters, Switzerland; www.kinematica.ch) with a sieve diameter of 0.5 mm. The ground material was then sieved through a number 40 sieve (425 µm openings). The recovered OPEFB powder was stored in a sealed plastic container at room temperature (~27 °C). This material was used in all experiments.

The cellulose, hemicellulose, and lignin content of OPEFB were determined using an automated analyzer (Velp FIWE, VELP Scientifica Srl, Usmate, Italy; www.velp.com). The morphology of the OPEFB particles was imaged using a scanning electron microscope (ZEISS MERLIN Compact; Carl Zeiss AG, Oberkochen, Germany; www.zeiss.com).

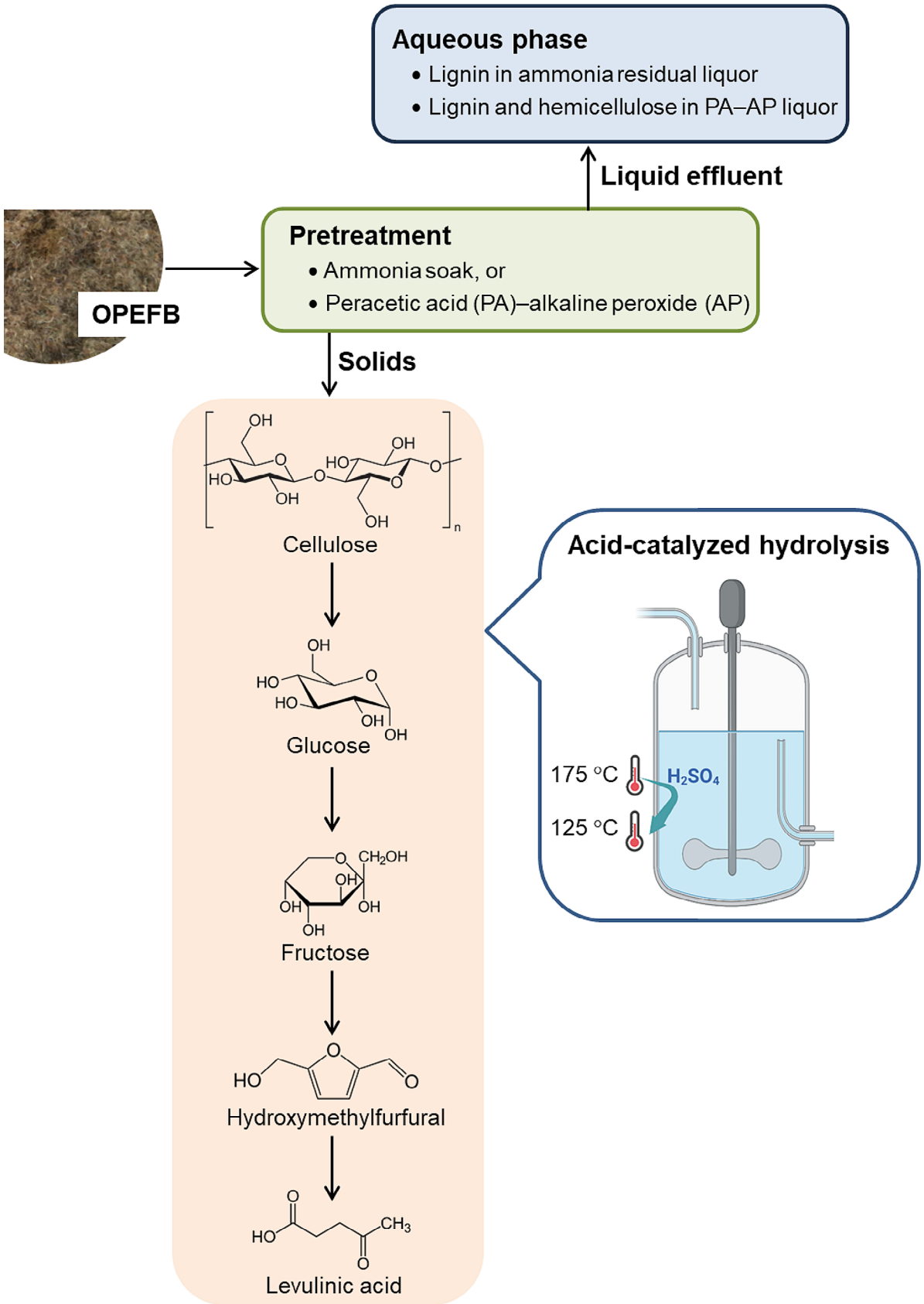

Fig. 1 Production scheme of levulinic acid (LA) from OPEFB as used in the present study: The two pretreatment options examined for delignification of OPEFB and the two-stage temperature regimen of acid-catalyzed hydrolysis for obtaining LA from delignified cellulose are shown

OPEFB Pretreatment

Two methods of OPEFB pretreatment were compared for delignification prior to conversion of the delignified cellulose to LA. These pretreatment methods were: (1) an ammonia soak pretreatment; and (2) a two-step pretreatment involving peracetic acid (PA) and then alkaline peroxide (AP).

Ammonia Pretreatment

The method used was adapted from Gozan et al. [24]. OPEFB was suspended in aqueous ammonia (13.13% w/w ammonia) for 14 h at room temperature such that the mass ratio of OPEFB to ammonia solution was 1:6. The OPEFB solids were then recovered, washed with deionized water until the pH became neutral, and dried to a constant weight in an oven at 105 °C. The recovered solid product was designated as the ammonia pretreated OPEFB. All material solubilized by the aqueous ammonia was washed out.

Two-Step Pretreatment with Peracetic Acid (PA) and Alkaline Peroxide (AP)

The method used was from Palamae et al. [21]. In the first step, the OPEFB powder was fully suspended for 9 h at 35 °C in concentrated peracetic acid (PA; prepared as in Palamae et al. [21]) such that 20 mL of PA solution was added to each g of OPEFB. This slurry was then neutralized with 6 M NaOH and the solids were recovered by filtration through a nylon mesh (45 µm openings). The solids were further washed with deionized water and dried in an oven (80 ° C, 48 h). In the second step, dry solids (2 g) were mixed with alkaline peroxide solution (34.8 mL; comprised of 80.0 g NaOH per L of water mixed with 5.2 mL of hydrogen peroxide (350.0 g H_2O_2 L^{-1})) for 12 h at 40 °C. The solids were recovered on a nylon mesh, washed first with dilute HCl and then with deionized water until the pH of the wash became neutral. The solids were dried to a constant weight in an oven (105 °C) and kept for further use. The solid product obtained was designated as the OPEFB pretreated by the PA–AP process. The lignin and the hemicellulose that were solubilized by the PA–AP treatment, were washed out.

Hydrolysis of the Pretreated OPEFB to LA

A stainless-steel pressure vessel coated inside with an inert protective layer of polytetrafluoroethylene (Fig. 2) was used for acid catalyzed hydrolysis of pretreated OPEFB to LA. The total volume of the reactor vessel was 100 mL and it contained 70 mL of the reaction mixture. The reaction mixture comprised pretreated OPEFB (5% w/v), H_2SO_4 (2.5% w/v, or 5% w/v), and deionized water. The reaction temperature was 125 °C, 150 °C, or 175 °C in different experiments. The initial gauge pressure of the reactor was set at 5 bar using pressurized nitrogen (Fig. 2) to prevent boiling.

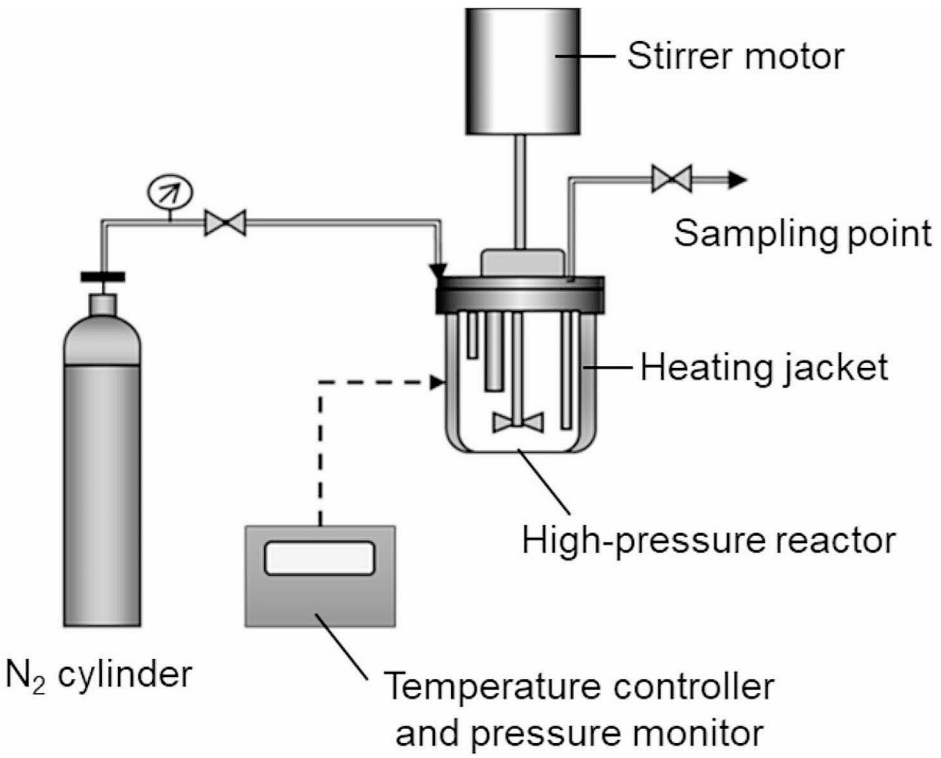

Fig. 2 High-pressure stirred reactor for acid-catalyzed hydrolysis of pretreated OPEFB

Table 1 OPEFB solids compositions before and after pretreatment

Constituent	Untreated OPEFB[a]	OPEFB pretreated with ammonia[b]	OPEFB pretreated by PA–AP process[c]
Cellulose (% w/w)	27.6 ± 3.6	51.7 ± 1.8	75.3 ± 0.8
Hemicellulose (% w/w)	28.5 ± 0.4	23.5 ± 0.8	6.9 ± 0.2
Lignin (% w/w)	29.3 ± 3.8	16.0 ± 2.6	1.5 ± 0.1

[a] Based on the total untreated OPEFB. The balance comprised everything else, including: ash; the extractable waxes; and the readily solubilized protein, starch, and other small molecules

[b] The balance comprised residual ash

[c] The balance comprised possible residual ash and insoluble derivative products of the reaction between acetic acid and cellulose [26], and acetic acid and lignin [27]

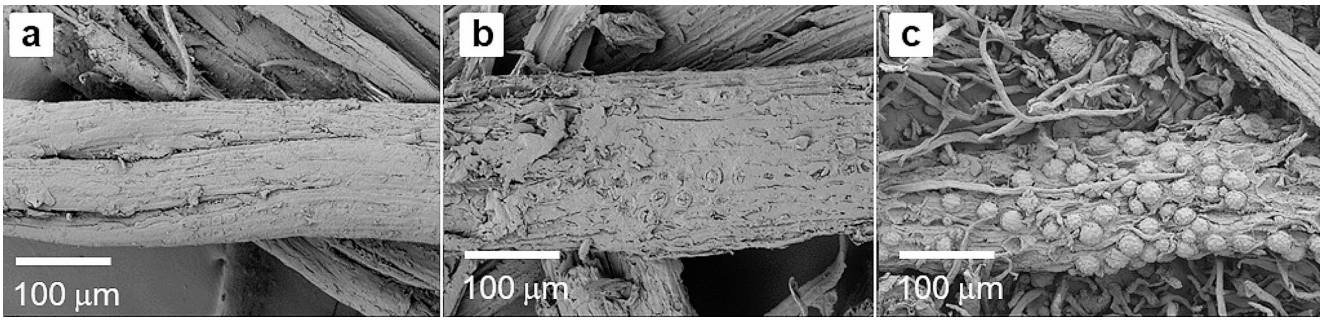

Fig. 3 SEM images of: (**a**) untreated OPEFB; (**b**) OPEFB pretreated by NH_3; and (**c**) OPEFB pretreated by the two-step PA–AP process

The reactor had a sampling tube immersed in the working suspension and a valve that could be opened to draw a small sample without releasing too much pressure (Fig. 2). In addition, the reactor had a mechanical stirrer (Fig. 2) operated at a rotational speed of 100 rpm to ensure uniform mixing. The reactor liquid phase was sampled at 20, 40, 80, and 120 min after the start of the reaction, for analyses. The samples were measured for LA, HMF, and glucose (GLC), by liquid chromatography with a tandem mass spectrometry (LC-MS/MS), as described by Saengsen et al. [25]. The data reported are the averaged values and standard deviation of measurements on triplicate samples.

Results and Discussion

OPEFB Composition before and after Pretreatment

The compositions of the native and variously pretreated OPEFB samples are shown in Table 1. Both the delignification pretreatments reduced the lignin content of the residual solids, but the PA–AP treatment removed nearly 95% of the original lignin whereas the ammonia treatment removed only around 45%. In both treatments, the lignin was removed by decomposition into smaller water-soluble molecules, and the hydrolysis of covalent linkages that bound lignin to xylan in hemicellulose. The PA–AP treatment solubilized nearly 76% of the original hemicellulose whereas the ammonia treatment solubilized ~ 18%. Better solubilization of hemicellulose by the PA–AP process effectively contributed to delignification. Scanning electron micrographs (SEM) of the untreated and the variously pretreated OPEFB (Fig. 3) confirmed superior delignification by the PA–AP process. The untreated OPEFB fibers had a relatively smooth surface due to lignin and hemicellulose forming a protective layer that covered the cellulose fibers (Fig. 3a). The ammonia pretreatment clearly removed some of the lignin and hemicellulose, creating open spaces from where the material had been solubilized (Fig. 3b), but lignin and hemicellulose solubilization and consequent generation of void spaces was much greater in the PA–AP treated samples (Fig. 3c). By removing the protective lignin and hemicellulose, the PA–AP treatment better exposed the cellulose to the reagents in the next step of acid-catalyzed hydrolysis. The round nodule-like structures in Fig. 3c are the silica deposits, or silica bodies, commonly seen on the surfaces of biomass fibers once the covering of lignin and hemicellulose is dissolved away [21].

Yield Profiles of LA, GLC, and HMF in the Hydrolysis Reaction Mixture

The molar yields of LA, GLC, and HMF on cellulose were calculated using the following equation:

$$Y_i\,(\%) = C_i V_R \left(\frac{MW_{\text{cellulose}}}{y_{\text{cellulose}} W_{\text{biomass}}} \right) \times 100 \qquad (1)$$

where Y_i was the yield (%, mol/mol) of component i (i.e., LA, GLC, or HMF), C_i was the measured concentration of

the component i (mol L^{-1}), V_R (L) was the reaction volume, $y_{cellulose}$ was the mass fraction of cellulose ((% w/w as in Table 1)/100) in OPEFB, $W_{biomass}$ (g) was the initial weight of the pretreated OPEFB, and $MW_{cellulose}$ was the molar mass of cellulose (162.1 g mol^{-1}).

The yield (%, mol/mol) profiles of LA, GLC, and HMF in the hydrolysis reaction mixture are shown in Fig. 4. The data are average values of triplicate samples. The data revealed the following:

1. For otherwise equivalent conditions, the LA yield at any instance was always higher from the OPEFB pretreated with the PA–AP process compared to the yield from the ammonia treated OPEFB (Fig. 4a, b).
2. Under the best conditions overall, the PA–AP pretreatment followed by acid hydrolysis with 5% (w/v) H_2SO_4 at 175 °C resulted in a LA yield of 57.4% at 120 min whereas for the same conditions of acid-catalyzed hydrolysis, the LA yield from ammonia pretreated OPEFB was ~45% (Fig. 4b). These differences were explained by the much greater delignification of OPEFB that was achieved with the PA–AP pretreatment compared to the ammonia treatment (Table 1).
3. The difference in LA yields from OPEFB pretreated by the two different methods was larger, if the subsequent acid hydrolysis was carried out using a lower concentration (i.e., 2.5% w/v H_2SO_4) of the acid at 175 °C, but for a shorter period of 40 min: thus, the LA yield from the PA–AP treated OPEFB was 38.8% whereas it was only 18.2% from OPEFB that had been pretreated with ammonia (Fig. 4a). The cause of the poor yield from ammonia treated OPEFB was once again the large amount of residual lignin in the biomass that made the subsequent acid-catalyzed hydrolysis less effective [28].
4. Irrespective of the type of pretreatment, the yield of LA increased both with an increase in the temperature of acid hydrolysis and an increase in the concentration of H_2SO_4, the catalyst (Fig. 4a and b). At the most effective reaction temperature of 175 °C, the reaction had essentially reached equilibrium by 120 min as there was no further increase in LA yield (Fig. 4a and b).
5. Depending on the hydrolysis temperature, the concentrations and hence the yields of the two intermediates (i.e., GLC and HMF) initially rose as the reaction progressed and then declined as the intermediates were consumed to generate LA (Fig. 4c, d, e, and f). The peaking pattern of the yield profiles of GLC and HMF was consistent with their being intermediates in the conversion of OPEFB cellulose to LA.
6. At any instance during the hydrolysis reaction, the yield of HMF was lower than the yield of GLC, consistent with the scheme in Fig. 1 where HMF was derived from GLC via fructose, suggesting that conversion of HMF to LA was faster than the decomposition of GLC to HMF [29]. After peaking at some point during the reaction, the concentrations of the two intermediates declined but this did not translate into a corresponding rapid increase in the yield of LA. This was explained by a possible degradation of LA to products such as 3-acetylpropanol [30] especially at the higher reaction temperature of 175 °C.
7. The above-mentioned peaks in the yield profiles of HMF and GLC were not noticeable under conditions of a slower reaction, e.g., a combination of the lower catalyst concentration (2.5% w/v H_2SO_4) and lower temperatures (125 °C and 150 °C) (Fig. 4c–f). This demonstrated that under these milder conditions, the LA formation reaction was slower than the reactions involved in the formation of the intermediates.

Based on the evidence (Fig. 4), HMF was an important intermediate in acid-catalyzed hydrolysis of OPEFB to LA. In principle, the hydrolysis reaction could be divided into two periods: first, during which the rate of production of HMF exceeded the rate of its conversion to LA, resulting in accumulation of HMF; and second, during which the rate of production of LA exceeded the rate of production of HMF, resulting in a decline in the concentration of the intermediate. The formation of LA is known to be favored by a lower reaction temperature compared to the formation of HMF [10]. Therefore, a dual temperature scheme involving a phase of a higher initial temperature followed by a second phase of reduced temperature may have the potential to reduce the energy requirements of producing LA from OPEFB without sacrificing the LA yield.

Yield of Levulinic Acid

In addition to the percent molar yield of LA on cellulose in OPEFB (Eq. 1), the percent mass yield of LA on the mass of pretreated OPEFB was also calculated. This yield is shown in Fig. 5 for the various process combinations used in this work (i.e., (1) the PA–AP pretreatment followed by acid hydrolysis (either 2.5%, or 5% w/v H_2SO_4) at three different temperatures (125, 150, 175 °C); and (2) the ammonia pretreatment followed by acid hydrolysis at the three mentioned temperatures).

Irrespective of the temperature of the subsequent acid-catalyzed hydrolysis, the ammonia pretreatment of OPEFB was the least effective for producing LA (Fig. 5). Irrespective of the pretreatment, whether PA–AP or ammonia, the yield of LA was enhanced both by using a higher temperature during acid-catalyzed conversion, and by using a higher

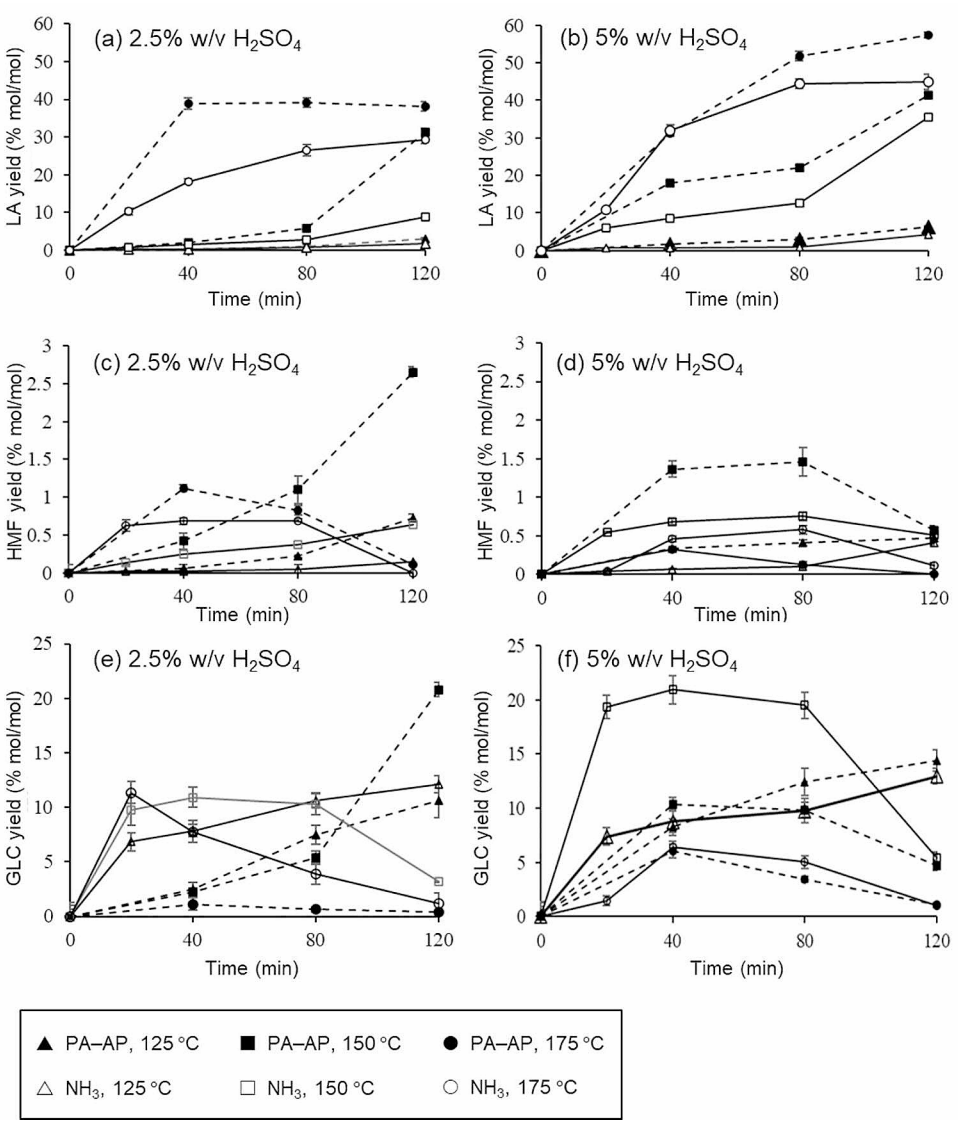

Fig. 4 The molar yield (% mol/mol) profiles of LA, GLC, and HMF as functions of reaction time: (**a**) LA yield using 2.5 w/v H_2SO_4; (**b**) LA yield using 5 w/v H_2SO_4; (**c**) HMF yield using 2.5 w/v H_2SO_4; (**d**) HMF yield using 5 w/v H_2SO_4; (**e**) GLC yield using 2.5 w/v H_2SO_4; and (**f**) GLC yield using 5% w/v H_2SO_4. The solid lines are for the PA–AP pretreated material and the dashed lines are for the ammonia pretreated material

concentration of the acid catalyst in the reaction mixture (Fig. 5). A two-step PA–AP pretreatment followed by acid-catalyzed hydrolysis using 5% w/v sulfuric acid at 175 °C for 120 min resulted in the highest yield of LA (31.1% w/w on pretreated OPEFB) (Fig. 5). In contrast, the best combination of the ammonia pretreatment and acid-catalyzed hydrolysis achieved a LA yield of 16.7% (Fig. 5), barely 54% of the yield afforded by the PA–AP process.

Compared with the literature data for 12 different types of lignocellulosic biomass samples, the PA–AP pretreatment used in the present work enabled a higher yield of LA (Table 2). Thus, an effective delignification of the biomass was an important prerequisite for attaining a high yield of LA. For a great majority (> 83%) of the cases in Table 2, the LA yield was less than 25% w/w. LA can be made by digestion of simple sugars with hydrochloric acid, but the yields are no better than some of the best results summarized in Table 2. For example, the following maximum yields (w/w) have been reported [31]: 14.5% on sucrose; 24.4% on glucose; and 25.1% on fructose. The relatively low yields were explained by the side reactions that converted some of the substrate to various other products [31]. The maximum theoretical yield of LA on cellulose is 71.6% (mol/mol) [23], or 51.2% w/w. LA yield in the range of 31–41% (w/w) have been reported using delignified rice straw, delignified corn stover, delignified sweet sorghum bagasse, and delignified *Miscanthus* [23]. The yields of LA based on the original untreated biomass were lower after the PA–AP pretreatment compared with the yields after the ammonia soak pretreatment. This was because the PA–AP pretreatment resulted in a large loss (40%) of the original untreated biomass through near complete removal of the lignin and hemicellulose. In contrast, the ammonia soak pretreatment removed only a part of the original lignin and, consequently, less of the original biomass (only 13%) was lost after this pretreatment. Thus, on a mass basis, the yield of LA on the untreated

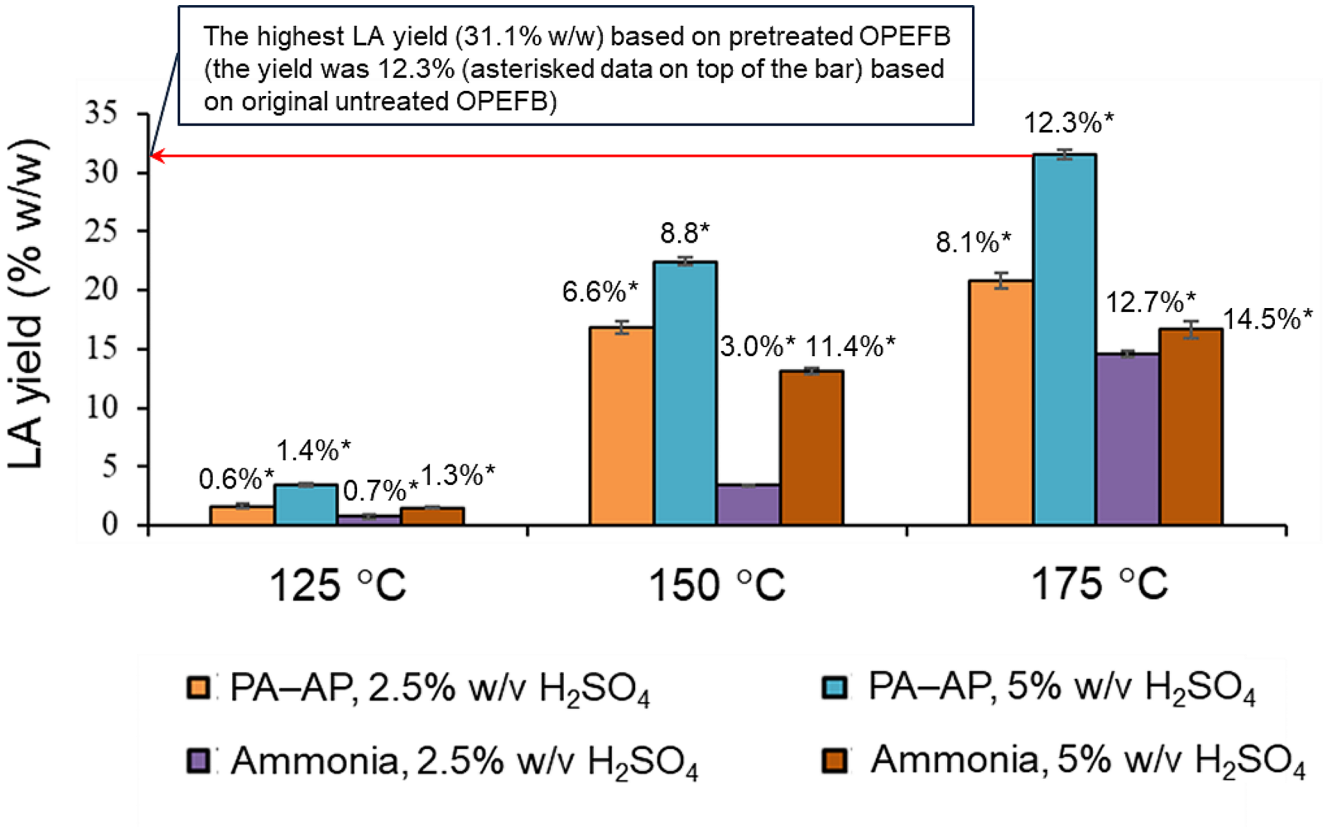

Fig. 5 LA yield (% w/w based on initial mass of pretreated OPEFB, shown on the y-axis) from OPEFB pretreated with the ammonia process and the two-step PA–AP process. The asterisked data are the LA yields (% w/w) based on the original untreated biomass. The asterisked data are not related to the scale on the y-axis. The experimental conditions were: either PA–AP pretreatment followed by reaction of the pretreated OPEFB with either 2.5% w/v H_2SO_4, or 5% w/v H_2SO_4, at one of the three temperatures specified underneath the bars; or aqueous ammonia pretreatment followed by reaction of the pretreated OPEFB with either 2.5% w/v H_2SO_4, or 5% w/v H_2SO_4, at one of the three temperatures specified underneath the bars. The reaction time was always 120 min

biomass was in several cases higher for the ammonia pretreatment compared to the PA–AP pretreatement (asterisked data; Fig. 5).

The Two-Stage Acid Hydrolysis at Different Temperatures

The two-stage acid-catalyzed hydrolysis of the pretreated OPEFB was performed using 5% w/v H_2SO_4 with a total reaction time of 120 min. The temperature in Stage 1 was 175 °C and in Stage 2 it was 125 °C. The holding times at the two temperatures varied, as shown in Fig. 6. The reaction was timed only when the reactor was at the specified temperatures. Between Stage 1 and Stage 2, the reactor was cooled rapidly by immersion in cold water until the required temperature was reached. The effects of intermediate cooling on the reaction were disregarded.

The data showed that a two-stage reaction with a temperature of 175 °C for 15 min followed by 125 °C for 105 min, resulted in a final LA yield of 41.0% from cellulose in the OPEFB pretreated by the PA–AP process (Fig. 6a). An identical two-stage temperature–time regimen gave a LA yield of 27.4% from cellulose in the biomass that had been pretreated by the ammonia process (Fig. 6b). In the above-mentioned two-stage scheme, the time-averaged processing temperature was 131.25 °C, but the yields of LA were quite comparable to the yields that were obtained earlier (section entitled Yield Profiles of LA, GLC, and HMF in the Hydrolysis Reaction Mixture) at a constant processing temperature of 150 °C for a reaction period of 120 min (Fig. 4c).

With a fixed total reaction period of 120 min, increasing the duration of the reaction at 175 °C to more than 15 min at the expense of the duration at 125 °C, did not increase the final yield of LA (Fig. 6a and b), possibly because the concentrations of the GLC and HMF intermediates began to decline after 15 min, as had occurred at ~40 min during processing at the lower constant temperature of 150 °C (Fig. 4d and f).

Table 2 Comparison of the LA yields from various biomass types and treatments

Biomass type	Pretreatment	Hydrolysis conditions			LA yield (% w/w)	Reference
		Catalyst	Temperature (°C)	Time (h)		
Wheat straw	-	H_2SO_4 (3.5%)	209.3	0.6	19.9[a]	Chang et al. [32]
Water hyacinth	H_2SO_4	H_2SO_4 (1 M)	175	0.5	35.0[a], 9.0[b]	Girisuta et al. [33]
Kenaf	-	Chromium chloride/HY zeolite	145.2	2.45	15.0[a]	Ya'aini et al. [34]
Olive tree pruning	-	HCl (37%), microwave irradiation	200	0.25	20.1[a]	Galletti et al. [7]
Poplar sawdust	Thermal	HCl (37%)	200	1	29.3[a]	Galletti et al. [7]
Rice straw	-	$[C_3SO_3HMIM]$ $[HSO_4]$	180	0.5	29.3[a]	Liu et al. [35]
Rice straw	Steam explosion	$S_2O_8^{2-}/ZrO^{2-}SiO^{2-}$	200	0.17	22.8[a]	Chen et al. [36]
Rice straw	-	HCl (15%)	200	3	16.6[a]	Kumar et al. [15]
Paddy straw	-	HCl (4.45%)	220	0.75	23.7[a]	Yan et al. [37]
Bagasse	-	HCl (4.45%)	220	0.75	22.8[a]	Yan et al. [37]
Cotton straw	Steam	H_2SO_4 (0.2 M)	120/180	0.3/1	9.5[b]	Yang et al. [38]
Giant reed	-	HCl (37%)	180	1	23.3[a]	Galletti et al. [39]
OPF[c]	-	[SMIM][$FeCl_4$]	154.5	3.7	24.8[a]	Ramli and Amin [40]
OPMF[d]	-	$InCl^{3-}$[HMIM] $[HSO_4]$	177	4.8	18.4[a]	Tiong et al. [41]
OPEFB	-	$InCl^{3-}$[HMIM] $[HSO_4]$	177	4.8	17.7[a]	Tiong et al. [41]
OPEFB	-	Chromium chloride/HY zeolite	145.2	2.45	15.5[a]	Ya'aini et al. [34]
OPEFB	PA–AP process	H_2SO_4 (5%)	175/125	0.25/1.75	31.1[a] (12.3[b])	This work
OPEFB	Ammonia process	H_2SO_4 (5%)	175/125	0.25/1.75	16.7[a] (14.5[b])	This work

[a] Calculated as: (mass of LA produced/mass of the total pretreated biomass fed to the reactor) × 100%

[b] Calculated as: (mass of LA/initial mass of the untreated biomass) × 100%

[c] OPF = oil palm fronds

[d] OPMF = oil palm mesocarp fiber

Reaction Kinetics

The kinetics of the acid-catalyzed hydrolysis of OPEFB to LA were modeled using the reaction scheme shown in Fig. 7. The cellulose in OPEFB was assumed to initially decompose to glucose which was then dehydrated to HMF and the latter was hydrolyzed to LA, the final product. A part of the glucose was assumed to degrade to humins, as generally occurs in acid-catalyzed hydrolysis [42].

Based on mass balances of the components (CEL, GLC, HMF, LA), a kinetic model of the acid-catalyzed hydrolysis could be written as follows:

$$\frac{d\,[\mathrm{CEL}]}{dt} = -k_{GLN}\,[\mathrm{CEL}] \tag{2}$$

$$\frac{d\,[\mathrm{GLC}]}{dt} = k_{GLN}\,[\mathrm{CEL}] - (k_{GLC1} + k_{GLC2})\,[\mathrm{GLC}] \tag{3}$$

$$\frac{d\,[\mathrm{HMF}]}{dt} = k_{GLC1}\,[\mathrm{GLC}] - k_{HMF}\,[\mathrm{HMF}] \tag{4}$$

$$\frac{d\,[\mathrm{LA}]}{dt} = k_{HMF}\,[\mathrm{HMF}] \tag{5}$$

where [CEL], [GLC], [HMF], and [LA] were the molar concentrations of cellulose, glucose, HMF, and LA, respectively, at time t, and k_{GLN}, k_{GLC1}, k_{GLC2}, and k_{HMF} were rate constants associated with the reactions identified in Fig. 7.

Equations (2)–(5) were used to obtain the following expressions for the concentrations of the components:

$$[\mathrm{CEL}] = [\mathrm{CEL}]_0 exp\,(-k_{GLN}t) \tag{6}$$

$$[\mathrm{CEL}] = \frac{k_{GLN}[\mathrm{CEL}]_0}{(k_{GLC1} + k_{GLC2}) - k_{GLN}} \left(exp\,(-k_{GLN}t) - exp\,(-\,(k_{GLC1} + k_{GLC2})\,t)\right) \tag{7}$$

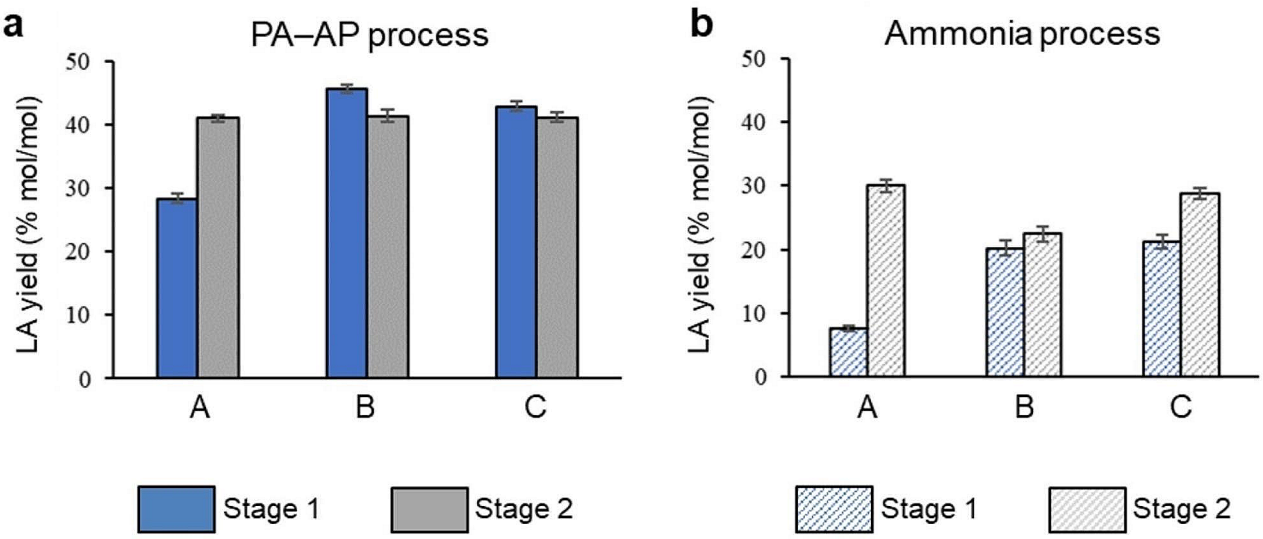

Acid-catalyzed hydrolysis conditions for the Processes (a) and (b) above

Bar group:	A	B	C
Stage 1:	175 °C, 15 min	175 °C, 30 min	175 °C, 45 min
Stage 2:	125 °C, 105 min	125 °C, 90 min	125 °C, 75 min

Fig. 6 Yield of LA on pretreated OPEFB under different temperature–time regimens (175 °C for the specified time (Stage 1) followed by 125 °C for the remaining period (Stage 2); the total reaction time (Stage 1 + Stage 2) was always 120 min): (**a**) OPEFB pretreated with the PA–AP process; and (**b**) OPEFB pretreated using the ammonia process. The data shown are averages of triplicate samples

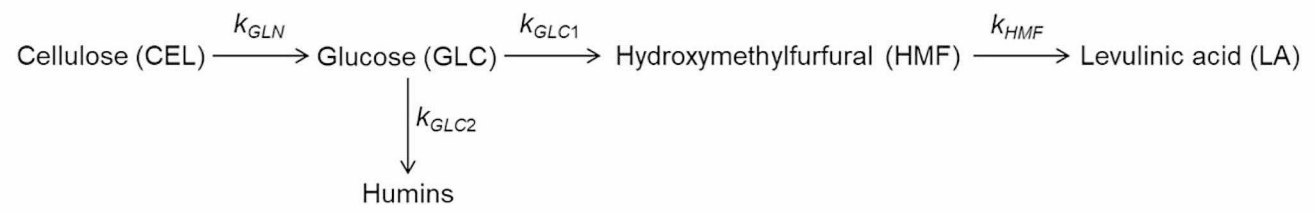

Fig. 7 The hydrolysis scheme of OPEFB cellulose to levulinic acid. The rate constants (k_{GLN}, k_{GLC1}, k_{GLC2}, k_{HMF}) for the various reactions are shown

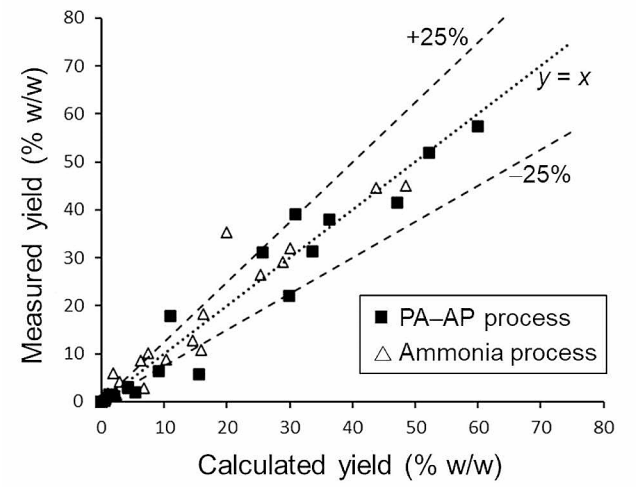

Fig. 8 A parity plot comparing the measured yield (%, w/w) of LA on cellulose and the yield predicted using Eq. (9). The diagonal line ($y=x$) represents an exact agreement between the measured and the calculated values

$$[\mathrm{HMF}] = \frac{k_{GLN}k_{GLC}[\mathrm{CEL}]_0}{(k_{GLC1}+k_{GLC2})-k_{GLN}} \left(\frac{exp\,(-k_{GLN}t)}{k_{HMF}-k_{GLN}} - \frac{exp\,(-(k_{GLC1}+k_{GLC2})\,t)}{k_{HMF}-(k_{GLC1}+k_{GLC2})}\right) + \frac{k_{GLN}k_{GLC}[\mathrm{CEL}]_0 exp\,(-k_{HMF}t)}{(k_{HMF}-k_{GLN})\,(k_{HMF}-(k_{GLC1}+k_{GLC2}))} \quad (8)$$

$$[\mathrm{LA}] = \frac{k_{GLN}k_{GLC}k_{HMF}[CEL_0]}{(k_{GLC1}+k_{GLC2})-k_{GLN}} \left(\frac{exp\,(-k_{GLN}t)-1}{k_{GLN}\,(k_{GLN}-k_{HMF})} - \frac{exp\,(-(k_{GLC1}+k_{GLC2})\,t)-1}{(k_{GLC1}+k_{GLC2})\,((k_{GLC1}+k_{GLC2})-k_{HMF})}\right) + \frac{k_{GLN}k_{GLC}\,[CEL_0]\,(exp\,(-k_{HMF}t)-1)}{(k_{HMF}-k_{GLN})\,((k_{GLC1}+k_{GLC2})-k_{HMF})} \quad (9)$$

where $[\mathrm{CEL}]_0$ was the initial concentration of cellulose.

The concentration profiles modelled with Eqs. (6)–(9) were fitted to the experimentally measured profiles (Fig. 4) to estimate the values of the rate constants k_{GLN}, k_{GLC1}, k_{GLC2}, and k_{HMF}. The initially assumed values of these constants were adjusted until the computed profiles best fitted the experimental data. The Solver functionality of Microsoft Excel was used to match the computed profiles to the experimental data shown in Fig. 4.

The values of the different rate constants determined as above, at different constant reaction temperatures, were used in the modified Arrhenius equation to calculate the activation energies of the reactions. The equation used was the following:

$$k = A_0[\mathrm{Acid}]^n exp^{-E/RT} \quad (10)$$

where A_0 was the preexponential factor, n was the reaction order based on the acid catalyst, E was the activation energy, [Acid] was the molar concentration of H_2SO_4, T was the absolute temperature of the reaction, and R (8.314 $J{\cdot}K^{-1}$ mol^{-1}) was the gas constant. The above analysis assumed the reactions to be pseudo first-order.

The calculated values of the various constants (i.e., k_{GLN}, k_{GLC1}, k_{GLC2}, k_{HMF}, A_0, n, E) for the hydrolysis of pretreated OPEFB to LA are shown in Table 3, for the two pretreatment methods. The yield of LA on cellulose calculated using Eq. (9) with the constants shown in Table 3 is compared in Fig. 8 with the experimentally measured yield at various times during the reaction. Irrespective of the pretreatment method, whether the PA–AP pretreatment, or soaking in ammonia solution, the experimentally measured yield was within ±25% of the calculated yield (Eq. 9) for most of the data (Fig. 8) over the entire range of the reaction conditions (i.e., temperatures of 125–175 °C; H_2SO_4 concentrations of 2.5 and 5.0%).

The values of the kinetic constants reported here (Table 3) were comparable to the data in the literature. For example, Lopes et al. [43] examined the production of LA from sugarcane bagasse, rice husk, and soybean straw, and reported the following values of the kinetic constants: the k_{GLN} to be in the range of 3.03×10^{-3} to 3.88×10^{-2} min^{-1} (our values were $(2.15–2.16)\times10^{-2}$ min^{-1}; Table 3); the k_{GLC1} to be in the range of 1.36×10^{-2} to 7.34×10^{3} min^{-1}; the k_{GLC2} to be in the range of 2.07×10^{-2} to 6.51×10^{3} min^{-1} (our values for this ranged from 6.1×10^{-1} to 8.9×10^{-1} min^{-1}; obtained

Table 3 Kinetic parameters of hydrolysis[a] of pretreated OPEFB to levulinic acid

Rate constants		A_0 (min^{-1})	n	E (kJ mol^{-1})
OPEFB pretreated with the PA–AP process				
k_{GLN} (min^{-1})	2.15×10^{-2}	2.278×10^{8}	0.137	85.657
k_{GLC1} (min^{-1})	1.17×10^{-1}	4.058×10^{6}	0.963	62.263
($k_{GLC1}+k_{GLC2}$) (min^{-1})	1.78×10^{-1}	1.209×10^{11}	0.279	100.800
k_{HMF} (min^{-1})	1.44	3.351×10^{5}	0.594	44.532
OPEFB pretreated with NH_3				
k_{GLN} (min^{-1})	2.16×10^{-2}	1.002×10^{4}	0.119	47.682
k_{GLC1} (min^{-1})	1.02×10^{-1}	3.592×10^{15}	1.663	136.269
($k_{GLC1}+k_{GLC2}$) (min^{-1})	1.91×10^{-1}	2.592×10^{11}	0.944	100.051
k_{HMF} (min^{-1})	5.14×10^{-1}	4.646×10^{5}	0.048	50.980

[a] Hydrolysis was performed at 175 °C using 5% w/v sulfuric acid

by subtracting k_{GLC1} from (k_{GLC1} + k_{GLC2}) in Table 3); and k_{HMF} in the range of 3.42×10^{-2} to 11 min^{-1} (our values were in the range 5.14×10^{-1} to 1.44 min^{-1}; Table 3). (The parameters A_0, n and E reported in the literature [43] were also comparable to the data of the present study.)

Irrespective of the pretreatment method used, the rate constant k_{GLN} (Fig. 7) had the lowest values compared to the other rate constants (Table 3), suggesting the decomposition of cellulose to glucose to be the rate-limiting step in production of LA from pretreated OPEFB. This was consistent with earlier reports of production of LA from entirely different types of lignocellulosic biomass such as sugarcane bagasse, rice husk, and soybean straw [43], including the biomass of the cyanobacterium *Spirulina platensis* ([44]. Furthermore, in Table 3, the rate constant k_{HMF} (Fig. 7) had highest value among the rate constants, and the corresponding reaction (Fig. 7) had the lowest activation energy. This was consistent with other observations relating to acid-catalyzed production of LA from other biomass types [24, 29]. The low activation energy of the HMF → LA reaction (Fig. 7; Table 3) implied that it was comparatively less sensitive to temperature than the other reactions in Fig. 7. This supported the adoption of the two-stage strategy for the hydrolysis reaction, that is, a higher temperature in the first stage and a lower temperature in the subsequent stage. The value of k_{GLC2} (the rate constant for humin formation from glucose; Fig. 7) for the OPEFB that had been pretreated with the PA–AP was ~30% lower than that for the OPEFB that had been pretreated with ammonia, suggesting less humin formation during LA production from the PA–AP pretreated OPEFB.

The k_{HMF} for the reaction that used the better delignified OPEFB, i.e., OPEFB pretreated by the PA–AP process, was nearly 2.8-fold greater compared to the k_{HMF} of the process that used the ammonia-pretreated OPEFB (Table 3), suggesting that glucose was more readily produced from the PA–AP pretreated OPEFB, and therefore more LA could be produced from this biomass.

In addition, the activation energy of the GLC → HMF reaction step (Fig. 7) of acid-catalyzed hydrolysis of ammonia pretreated OPEFB was higher than of the PA–AP pretreated OPEFB (Table 3). Therefore, to generate a given quantity of LA, the ammonia pretreated biomass would have required a higher reaction temperature and a higher concentration of the acid catalyst, than the biomass pretreated by the PA–AP process.

Conclusion

The PA–AP pretreatment in combination with a suitable temperature–time regimen during acid hydrolysis (either 175 °C for 15 min followed by 125 °C for 105 min, or a constant 150 °C for 120 min) of OPEFB proved to be most effective for converting OPEFB to levulinic acid. The best acid hydrolysis treatment required 5% (w/v) sulfuric acid and 5% (w/v) pretreated OPEFB solids in the reaction mixture for a total treatment time of 120 min. The optimal combination of PA–AP process and the acid catalyzed hydrolysis resulted in a levulinic acid yield of 31% (w/w) on pretreated OPEFB (12% w/w based on the original untreated biomass). Compared to the ammonia pretreatment, the PA–AP pretreatment was better in removing lignin from OPEFB and a good delignification assured a higher yield of LA during the subsequent acid hydrolysis. The achieved yield was nearly 75% greater than the highest yield previously reported in the literature for LA production from OPEFB (Table 2). A kinetic analysis of the acid-catalyzed production of LA acid from the pretreated OPEFB cellulose revealed the rate limiting step to be the hydrolysis of cellulose to glucose.

Acknowledgements This research was supported by Thailand Science Research and Innovation Fund Contract No. FRB650082/0227. Support is gratefully acknowledged from the Office of the Permanent Secretary of the Ministry of Higher Education, Science, Research and Innovation, under the Reinventing University System / Visiting Professor Program.

CRediT Authorship Contribution Statement **Litavadee Chuaboon**: Methodology, Validation, Investigation, Formal analysis, Visualization, Resource, Writing – original draft, Writing – review & editing. **Chatcha Saengsen**: Methodology, Validation, Investigation. **Orawan Sookbampen**: Methodology, Validation. **Euntae Yang**: Writing – review & editing. **Hafiza Shukor**: Writing – review & editing. **Yusuf Chisti**: Visualization, Writing – review & editing. **Wichitpan Rongwong**: Conceptualization, Methodology, Investigation, Project administration, Validation, Writing – original draft, Writing – review & editing, Resources, Supervision, Funding acquisition.

Data Availability Data will be made available on request.

Declarations

Declaration of Competing Interest The authors declare that they have no known competing financial interests or personal relationships that could have appeared to influence the work reported in this paper.

References

1. Werpy, T., Petersen, G.: Top Value Added Chemicals from Biomass: Volume I—results of Screening for Potential Candidates from Sugars and Synthesis gas. National Renewable Energy Laboratory, Golden, CO, USA (2004). https://doi.org/10.2172/15008859

2. Bozell, J.J., Moens, L., Elliott, D.C., Wang, Y., Neuenscwander, G.G., Fitzpatrick, S.W., Bilski, R.J., Jarnefeld, J.L.: Production of levulinic acid and use as a platform chemical for derived products. Resour. Conserv. Recycl. **28**, 227–239 (2000). https://doi.org/10.1016/S0921-3449(99)00047-6
3. Deng, F., Amarasekara, A.S.: Catalytic upgrading of biomass derived furans. Ind. Crops Prod. **159**, 113055 (2021). https://doi.org/10.1016/j.indcrop.2020.113055
4. Silva, J.F.L., Grekin, R., Mariano, A.P., Filho, R.M.: Making levulinic acid and ethyl levulinate economically viable: A worldwide technoeconomic and environmental assessment of possible routes. Energy Technol. **6**, 613–639 (2018). https://doi.org/10.1002/ente.201700594
5. Victor, A., Sharma, P., Pulidindi, I.N., Gedanken, A.: Levulinic acid is a key strategic chemical from biomass. Catalysts. **12**, 909 (2022). https://doi.org/10.3390/catal12080909
6. Elumalai, S., Agarwal, B., Sangwan, R.S.: Thermo-chemical pretreatment of rice straw for further processing for levulinic acid production. Bioresour Technol. **218**, 232–246 (2016). https://doi.org/10.1016/j.biortech.2016.06.037
7. Galletti, A.M.R., Antonetti, C., De Luise, V., Licursi, D., Nassi, N.: Levulinic acid production from waste biomass. BioResour. **7**, 1824–1835 (2012)
8. Morone, A., Apte, M., Pandey, R.A.: Levulinic acid production from renewable waste resources: Bottlenecks, potential remedies, advancements and applications. Renew. Sustain. Energy Rev. **51**, 548–565 (2015). https://doi.org/10.1016/j.rser.2015.06.032
9. Mthembu, L.D., Gupta, R., Deenadayalu, N.: Advances in biomass-based levulinic acid production. Waste Biomass Valorization. **14**, 1–22 (2023). https://doi.org/10.1007/s12649-022-01948-x
10. Mukherjee, A., Dumont, M.-J., Raghavan, V.: Review: Sustainable production of hydroxymethylfurfural and levulinic acid: Challenges and opportunities. Biomass Bioenergy. **72**, 143–183 (2015). https://doi.org/10.1016/j.biombioe.2014.11.007
11. Nutongkaew, P., Waewsak, J., Riansut, W., Kongruang, C., Gagnon, Y.: The potential of palm oil production as a pathway to energy security in Thailand. Sustain. Energy Technol. Assess. **35**, 189–203 (2019). https://doi.org/10.1016/j.seta.2019.07.002
12. Sukiran, M.A., Abnisa, F., Daud, W., Abu Bakar, W.M.A., Loh, N.: A review of torrefaction of oil palm solid wastes for biofuel production. Energy Convers. Manag. **149**, 101–120 (2017). https://doi.org/10.1016/j.enconman.2017.07.011
13. Sajid, M., Farooq, U., Bary, G., Azim, M.M., Zhao, X.: Sustainable production of levulinic acid and its derivatives for fuel additives and chemicals: Progress, challenges, and prospects. Green. Chem. **23**, 9198–9238 (2021). https://doi.org/10.1039/D1GC02919C
14. Baruah, J., Nath, B.K., Sharma, R., Kumar, S., Deka, R.C., Baruah, D.C., Kalita, E.: Recent trends in the pretreatment of lignocellulosic biomass for value-added products. Front. Energy Res. **6**, 141 (2018). https://doi.org/10.3389/fenrg.2018.00141
15. Kumar, P., Barrett, D.M., Delwiche, M.J., Stroeve, P.: Methods for pretreatment of lignocellulosic biomass for efficient hydrolysis and biofuel production. Ind. Eng. Chem. Res. **48**, 3713–3729 (2009). https://doi.org/10.1021/ie801542g
16. Mosier, N., Wyman, C., Dale, B., Elander, R., Lee, Y.Y., Holtzapple, M., Ladisch, M.: Features of promising technologies for pretreatment of lignocellulosic biomass. Bioresour Technol. **96**, 673–686 (2005). https://doi.org/10.1016/j.biortech.2004.06.025
17. Tocco, D., Carucci, C., Monduzzi, M., Salis, A., Sanjust, E.: Recent developments in the delignification and exploitation of grass lignocellulosic biomass. ACS Sustain. Chem. Eng. **9**, 2412–2432 (2021). https://doi.org/10.1021/acssuschemeng.0c07266
18. Muranaka, Y., Suzuki, T., Sawanishi, H., Hasegawa, I., Mae, K.: Effective production of levulinic acid from biomass through pretreatment using phosphoric acid, hydrochloric acid, or ionic liquid. Ind. Eng. Chem. Res. **53**, 11611–11621 (2014). https://doi.org/10.1021/ie501811x
19. Rackemann, D.W., Bartley, J.P., Harrison, M.D., Doherty, W.O.S.: The effect of pretreatment on methanesulfonic acid-catalyzed hydrolysis of bagasse to levulinic acid, formic acid, and furfural. RSC Adv. **6**, 74525–74535 (2016). https://doi.org/10.1039/C6RA14772K
20. Kim, J.S., Lee, Y.Y., Kim, T.H.: A review on alkaline pretreatment technology for bioconversion of lignocellulosic biomass. Bioresour Technol. **199**, 42–48 (2016). https://doi.org/10.1016/j.biortech.2015.08.085
21. Palamae, S., Dechatiwongse, P., Choorit, W., Chisti, Y., Prasertsan, P.: Cellulose and hemicellulose recovery from oil palm empty fruit bunch (EFB) fibers and production of sugars from the fibers. Carbohydr. Polym. **155**, 491–497 (2017). https://doi.org/10.1016/j.carbpol.2016.09.004
22. Zhao, C., Shao, Q., Chundawat, S.P.S.: Recent advances on ammonia-based pretreatments of lignocellulosic biomass. Bioresour Technol. **298**, 122446 (2020). https://doi.org/10.1016/j.biortech.2019.122446
23. Pulidindi, I.N., Kim, T.H.: Conversion of levulinic acid from various herbaceous biomass species using hydrochloric acid and effects of particle size and delignification. Energies. **11**, 621 (2018). https://doi.org/10.3390/en11030621
24. Gozan, M., Panjaitan, J.R.H., Tristantini, D., Alamsyah, R., Yoo, Y.J.: Evaluation of separate and simultaneous kinetic parameters for levulinic acid and furfural production from pretreated palm oil empty fruit bunches. Int. J. Chem. Eng. 1920180 (2018). (2018). https://doi.org/10.1155/2018/1920180
25. Saengsen, C., Sookbampen, O., Wu, S., Seetasang, S., Rongwong, W., Chuaboon, L.: The potency of HPLC-DAD and LC-MS/MS combined with ion chromatography for detection/purification of levulinic acid and bio-compounds from acid hydrolysis of OPEFB. RSC Adv. **12**, 28638–28646 (2022). https://doi.org/10.1039/D2RA03563D
26. Hiller, L.A. Jr.: The reaction of cellulose with acetic acid. J. Polym. Sci. **14**, 555–577 (1954). https://doi.org/10.1002/pol.1954.120147805
27. Mouthier, T., Appeldoorn, M.M., Pel, H., Schols, H.A., Gruppen, H., Kabel, M.A.: Corn stover lignin is modified differently by acetic acid compared to sulfuric acid. Ind. Crops Prod. **121**, 160–168 (2018). https://doi.org/10.1016/j.indcrop.2018.05.008
28. Alonso, D.M., Wettstein, S.G., Mellmer, M.A., Gurbuz, E.I., Dumesic, J.A.: Integrated conversion of hemicellulose and cellulose from lignocellulosic biomass. Energy Environ. Sci. **6**, 76–80 (2013). https://doi.org/10.1039/C2EE23617F
29. Girisuta, B., Janssen, L.P.B.M., Heeres, H.J.: Kinetic study on the acid-catalyzed hydrolysis of cellulose to levulinic acid. Ind. Eng. Chem. Res. **46**, 1696–1708 (2007). https://doi.org/10.1021/ie061186z
30. Chen, W., Hu, H., Cai, Q., Zhang, S.: Synergistic effects of furfural and sulfuric acid on the decomposition of levulinic acid. Energy Fuels. **34**, 2238–2245 (2020). https://doi.org/10.1021/acs.energyfuels.9b03971
31. Thomas, R.W., Schuette, H.A.: Studies on levulinic acid. I. its preparation from carbohydrates by digestion with hydrochloric acid under pressure. J. Am. Chem. Soc. **53**, 2324–2328 (1931). https://doi.org/10.1021/ja01357a043
32. Chang, C., Cen, P., Ma, X.: Levulinic acid production from wheat straw. Bioresour Technol. **98**, 1448–1453 (2007). https://doi.org/10.1016/j.biortech.2006.03.031
33. Girisuta, B., Danon, B., Manurung, R., Janssen, L.P.B.M., Heeres, H.J.: Experimental and kinetic modelling studies on the acid-catalysed hydrolysis of the water hyacinth plant to levulinic acid. Bioresour Technol. **99**, 8367–8375 (2008). https://doi.org/10.1016/j.biortech.2008.02.045

34. Ya'aini, N., Amin, N.A.S., Asmadi, M.: Optimization of levulinic acid from lignocellulosic biomass using a new hybrid catalyst. Bioresour Technol. **116**, 58–65 (2012). https://doi.org/10.1016/j.biortech.2012.03.097
35. Liu, L., Li, Z., Hou, W., Shen, H.: Direct conversion of lignocellulose to levulinic acid catalyzed by ionic liquid. Carbohydr. Polym. **181**, 778–784 (2018). https://doi.org/10.1016/j.carbpol.2017.11.078
36. Chen, H., Yu, B., Jin, S.: Production of levulinic acid from steam exploded rice straw via solid superacid, $S_2O_8^{2-}/ZrO_2–SiO_2–Sm_2O_3$. Bioresour Technol. **102**, 3568–3570 (2011). https://doi.org/10.1016/j.biortech.2010.10.018
37. Yan, L., Yang, N., Pang, H., Liao, B.: Production of levulinic acid from bagasse and paddy straw by liquefaction in the presence of hydrochloride acid. Clean. – Soil. Air Water. **36**, 158–163 (2008). https://doi.org/10.1002/clen.200700100
38. Yang, Z., Kang, H., Guo, Y., Zhuang, G., Bai, Z., Zhang, H., Feng, C., Dong, Y.: Dilute-acid conversion of cotton straw to sugars and levulinic acid via 2-stage hydrolysis. Ind. Crops Prod. **46**, 205–209 (2013). https://doi.org/10.1016/j.indcrop.2013.01.031
39. Galletti, A.M.R., Antonetti, C., Ribechini, E., Colombini, M.P., Di Nasso, N.N., Bonari, E.: From giant reed to levulinic acid and gamma-valerolactone: A high yield catalytic route to valeric biofuels. Appl. Energy. **102**, 157–162 (2013). https://doi.org/10.1016/j.apenergy.2012.05.061
40. Ramli, N.A.S., Amin, N.A.S.: Optimization of biomass conversion to levulinic acid in acidic ionic liquid and upgrading of levulinic acid to ethyl levulinate. BioEnergy Res. **10**, 50–63 (2017). https://doi.org/10.1007/s12155-016-9778-3
41. Tiong, Y.W., Yap, C.L., Gan, S., Yap, W.S.P.: Optimisation studies on the conversion of oil palm biomass to levulinic acid and ethyl levulinate via indium trichloride-ionic liquids: A response surface methodology approach. Ind. Crops Prod. **128**, 221–234 (2019). https://doi.org/10.1016/j.indcrop.2018.10.087
42. Dussan, K., Girisuta, B., Haverty, D., Leahy, J.J., Hayes, M.H.B.: Kinetics of levulinic acid and furfural production from Miscanthus´giganteus. Bioresour Technol. **149**, 216–224 (2013). https://doi.org/10.1016/j.biortech.2013.09.006
43. Lopes, E.S., Rivera, E.C., de Jesus Gariboti, J.C., Feistel, L.H.Z., Dutra, J.V., Filho, M., Tovar, R.: Kinetic insights into the lignocellulosic biomass-based levulinic acid production by a mechanistic model. Cellulose. **27**, 5641–5663 (2020). https://doi.org/10.1007/s10570-020-03183-w
44. Ringgani, R., Azis, M.M., Rochmadi, Budiman, A.: Kinetic study of levulinic acid from *Spirulina platensis* residue. Appl. Biochem. Biotechnol. **194**, 2684–2699 (2022). https://doi.org/10.1007/s12010-022-03806-x

Waste and Biomass Valorization (2024) 15:5755–5769
https://doi.org/10.1007/s12649-024-02457-9

ORIGINAL PAPER

Techno-Economic Assessment of Ferulic Acid Bioproduction from Agro-industrial Waste Using *Aspergillus niger*

Apriliana Cahya Khayrani[1,2,4,5] · Ibnu Maulana Hidayatullah[1,2,5] · Ignatius Lintang Satyawan[2,3] · Fatimah Azizah Riyadi[1,2,5] · Nonni Soraya Sambudi[6] · Nor Hasmaliana Abdul Manas[7,8]

Received: 25 September 2023 / Accepted: 2 February 2024 / Published online: 27 March 2024

Abstract

As one of the leading countries in the agro-industrial sector, Indonesia has a wealth of biomass that can be converted into value-added commodities. The processing of this biomass generates waste containing cellulose, hemicellulose, and lignin, varying with biomass type. Valorizing this biomass presents an opportunity to enhance the profitability of agro-industries while simultaneously producing valuable chemicals like ferulic acid. Ferulic acid is a promising platform chemical that has numerous applications and significant derivative potential. This study conducts a techno-economic and profitability analysis for ferulic acid production using ferulic acid esterase (FAE) enzyme secreted from *Aspergillus niger*. We utilized SuperPro Designer v13.0 software to simulate the process, considering four scenarios: Oil palm empty fruit bunch (OPEFB), corn stover, sugarcane (SC) bagasse, and rice straw as raw materials. The results indicate that SC bagasse is the most optimal raw material, yielding 24.31% ferulic acid. This scenario offers a gross margin of 63.17%, a return on investment (ROI) of 36.27%, and a payback period of 2.76 years at an internal rate of return (IRR) of 27.47%, outperforming other scenarios. Therefore, using SC bagasse as the substrate shows the best overall assessment and simulation results. Our findings not only provide practical insights for the economic viability and sustainability of using different biomass types for high-value biochemical production but also pave the way for further exploration into the efficient utilization of regional biomass resources.

Apriliana Cahya Khayrani, Ibnu Maulana Hidayatullah and Ignatius Lintang Satyawan contributed equally to this work.

✉ Apriliana Cahya Khayrani
apriliana.cahya@ui.ac.id

[1] Department of Chemical Engineering, Bioprocess Engineering Program, Universitas Indonesia, Kampus UI Depok, Depok, West Java 16424, Indonesia

[2] Department of Chemical Engineering, Faculty of Engineering, Universitas Indonesia, Kampus UI Depok, Depok, West Java 16424, Indonesia

[3] Department of Life Sciences, Chung-Ang University, Seoul, Republic of Korea

[4] Research Center of Biomedical Engineering, Universitas Indonesia, Kampus UI Depok, Depok, West Java 16424, Indonesia

[5] Research Center of Biomass Valorization, Universitas Indonesia, Kampus UI Depok, Depok, West Java 16424, Indonesia

[6] Department of Chemical Engineering, Faculty of Industrial Technology, Universitas Pertamina, Jakarta 12220, Indonesia

[7] Faculty of Chemical and Energy Engineering, Universiti Teknologi Malaysia, Johor, Malaysia

[8] Institute of Bioproduct Development, Universiti Teknologi Malaysia, Johor, Malaysia

Graphical Abstract

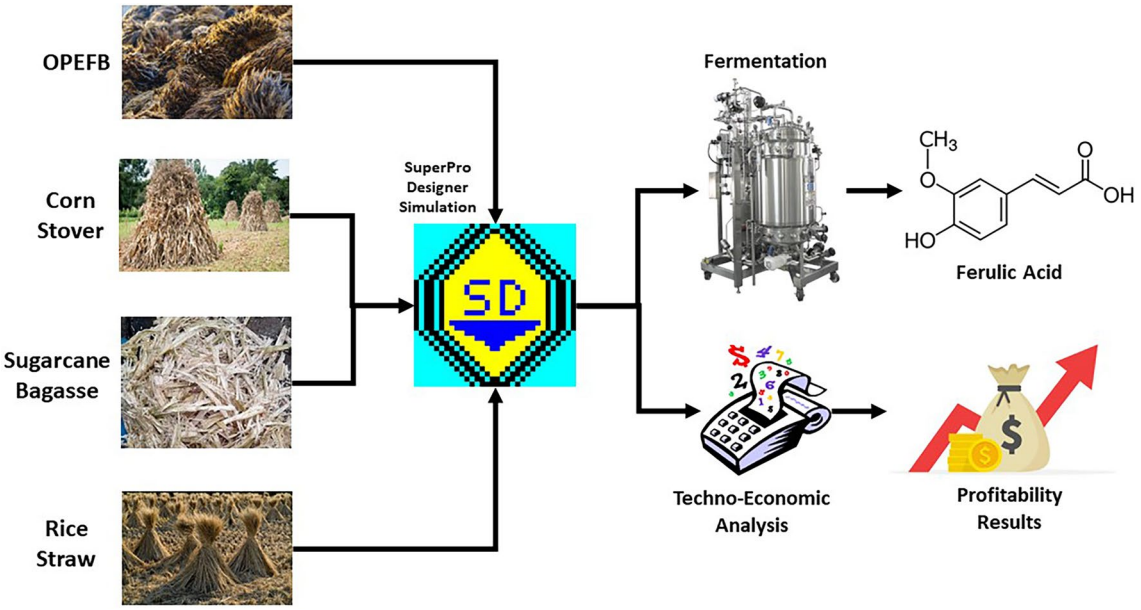

Keywords Agro-industrial biomass · *Aspergillus niger* · Ferulic acid · SuperPro designer

Statement of Novelty

At the forefront of Indonesia's agro-industrial landscape, this study introduces an innovative approach to biomass utilization, emphasizing a comprehensive techno-economic and profitability analysis for ferulic acid production. The analysis utilizes the ferulic acid esterase (FAE) enzyme secreted from *Aspergillus niger*. By employing SuperPro Designer v13.0 software, this work advances the field by simulating the process, taking into account four distinct biomass wastes: oil palm empty fruit bunch (OPEFB), corn stover, sugarcane (SC) bagasse, and rice straw as raw materials. This study not only explores the economic potential of producing ferulic acid but also highlights the diverse utilization of different biomass types. It introduces a fresh perspective on sustainable agro-industrial practices by encouraging resource-efficient approaches in the industry.

Introduction

Indonesia is the largest palm oil-producing country in the world. Based on data published by Index Mundi [1], the total production is estimated at 46,000,000 metric tons (MT) in 2022. This also means that waste production from palm oil processing facilities is the largest. In palm oil biomass waste, especially oil palm empty fruit bunch (OPEFB), there are cellulose, hemicellulose, and lignin [2, 3], which can be processed into precursors or products that can provide added value because of their benefits. In this research, the composition of OPEFB based on the study conducted by Zainudin [4] which contains 12.39% lignin, 45.06% cellulose, 28.51% hemicellulose, and 14.04% ash was employed as the initial raw material composition by weight for process simulation input.

In 2020, Indonesia's corn (*Zea mays*) production was estimated to have reached 24,050,000 MT [5]. Not only that, but corn cultivation also produces biomass waste in the form of corn stover, which is rich in cellulose, hemicellulose, and lignin [6]. By weight, corn stover is mostly made up of ~ 38% cellulose, ~ 30% hemicellulose, and ~ 20% lignin along with

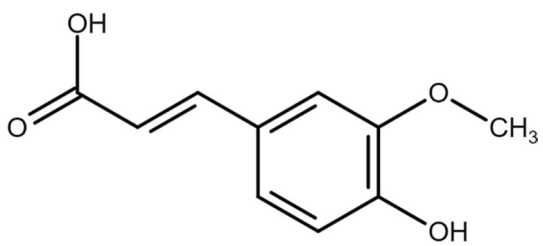

Fig. 1 Representative chemical structure of ferulic acid

small fractions of ash and extractives [7]. Because hemicellulose is abundant in corn stover, it is a promising substrate to produce ferulic acid, a hydrolysis product of hemicellulose [8, 9].

Apart from oil palm and corn, sugarcane (*Saccharum officinarum*) is also a popular source of lignocellulosic biomass [10]. Based on data published by Badan Pusat Statistik [11], the Indonesian sugarcane plantation sector is projected to grow in 2021 relative to 2020 by 2,700 hectares (4.76%) from the original 56,860 hectares to 59,380 hectares. The massive production scale of sugarcane in Indonesia resulted in great output of a side product called bagasse, which is a common biomass waste generated by its washing, processing, and separation of the juice [12]. In comparison to other substrates, sugarcane bagasse consists of around 23% lignin, 46% cellulose, 27% hemicellulose, and traces of ash [13].

In Indonesia, rice (*Oryza sativa*) is also another form of field crops that is extensively grown. Rice production output in Indonesia is anticipated to 54.42 million metric tons in 2021 (BPS, 2022). Additionally, rice farming yields rice straw, a biomass residue product that is high in cellulose, hemicellulose, and lignin [14]. Since hemicellulose makes up 28.45% of the weight of rice straw, it is a potential substance for producing ferulic acid, a lignocellulosic materials breakdown result [15].

In this study, ferulic acid is chosen as the subject because it is known as an active pharmaceutical ingredient [16]. Ferulic acid is chemical class of the phenolic acid group frequently present in plant tissues with the IUPAC name (2E)-3-(4-hydroxy-3-methoxyphenyl)prop-2-enoic acid (Fig. 1). Phenolic acids are secondary metabolites with diverse chemical structures and biological characteristics. In the plants, primarily exist in a bound state, either as esters or glycosides, lignin components, and hydrolysis tannins [17, 18]. Ferulic acid is a prevalent derivative of cinnamic acid, along with caffeic, p-coumaric, synapine, syryte, and vanillin acids [17]. Ferulic acid exhibits superior bioavailability and extended plasma retention compared to other phenolic acids, moreover, often regarded as a highly effective antioxidant [19]. Ferulic acid has numerous physiological functions, including anti-inflammatory [20, 21], antimicrobial [22], anticancer [23], anti-thrombotic [24], hypocholesterolemic activity [25], immunostimulant, and [21] cardiovascular protection. It's used in sports supplements, pharmaceutics, food, and skin care as a photoprotective agent and brightening component [26].

Since ferulic acid can be produced from hydrolysis of hemicellulose, this study explores the economic advantages of agro-industrial biomass as a raw material of crude ferulic acid production through process simulation using SuperPro Designer software. The simulation provides a quick calculation and estimation of the production process results from the feed to the final product. After simulation, techno-economic assessments are conducted to gain insight into whether agro-industrial biomass can be economically advantageous compared to other biomass sources of ferulic acid such as corn stover and sugarcane bagasse.

To develop the general flow of the production process and to identify the best substrate for optimum process scenario through mathematical calculation, the process simulation of ferulic acid production with SuperPro Designer followed by techno-economic assessment can be considered. The process starts with washing of the biomass followed by drying and grinding. Then, the biomass grounds are delignified in an

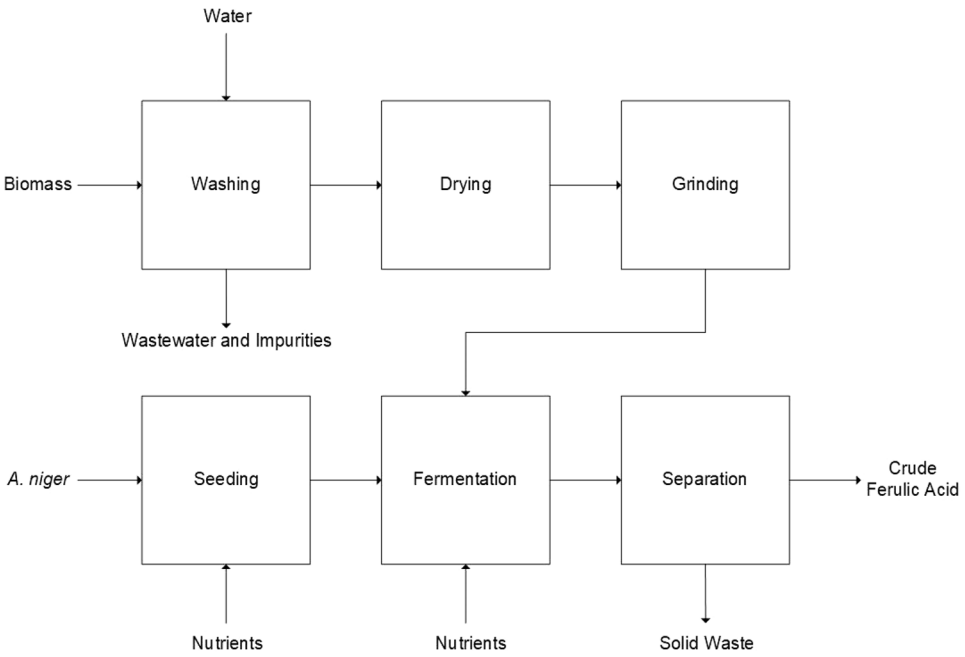

Fig. 2 Block flow diagram of ferulic acid production

alkaline pretreatment using 1M NaOH [27] , which is filtered to remove the dissolved lignin. The biomass is then fed into a bioreactor along with the fungal cell culture, and fermentation occurs for the fungi to grow and express the ferulic acid esterase (FAE) enzyme. This same enzyme acts as a catalyst for water molecules in hydrolysis to break down arabinoxylan within the biomass and release ferulic acid [28]. At the end of the process, the result of fermentation is introduced into a freeze-dryer to disrupt the cells and separate water contents to obtain ferulic acid and residual FAE. After the overall process simulation is complete, a techno-economic assessment can be conducted to calculate the total cost of the facility construction project, production materials, and operational expenses, as well as provide insight into its profitability, sensitivity, and return on investment based on the global market price of ferulic acid.

After the stoichiometric mass balance calculation results are obtained, the prices for materials, industrial microorganism culture, equipment, utilities, and operator salaries are adjusted according to the provincial minimum wage of Riau province, the largest palm oil-producing region in Indonesia, to conduct a study of the required economic parameters, namely Net present value (NPV), Internal rate of return (IRR), gross margin, and payback period (PBP). The assumed location of the plant is in Riau province, Indonesia. The data were collected in the form of reports and executive summaries exported from the SuperPro Designer v13.0 and analyzed to synthesize the conclusions and suggestions regarding the research.

Materials and Methods

This research begins with a literature study of journals, reviews, articles, and scientific works related to ferulic acid production from agro-industrial wastes using enzymatic hydrolysis. Then, the data and parameters obtained from the literature study are inputted into the SuperPro Designer v13.0 software for computation and process simulation to obtain an overview of the production process and the stoichiometric mass balance calculation results. This process simulation is divided into four scenarios, namely Scenario A, which uses OPEFB. Scenario B uses corn stover, Scenario C uses sugarcane bagasse, and Scenario D uses rice straw.

Table 1 Post-washing composition of the scenario A feed

Component	Flowrate (kg/batch)	Mass composition (%)
Ash	0.016	0.0016
Cellulose	523.343	50.889
Hemicellulose	331.125	32.198
Lignin	143.901	13.992
Water	30.000	2.917
Total	1028.385	100

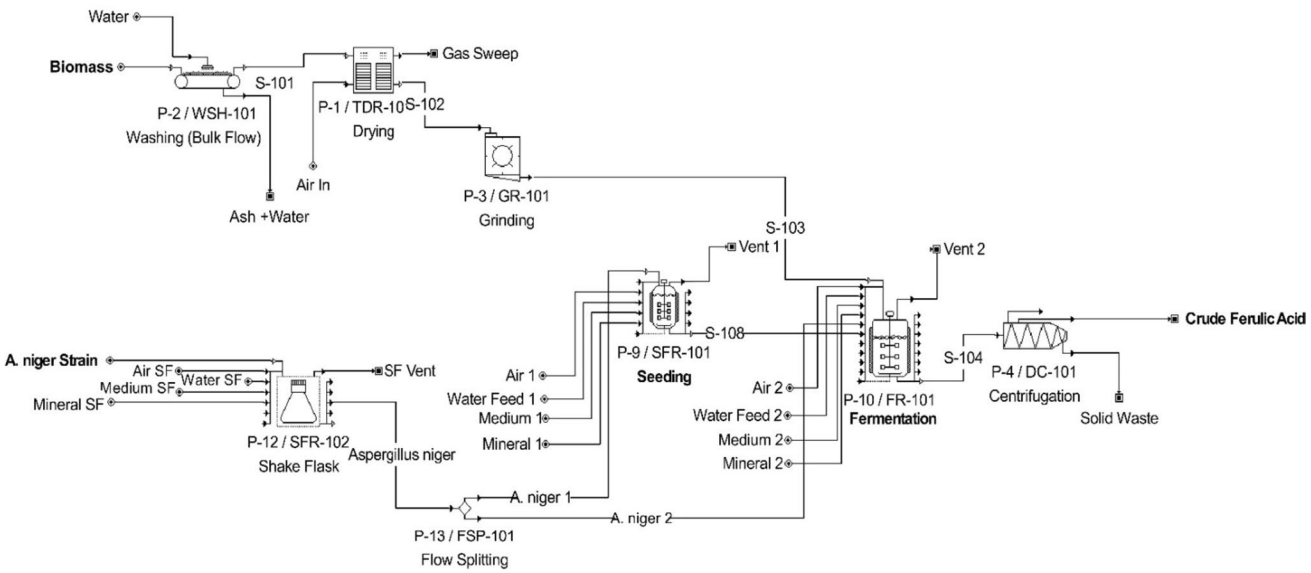

Fig. 3 Complete process flow diagram of ferulic acid production using *Aspergillus niger*

Table 2 Composition of the scenario A product

Component	Flowrate (kg/batch)	Mass composition (%)
Carbohydrates	0.454	0.100
Cell	33.437	7.386
Cellulose	5.233	1.156
FAE	16.096	3.555
Ferulic Acid	298.193	65.865
Hemicellulose	3.304	0.729
Laccase	26.827	5.925
Lignin Peroxidase	20.388	4.503
Potassium	0.019	0.004
Proteins	0.099	0.022
Sulfur	0.013	0.003
Water	48.667	10.7496
Total	452.734	100

Table 3 Post-washing composition of the scenario B feed

Component	Flowrate (kg/batch)	Mass composition (%)
Ash	1.050	0.113
Cellulose	380.800	41.121
Hemicellulose	307.200	33.173
Lignin	207.000	22.353
Water	30.000	3.240
Total	926.050	100

Process Mass Balance Evaluation

Preparation of Materials

The production process of ferulic acid from agro-industrial biomass is modeled after the processes described in studies published by Converti et al. [29], Sharma et al. [30], and Ou et al. [31] with some modifications to adapt to the SuperPro Designer software. The process is conducted in a batch with the starting number of biomass materials at 1000 kg per batch (Fig. 2).

First, the biomass is washed to remove any debris and other physical impurities. Then, the biomass is put into a machine dryer to remove any moisture. After the biomass is dried, it can be processed in a grinder to turn it into ground, allowing for a smaller surface area, which allows easier processing. The biomass grounds are then used as the carbon source and substrate for fermentation using *Aspergillus niger* to produce ferulic acid. *Aspergillus niger* was previously reported to have the ability to secrete enzymes for delignification, such as lignin

Table 4 Composition of the scenario B product

Component	Flowrate (kg/batch)	Mass composition (%)
Carbohydrates	0.454	0.114
Cell	24.355	6.095
Cellulose	3.808	0.953
FAE	11.712	2.931
Ferulic Acid	276.776	69.267
Hemicellulose	3.067	0.768
Laccase	19.520	4.885
Lignin Peroxidase	14.835	3.713
Potassium	0.020	0.005
Proteins	0.100	0.025
Sulfur	0.013	0.003
Water	44.916	11.241
Total	399.576	100

Table 5 Post-washing composition of the scenario C feed

Component	Flowrate (kg/batch)	Mass composition (%)
Ash	0.400	0.040
Cellulose	460.000	46.446
Hemicellulose	270.000	27.262
Lignin	230.000	23.223
Water	30.000	3.029
Total	990.400	100

Table 6 Composition of the scenario C product

Component	Flowrate (kg/batch)	Mass composition (%)
Carbohydrates	0.454	0.118
Cell	29.401	7.676
Cellulose	4.600	1.201
FAE	14.148	3.694
Ferulic Acid	243.107	63.468
Hemicellulose	2.694	0.703
Laccase	23.580	6.156
Lignin Peroxidase	17.921	4.679
Potassium	0.020	0.005
Proteins	0.100	0.026
Sulfur	0.013	0.003
Water	47.001	12.271
Total	383.039	100

peroxidase and laccase [32] and ferulic acid esterase [33] to produce ferulic acid. Before the fermentation, an inoculum of *Aspergillus niger* is prepared during a seeding process and nourished with water, minerals, and flour-based medium until the culture weight of 1.23 kg is achieved. The post-seeding culture is introduced into a 200L fermenter along with the delignified biomass. During the 48 h of fermentation, the biomass is hydrolyzed with the help of ferulic acid esterase (FAE) enzyme catalyst secreted by the *Aspergillus niger*, releasing ferulic acid as the product. The complete process flow diagram and the equipment employed in the proposed production facility can be seen in Fig. 3

Results and Discussion

Material Balance Analysis

The material balance of each scenario is conducted to determine the yield of the ferulic acid production from each scenario. The calculation starts from the initial composition of lignocellulosic biomass post-washing and the final composition of the product. The mass flow of ferulic acid, the mass flow of hemicellulose residue in the product, and the initial mass flow of hemicellulose are the parameters of ferulic acid yield calculation. In this production process, the hemicellulose of the agro-industrial biomass is the material that is broken down to release ferulic acid. The yield of ferulic acid against the initial mass of biomass raw materials production ($Y_{P/S}$) from each scenario is calculated using Eq. 1 [34].

$$Y_{P/S}(\%) = \frac{Mass\ of\ Ferulic\ Acid}{Initial\ Mass\ of\ Biomass} \times 100\% \quad (1)$$

Material Balance of Scenario A

Scenario A employs the utilization of 1000 kg OPEFB as the raw material of ferulic acid production, with the use of a machine dryer to remove moisture. In this scenario, the primary composition of the feed per batch consists of 523 kg of cellulose, 331.12 kg of hemicellulose, and 143.90 kg of lignin (Table 1). After the raw material is pretreated and processed, the product contains 298.19 kg of ferulic acid, 16.096 kg of ferulic acid esterase, and 3.30 kg of residual hemicellulose (Table 2). Based on the calculation using Eq. 1, the yield of ferulic acid from OPEFB is 26.83%.

Table 7 Post-washing composition of the scenario D feed

Component	Flowrate (kg/batch)	Mass composition (%)
Ash	1.938	0.231
Cellulose	341.000	40.685
Hemicellulose	284.000	33.885
Lignin	181.200	21.619
Water	30.000	3.579
Total	838.138	100

Table 8 Composition of the scenario D product

Component	Flowrate (kg/batch)	Mass composition (%)
Carbohydrates	0.454	0.123
Cell	21.819	5.902
Cellulose	3.410	0.923
FAE	10.488	2.837
Ferulic Acid	255.887	69.222
Hemicellulose	2.835	0.767
Laccase	17.480	4.729
Lignin Peroxidase	13.285	3.594
Potassium	0.020	0.005
Proteins	0.100	0.027
Sulfur	0.013	0.004
Water	43.869	11.867
Total	369.660	100

Material Balance of Scenario B

Scenario B employs the utilization of 1000 kg corn stover as the raw material of ferulic acid production, with the use of a machine dryer to remove moisture. In this scenario, the primary composition of the feed per batch consists of 380.8 kg of cellulose, 307.2 kg of hemicellulose, and 207 kg of lignin

Table 9 Direct capital cost of biomass facility project

No	Project item	Cost (US$)
1	Equipment purchase	110,000
2	Installation	51,000
3	Piping	39,000
4	Instrumentation	44,000
5	Insulation	3,000
6	Electrical	11,000
7	Buildings	50,000
8	Yard improvement	17,000
9	Auxiliary facilities	44,000
10	Engineering	92,000
11	Construction	129,000
12	Contractor's fee	30,000
13	Contingency	59,000
Direct Fixed Capital Cost		679,000

Table 10 Raw material cost of scenario A (OPEFB)

Bulk Material	Unit Cost (US$)	Annual Amount	Unit	Annual Cost (US$)	Cost (US$/ton MP)	Cost distribution (%)
A. niger	2.52	450.00	g	1,134.00	50.47	2.62
Sterile Air	0.00	43,961.00	kg	0.00	0.00	0.00
EFB	21.95	30.00	ton	653.00	29.08	1.51
Mineral Solution	26.00	156.00	L	4,061.00	180.75	9.38
NaOH	29.03	1,274.00	ton	36,989.00	1646.31	85.41
Water	0.00	12,285.00	kg	10.00	0.44	0.02
Wheat Flour	1.02	288.00	kg	294.00	13.07	0.68
Total				43,141.00	1,920.13	100.00

Table 11 Raw material cost of scenario B (corn stover)

Bulk Material	Unit Cost (US$)	Annual Amount	Unit	Annual Cost (US$)	Cost (US$/ton MP)	Cost distribution (%)
A. niger	2.52	450.00	g	1,134.00	46.60	2.63
Sterile Air	0.00	46,082.00	kg	0.00	0.00	0.00
Corn Stover	34.59	30.00	ton	1,029.00	0.00	0.00
Mineral Solution	26.00	156.00	L(STP)	4,061.00	166.88	9.43
NaOH	29.03	1,288.00	ton	37,389.00	1536.45	86.84
Water	0.00	12,285.00	kg	10.00	0.41	0.02
Wheat Flour	1.02	288.00	kg	294.00	12.07	0.68
Total				30,274.00	2,925.13	100.00

Table 12 Raw material cost of scenario C (sugarcane bagasse)

Bulk Material	Unit Cost (US$)	Annual Amount	Unit	Annual Cost (US$)	Cost (US$/ton MP)	Cost distribution (%)
A. niger	2.52	325.00	g	819.00	82.22	2.69
Sterile Air	0.00	27,204.00	kg	0.00	0.00	0.00
Mineral Solution	26.00	113.00	L	2,933.00	294.44	9.63
NaOH	29.03	881.00	ton	25,573.00	2,567.28	84.00
Sugarcane Bagasse	36.26	21.00	ton	779.00	78.25	2.56
Water	0.00	8,873.00	kg	7.00	0.72	0.02
Wheat Flour	1.02	208.00	kg	212.00	21.30	0.70
Total				30,324.00	3,044.20	100.00

Table 13 Raw material cost of scenario D (rice straw)

Bulk Material	Unit Cost (US$)	Annual Amount	Unit	Annual Cost (US$)	Cost (US$/ton MP)	Cost distribution (%)
A. niger	2.52	450.00	g	1,134.00	82.22	2.69
Air	0.00	33,227.00	kg	0.00	0.00	0.00
Mineral Solution	26.00	156.00	L	4.061.00	294.44	9.63
NaOH	29.03	1,167.00	ton	33,892.00	2,567.28	84.00
Rice Straw	0.03	27.00	ton	918.00	78.25	2.56
Water	0.00	12,285.00	kg	10.00	0.72	0.02
Wheat Flour	1.02	288.00	kg	294.00	21.30	0.70
Total				40,308	3,044.20	100.00

(Table 3). After the raw material is pretreated and processed into the product, the product contains 276.77 kg of ferulic acid, 11.71 kg of ferulic acid esterase, and 3.067 kg of residual hemicellulose (Table 4). Based on the calculation using Eq. 1, the yield of ferulic acid from corn stover is around 27.68%.

Material Balance of Scenario C

Scenario C employs the utilization of 1000 kg sugarcane bagasse as the raw material of ferulic acid production, with the use of a machine dryer to remove moisture. In this scenario, the primary composition of the feed per batch consists of 460 kg of cellulose, 270 kg of hemicellulose, and 230 kg of lignin (Table 5). After the raw material is pretreated and processed into the product, the product contains 243.11 kg of ferulic acid, 14.15 kg of ferulic acid esterase, and 2.69 kg of residual hemicellulose (Table 6). Based on the calculation using Eq. 1, the yield of ferulic acid from sugarcane bagasse is around 24.31%.

Material Balance of Scenario D

Scenario D uses 1000 kg of rice straw as the raw material for the manufacture of ferulic acid. In this case, the main components of the feed in each batch are 181.2 kg of lignin, 284 kg of hemicellulose, and 102 kg of cellulose (Table 7). The finished product comprises 341 kg of leftover hemicellulose and 255.89 kg of ferulic acid after the feedstock has been pretreated and handled into it. It also contains 10.49 kg of ferulic acid esterase (Table 8). The production of ferulic acid from rice straw is approximately 25.59%, according to the estimate made with Eq. 1.

Table 14 Equipment specification

Code	Type	Units	Capacity	Material of construction
WSH-101	Biomass Washer	1	600 kg/h	CS
TDR-101	Machine Dryer	1	11.28 m2	SS316
GR-101	Grinder	1	257.88 kg/h	CS
SFR-101	Shaker Incubator	1	4.00 L	CS
SFR-102	Seed Fermenter	1	1.46 L	SS316
FR-101	Fermenter	2	155.97 L	SS316
FDR-101	Freeze-Dryer	1	118.93 kg	SS316
FSP-101	Flow Splitter	1	2.09 kg/h	CS

Table 15 List of equipment cost

Code	Type	Units	Unit Cost (US$)	Cost (US$)
WSH-101	Biomass Washer	1	6,000	6,000
TDR-101	Machine Dryer	1	4,000	4,000
GR-101	Grinder	1	4,000	4,000
SFR-101	Shaker Incubator	1	8,000	8,000
SFR-102	Seed Fermenter	1	30,000	30,000
FR-101	Fermenter	2	70,000	140,000
FDR-101	Freeze-Dryer	1	10,000	10,000
Unlisted Equipment				50,000
Total				251,000

Economic Analysis

Economic evaluation is conducted to measure and determine the profitability of each scenario employed in this research. There are four scenarios provided in the process simulation and techno-economic analysis. The parameters for techno-economic analysis are based on the previous studies published by Hidayatullah et al. [35] and Harahap et al. [36], which include capital expenditure (CAPEX), operational expenditure (OPEX), revenues, production capacity, production cost, gross margin, return of investment (ROI), payback period (PBP), internal rate of return (IRR), and net present value (NPV) of the project scenarios. The parameters then subjected to sensitivity analysis to measure the impact of external factors such as changes in product price, raw materials, and labor cost against the economic simulation results.

Project Cost

Since the facility needs to be constructed before the production process can start, the project cost is the first to be determined at the early stages. The data from the Table 9 is obtained from the economic simulation results of the SuperPro Designer program and it shows that the factors affecting the disparity in project capital cost primarily came from equipment purchase, installation, buildings, engineering, and construction. In this case, the cost in the following table is

Table 16 List of labour costs of each scenario

Labor Type	Scenario	Unit Cost (US$/h)	Annual Amount (h)	Annual Cost (US$)
Operator	A	2.71	24,950	70,429
	B	2.71	19,021	51,623
	C	2.71	18,768	50,937
	D	2.71	25,907	70,313

the expected number needed for the project to be completed on time.

Raw Materials Cost

Raw material cost is an important part of techno-economic analysis because the process involves agro-industrial biomass of different types; oil palm empty fruit bunch (OPEFB), corn stover, and sugarcane bagasse. Consequently, the scenarios have different raw material costs as well (Table 10, 11, 12, 13). The materials' cost estimate is based on the price of the reagents and materials in the online marketplace such as Alibaba, which is inputted into the SuperPro Designer program as the estimate.

Process Equipment

Equipment Specification

SuperPro Designer used a designer mode to generate the specifications from every piece of equipment throughout this modeling. All equipment was estimated based on throughput into the piece of equipment. Optimum sizing and calculations determine the most suitable equipment specification for the whole process. The complete specification of the equipment is described in Table 14. This specification applies to all scenarios.

Equipment Cost

Equipment cost is also important in techno-economic analysis because every industrial processor needs equipment to process the raw materials into the precursors or the final product. The equipment cost input is based on the market price of bioprocess equipment by the vendor (Bailun Biotechnology, China) and this cost assessment was calculated using the SuperPro Designer software (Table 15). Around US$251,000.00 is required to procure all the necessary process equipment and its supporting elements to construct the facility.

Table 17 Utility cost comparison

Scenario	Utility	Unit Cost (US$/h)	Annual Amount	Unit	Annual Cost (US$)	Total Utility Cost (US$/year)
A	Power	0.10	10,599	kWh	1,060	1,553
	Steam	12.00	24	MT	292	
	Chilled Water	0.40	503	MT	201	
B	Power	0.10	7,575	kWh	758	1,087
	Steam	12.00	16	MT	190	
	Chilled Water	0.40	348	MT	139	
C	Power	0.10	7,691	kWh	769	1,127
	Steam	12.00	18	MT	213	
	Chilled Water	0.40	361	MT	144	
D	Power	0.10	9,607	kWh	961	1,378
	Steam	12.00	20	MT	242	
	Chilled Water	0.40	439	MT	176	

Table 18 Waste disposal cost comparison

Scenario	Type of Waste	Annual Amount	Unit	Annual Cost (US$)	Total Cost (US$/year)
A	NaOH + Lignin	5,596	Kg	1,007	4,193
	Cells + Water	11	m^3	3,185	
B	NaOH + Lignin	5,749	Kg	1,035	3,095
	Cells + Water	7	m^3	2,063	
C	NaOH + Lignin	6,110	Kg	1,100	3,442
	Cells + Water	8	m^3	2,342	
D	NaOH + Lignin	7,143	Kg	1,286	3,901
	Cells + Water	9	m^3	2,615	

Table 19 Annual operating cost data

Cost Item	Cost (US$)			
	A	**B**	**C**	**D**
Raw Materials	42,000	30,000	30,000	40,000
Labor-dependent	70,000	52,000	51,000	70,000
Facility-dependent	128,000	128,000	128,000	128,000
Laboratory QC / QA	11,000	8,000	8,000	11,000
Consumables	400	257	267	321
Waste Disposal	4,000	3,000	3,000	4,000
Utilities	2,000	1,000	1,000	1,000
Total	257,400	222,257	221,267	255,321

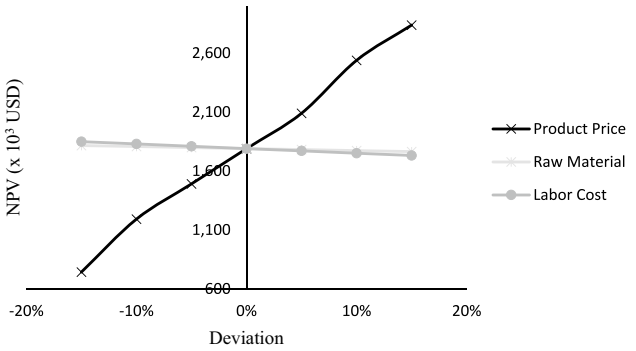

Fig. 4 Sensitivity analysis of product price, raw materials, and labor cost toward net present value (NPV)

Labor Cost

The labor costs in the following table were calculated utilizing the starting price out from the minimum labor wage of Riau province for the year 2023 (Gubernur [37]). An industrial worker is entitled to receive at least US$ 207.11 per month, which translates to US$1.18 per hour for this modeling. Several variables were added to the starting cost to accommodate for the benefits factor of 0.4, operational consumables factor of 0.1, supervisory factor of 0.2, and administrative of 0.6. The final unit cost generated after the SuperPro is US$2.71 per hour of labor (Table 16). After the process scheduling is complete, the SuperPro economic analysis feature calculates the total labor cost per annum of each scenario. From the following table, Scenario A has the highest annual labor cost, meanwhile Scenario C has the lowest labor cost due to the shortest time of manual work needed in the whole manufacturing process compared to another scenario.

Utility Cost

The economics of the power is based on the calculation of electricity prices based on the Perusahaan Listrik Negara (PLN) tariff for class B-2/TR of US$0.1/kWh in accordance to the Minister of Energy and Mineral Resources of the Republic of Indonesia Regulation No. 28 of Year 2016 [38]. Meanwhile, the cost of steam and chilled water utilities is based on the estimations of the SuperPro Designer software. Based on comparing utility costs for each scenario, it is known that Scenario A was the scenario with the highest consumption, and Scenario B was the lowest, so it is cost-effective for utility use. Utility usage was influenced by the composition of materials and the needs of each means of production. The difference in utility usage had no significant effect on yield. The comparison of each scenario's utility cost can be seen in Table 17. Based on the following table, electric power is the utility with the largest usage because it is an important workforce of the process equipment. Water and steam is utilized for the cleaning and

Table 20 Economic parameters of ferulic acid production using *Aspergillus niger*

Parameter	Unit	Scenario			
		A	**B**	**C**	**D**
Capital Expenditure (CAPEX)	US$	1,593,000	1,594,000	1,594,000	1,593,000
Operational Expenditure (OPEX)	US$/year	410,000	411,000	412,000	409,000
Revenues	US$/year	917,000	993,000	1,041,000	897,000
Raw Materials Cost	US$/year	43,000	44,000	45,000	43,000
Ferulic Acid Production Capacity	ton MP/year	22.47	24.33	25.51	21.98
Ferulic Acid Price	US$/kg	45.00	45.00	45.00	45.00
Unit Production Cost	US$/ton MP	18,242.63	16,871.84	16,144.18	18,605.40
Unit Production Revenue	US$/ton MP	40,823.31	40,823.31	40,823.31	40,823.31
Gross Margin	%	55.31	58.67	63.17	54.42
ROI	%	28.09	30.93	32.69	27.38
PBP	years	3.56	3.23	2.76	3.65
IRR	%	20.86	23.20	27.47	20.23
NPV	US$	1,589,000	1,915,000	2,116,000	1,508,000

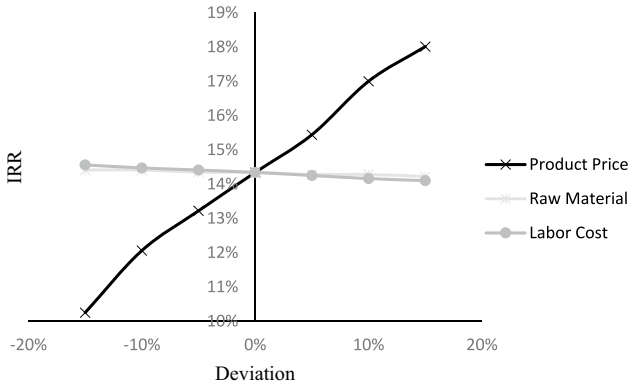

Fig. 5 Sensitivity analysis of product price, raw materials, and labour cost toward internal rate of return (IRR)

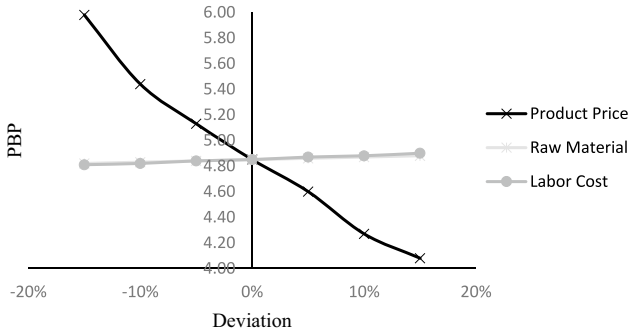

Fig. 6 Sensitivity analysis of product price, raw materials, and labor cost toward payback period (PBP)

Table 21 Yields of ferulic acid versus raw material mass

Scenario	Biomass	Yield (%)
A	OPEFB	26.97
B	Corn Stover	29.09
C	Sugarcane Bagasse	24.31
D	Rice Straw	26.89

sterilization-in-place of the equipment to maintain its cleanliness as part of the good manufacturing practices.

Waste Disposal

The plant utilized third-party waste disposal and treatment services. The waste generated in the processes are categorized into chemical waste and biological waste. Both types need special treatment to reduce its environmental risk before disposal. Statista [39] states that the typical pharmaceutical production waste treatment service cost is 0.17 euros per m^3, equivalent to US$0.18 per m^3. Based on the data in the following table (Table 18), it can be known that Scenario A had the largest waste output compared to other scenarios; with Scenario B, the scenario was the least (Table 18). The cost of waste treatment increased along with the rise in waste output. Scenario B is an environmentally friendly alternative to all other processes because it offers both economic and environmental advantages.

Operational Cost

The calculation of the economics of the power is based on the following factors: raw materials cost, labor costs, facility-dependent costs (equipment, maintenance, etc.), laboratory equipment uses, consumable items, waste output and use of disposal services, and total utilities. Based on the data shown in Table 19, it is shown that Scenario A has the highest operational cost of US$257,400. Meanwhile, Scenario C has the lowest operational cost of US$221,267. This could be affected by substrate-related factors such as substrate density.

Profitability Analysis

After the stoichiometric mass balance calculation results are obtained, the prices for materials, industrial microorganism culture, equipment, utilities, and operator salaries are adjusted according to the provincial minimum wage of Riau province as the largest palm oil-producing region in Indonesia to conduct a study of the required economic parameters, namely NPV, IRR, gross margin, and payback period (PBP) without sensitivity analysis (Table 20). The data is collected as reports and executive summaries exported from the SuperPro Designer software. They are used to synthesize the conclusions and suggestions regarding the research.

According to the economic study conducted in SuperPro Designer, all scenarios provide a Gross Margin of over 50% and a payback period of 3–4 years. This suggests that the biomass included in the simulation experiment have great potential for industrial-scale utilization. However, when evaluated in terms of NPV, IRR, ROI, and other economic indicators, scenario C exhibits the highest level of profitability. After the economic parameters are specified for sensitivity analysis, the sensitivity graph is generated and shown below in Figs. 4, 5 and 6.

The results showed that deviations in raw materials and labor costs are less influential in affecting the economic parameters of this study. However, an increase in both parameters will generate dropped NPV and slower IRR due to an escalated annual cost resulting in a longer payback period of the production facility. Conversely, if there is a decrease in raw material and labor costs, the NPV will increase and boost the IRR, eventually resulting in a faster payback period. The deviations in raw materials and labor costs are relatively stable and do not cause many changes in

Table 22 Previous studies regarding techno-economic analysis of biomass processing using SuperPro Designer

Research	Substrate	Process	Product	IRR	NPV	PBP
Karimah et al. [40]	OPEFB	Acid hydrolysis	Furfural	49.77%	US$ 39,210,000	1.75 years
Safaat & Wulan[43]	Napier Grass	Fermentation and Anaerobic digestion	Bioethanol and Biogas	11.32%,	US$ 23,382,883.03	7.2 years
Taiwo et al. [45]	Glucose	Fermentation	Cellulase Enzyme	36.95%	US$140,328,000	1.88 years
Fredsgaard et al. [44]	*Salicornia sp.*	Hydrogenation, hydrodeoxygenation, hydrocracking, and isomerization	Jet Fuel	10%	US$150,000,000	7 years
This research	OPEFB	Fermentation and enzymatic hydrolysis	Ferulic Acid	20.86%	US$1,589,000	3.56 years
	Corn Stover			23.20%	US$1,915,000	3.23 years
	SC Baggase			27.47%	US$2,116,000	2.76 years
	Rice Straw			20.23%	US$1,508,000	3.65 years

the parameters. However, based on the graphs above, ferulic acid price as the product is the most sensitive factor that can economically affect the parameters. Even a slight increase of 5% in ferulic acid price can boost the IRR to 22.11% and shorten the payback period from 3.56 years to 3.38 years. The sensitivity analysis results show that better profitability can be gained by maintaining relatively constant raw material costs and labor costs, while slightly increasing the product selling price.

Based on this in silico study of the bioproduction of ferulic acid from three different types of agro-industrial biomass, it can be concluded that each biomass type can produce ferulic acid with different yields. The yield of ferulic acid versus initial raw material mass can be seen in Table 21, where the ferulic acid from OPEFB has a yield of 26.97%, meanwhile, the ferulic acid from corn stover has a yield of 29.09%, then 25.54% from sugarcane bagasse, and 26.89% from rice straw as well. When comparing the economic assessment results, it is discovered that the revenue of unit production of all scenarios is similar, most likely due to the same selling price of ferulic acid at US$45.00 per kg. However, the profitability results of each scenario are different because they all have different values of product yield as well as material and operational costs. If the yield is greater and combined with a lower operational cost (OPEX), profitability can be considered optimum. A comparison between the OPEX results showed that Scenario D has the most affordable operational expenditure at a rate of US$409,000 / year, followed by Scenario A which costs US$410,000 / year, and Scenario C which is the highest at US$412,000 / year. When it comes to the PBP, it was discovered that the duration for Scenario C to achieve it only needs 2.76 years which is the shortest among all Scenarios. In this factor, Scenario D has the longest PBP at 3.65 years. On the other hand, the PBP duration for Scenario A is 3.56 years. This can be further explained by comparing the ROI results where an increase in ROI coincides with a shorter PBP in every scenario. Scenario C has the greatest ROI at 32.69%, meanwhile Scenario D has the least value at 27.38%. The ROI value of Scenario A itself stands at 28.09%. The same also applies to the IRR where Scenario C has the best IRR value at 27.47% and the IRR of Scenario D is 20.23%, which is the lowest. Scenario A is positioned between these at 20.86% IRR. Lastly, in the NPV results, Scenario D as the NPV of US$1,508,000, followed by Scenario A at US$1,589,000, then Scenario B at US$1,915,000, and Scenario C at US$2,116,000. Based on the data of the results, it can be taken into conclusion that Scenario D is the least profitable scenario because it has the lowest NPV, IRR, ROI, and the slowest PBP among all scenarios, despite it having the best advantage in terms of operational cost. From the results also, Scenario C can be considered as the most economically profitable scenario. However, in terms of the product yield, it is not as high as the yield of Scenario A, where the ferulic acid yield of 26.97% from OPEFB is greater than 25.54% yield from sugarcane bagasse (Table 21). Therefore, Scenario A can be considered the most optimum scenario in consideration of both the technical and economic aspects.

When compared with previous studies conducted by Karimah et al. [40] as shown in the Table 22 which utilizes the same substrate, OPEFB, and an almost identical hydrolysis-based process, the comparison shown that the IRR of this study is not as high as in the previous studies by Karimah et al. [40] which consequently has a faster payback period of initial investment in just 1.75 years, whereas in this study the IRR is 20.86% and the payback period is more than twice longer than the latter. One of the most possible factors that can explain this phenomenon could be the difference in the desired product market size. According to a study published by Grand View Research [41], the market size of furfural is calculated up to US$556,740,000 in the year 2022. On the other hand, the market size of ferulic acid in the same year is estimated to have reached the number of US$68,610,000 [42]. This means that in the global market, furfural has a higher demand than ferulic acid. However, this study has

a better IRR and faster payback period when compared with the result of the studies by Safaat & Wulan [43] and Fredsgaard et al. [44]. Despite the popularity of bioethanol and jet fuel in the current trend of global market, the factor could be the utilization of Napier grass and *Salicornia sp*. as a substrate is not as widespread as OPEFB and mostly experimental.

Therefore, the production of furfural could be more profitable than ferulic acid. In order to enhance the profitability of ferulic acid bioproduction, further research and development is needed to explore the potential use of ferulic acid in industries other than cosmeceuticals in order to increase its market demands, or by optimizing the production process through the use of a more affordable industrial microbe strain and reducing the usage of materials and energy in the production facility while keeping attention to the boundaries so that it would not negatively affect the yield nor the product output.

From the results of the techno-economic analysis of each scenario in this study, Scenario C, which utilizes SC Baggase, is the most profitable with a gross margin of 63.17%, and 36.27% ROI with the expected return in 2.76 years at IRR of 27.47%. Although ferulic acid from OPEFB has a lower yield than ferulic acid from corn stover, the profitability is influenced by the affordability of raw materials, different operating conditions, utilities and energy use, operating costs, and annual revenues.

Conclusions

This paper successfully conducted techno-economic analysis on the ferulic acid production using enzymes from *Aspergillus niger* culture. Based on the results of the study, difference in ferulic acid yields based on agro-industrial biomass type is affected by its hemicellulose content, especially arabinoxylan. In this case, it is discovered that the corn stover has the highest yield at 29.09% of ferulic acid in their product compared to OPEFB and sugarcane bagasse. Moreover, this research provided proof that utilization of SC Baggase as the raw material is the most optimum scenario with a gross margin of 63.17%, and 32.69% ROI with a payback period of 2.76 years at IRR of 27.47%. Regarding the economic sensitivity of the ferulic acid production process, better profitability can be gained by maintaining relatively constant raw material costs and labor costs, while slightly increasing the product selling price. In the future, validation is needed to confirm the process simulation results and product quality. In addition, economic aspects of cleanroom, energy use in laminar airflow systems, sterile equipment, and protective personnel equipment should also be considered, as every cosmeceutical manufacturing industry must comply with the principles of good manufacturing practices or GMP standards.

Funding This research was partly supported by Q2 Scheme Research Grant (Hibah Publikasi Artikel di Jurnal Internasional Kuartil Q2) No. NKB-678/UN2.RST/HKP.05.00/2022 from Directorate Research and Development Universitas Indonesia awarded to Apriliana Cahya Khayrani, Ph.D.

Data Availability Enquiries about data availability should be directed to the authors.

Declarations

Competing Interests The authors have not disclosed any competing interests.

References

1. Index Mundi (2023). Indonesia Palm Oil Production by Year. March 20, 2023. https://www.indexmundi.com/agriculture/?commodity=palm-oil&country=id&graph=production
2. Harsono, H., Putra, A.S., Maryana, R., Rizaluddin, A.T., H'ng, Y. Y., Nakagawa-izumi, A., & Ohi, H.: Preparation of dissolving pulp from oil palm empty fruit bunch by prehydrolysis soda-anthraquinone cooking method. J. Wood Sci. **62**(1), 65–73 (2015)
3. Rathamat, Z., Choorit, W., Chisti, Y., Prasertsan, P.: Two-step isolation of hemicellulose from oil palm empty fruit bunch fibers and its use in production of xylooligosaccharide prebiotic. Ind. Crops Prod. **160**, 113124 (2021)
4. Zainudin, M.H., Abdul Rahman, N.A., Abd-Aziz, S., Funaoka, M., Shinano, T., Shirai, Y., Wakisaka, M., Hassan, M.: Utilization of glucose recovered by phase separation system from acid-hydrolysed oil palm empty fruit bunch for bioethanol production. Pertanika J. Trop. Agric. Sci. **35**, 117–126 (2012)
5. ASEAN Statistical Yearbook. (2021). ASEAN Statistical Yearbook 2021. The Asian Secretariat. https://www.aseanstats.org/wp-content/uploads/2021/12/ASYB_2021_All_Final.pdf
6. Mourtzinis, S., Cantrell, K.B., Arriaga, F.J., Balkcom, K.S., Novak, J.M., Frederick, J.R., Karlen, D.L.: Carbohydrate and nutrient composition of corn stover from three southeastern USA locations. Biomass Bioenerg. **85**, 153–158 (2016)
7. Vincent, M., Pometto, A., III., Van Leeuwen, H.: Simultaneous Saccharification and Fermentation of Ground Corn Stover for the Production of Fuel Ethanol Using Phanerochaete chrysosporium, Gloeophyllum trabeum, Saccharomyces cerevisiae, and Escherichia coli K011. J. Microbiol. Biotechnol. **21**, 703–710 (2011)
8. Valério, R., Crespo, J.G., Galinha, C.F., Brazinha, C.: Effect of Ultrafiltration Operating Conditions for Separation of Ferulic Acid from Arabinoxylans in Corn Fibre Alkaline Extract. Sustainability **13**(9), 4682 (2021)
9. Valério, R., Serra, A.T., Baixinho, J., Cardeira, M., Fernández, N., Bronze, M.R., Brazinha, C.: Combined hydrothermal pretreatment and enzymatic hydrolysis of corn fibre: Production of ferulic acid extracts and assessment of their antioxidant and antiproliferative properties. Ind. Crops Prod. **170**, 113731 (2021)
10. Huang, J., Khan, M.T., Perecin, D., Coelho, S.T., Zhang, M.: Sugarcane for bioethanol production: Potential of bagasse in Chinese perspective. Renew. Sustain. Energy Rev. **133**, 110296 (2020)
11. Badan Pusat Statistik. (2022). Statistik Tebu Indonesia 2021. December 7, 2022. https://www.bps.go.id/publication/2022/11/

30/6392bf8e4265949485d85e72/statistik-tebu-indonesia-2021.html
12. Rabelo, S.C., da Costa, A.C., Vaz Rossel, C.E.: Industrial Waste Recovery. In: Santos, C., Caldas, C., Borem, A. (eds.) Sugarcane, pp. 365–381. Academic Press, Cambridge (2015)
13. Alonso-Pippo, W., Luengo, C.A., Felfli, F.F., Garzone, P., Cornacchia, G.: Energy recovery from sugarcane biomass residues: Challenges and opportunities of bio-oil production in the light of second-generation biofuels. Journal of Renewable and Sustainable Energy **1**(6), 063102 (2009)
14. Shoaib, A.M., El-Adly, R.A., Hassanean, M.H.M., Youssry, A., Bhran, A.A.: Developing a free-fall reactor for rice straw fast pyrolysis to produce bio-products. Egypt. J. Pet. **27**(2018), 1305–1311 (2018)
15. Sindhu, R., Binod, P., Janu, K.U., Sukumaran, R.K., Pandey, A.: Organosolvent pretreatment and enzymatic hydrolysis of rice straw for the production of bioethanol. World J. Microbiol. Biotechnol. **28**(2), 473–483 (2011). https://doi.org/10.1007/s11274-011-0838-8
16. Xiao, T., Lai, R., Liu, Z., Xiong, S., Li, X., Zeng, Y., Jiao, S., Tang, Y., Lu, Y., Zu, Y.: Active pharmaceutical ingredient-ionic liquids assisted follicular co-delivery of ferulic acid and finasteride for enhancing targeted anti-alopecia. Int. J. Pharm. **648**(December), 123642 (2023)
17. Bezerra, G.S.N., Pereira, M.A.V., Ostrosky, E.A., Barbosa, E.G., de Moura, M., de F. V., Ferrari, M., Aragão, C. F. S., & Gomes, A. P. B.: Compatibility study between ferulic acid and excipients used in cosmetic formulations by TG/DTG, DSC and FTIR. J. Therm. Anal. Calorim. **127**(2), 1683–1691 (2017)
18. Zduńska, K., Dana, A., Kolodziejczak, A., Rotsztejn, H.: Antioxidant Properties of Ferulic Acid and Its Possible Application. Skin Pharmacology and Physiology **31**, 332–336 (2018)
19. Yang, J., Chen, J., Hao, Y., Liu, Y.: Identification of the DPPH radical scavenging reaction adducts of ferulic acid and sinapic acid and their structure-antioxidant activity relationship. Lwt **146**(March), 111411 (2021)
20. Sun, X., Sun, P., Liu, L., Jiang, P., Li, Y.: Ferulic acid attenuates microglia-mediated neuroinflammation in retinal degeneration. BMC Ophthalmol. **21**(1), 1–9 (2021)
21. Li, D., Rui, Y., Guo, S., Luan, F., Liu, R., Zeng, N.: Ferulic acid: A review of its pharmacology, pharmacokinetics, and derivatives. Life Sci. **284**, 119921 (2021)
22. Borges, A., Ferreira, C., Saavedra, M.J., Simões, M.: Antibacterial activity and mode of action of ferulic and gallic acids against pathogenic bacteria. Microb. Drug Resist. **19**(4), 256–265 (2013)
23. Panwar, R., Sharma, A.K., Kaloti, M., Dutt, D., Pruthi, V.: Characterization and anticancer potential of ferulic acid-loaded chitosan nanoparticles against ME-180 human cervical cancer cell lines. Applied Nanoscience (Switzerland) **6**(6), 803–813 (2016)
24. Choi, J.H., Park, J.K., Kim, K.M., Lee, H.J., Kim, S.: In vitro and in vivo antithrombotic and cytotoxicity effects of ferulic acid. J. Biochem. Mol. Toxicol. **32**(1), e22004 (2018)
25. Luo, Z., Li, M., Yang, J., Li, J., Zhang, Y., Liu, F., El-Omar, E., Han, L., Bian, J., Gong, L., Wang, M.: Ferulic acid attenuates high-fat diet-induced hypercholesterolemia by activating classic bile acid synthesis pathway. Front. Nutr. **9**, 976638 (2022)
26. Zhang, L.W., Al-Suwayeh, S.A., Hsieh, P.W., Fang, J.Y.: A comparison of skin delivery of ferulic acid and its derivatives: Evaluation of their efficacy and safety. Int. J. Pharm. **399**(1–2), 44–51 (2010)
27. Saadon, S.Z.A.H., Osman, N.B., Yusup, S.: Pretreatment of fiber-based biomass material for lignin extraction. In: Yusup, S., Rashidi, N.A. (eds.) Value-Chain of Biofuels, pp. 105–135. Elsevier, Amsterdam (2022)
28. Pazo-Cepeda, M.V., Guadalupe, S., Aspromonte & Alonso, E.: Extraction of ferulic acid and feruloylated arab-inoxylo-oligosaccharides from wheat bran using hot water. Food Biosci. **44**, 101374 (2021)
29. Converti, A., Aliakbarian, B., Domínguez, J.M., Vázquez, G.B., Perego, P.: Microbial production of biovanillin. Bra-zilian Journal of Microbiology **41**(3), 519–530 (2010)
30. Sharma, A., Sharma, A., Singh, J., Sharma, P., Tomar, G.S., Singh, S., Nain, L.: A biorefinery approach for the prduction of ferulic acid from agroresidues through ferulic acid esterase of lactic acid bacteria. 3 Biotech. **10**(8), 1 (2020)
31. Ou, S., Zhang, J., Wang, Y., Zhang, N.: Production of Feruloyl Esterase from *Aspergillus niger* by Solid-State Fermen-tation on Different Carbon Sources. Enzyme Res. **2011**, 1–4 (2011)
32. Wang, X., Yao, B., Su, X.: Linking Enzymatic Oxidative Degradation of Lignin to Organics Detoxification. Int. J. Mol. Sci. **19**(11), 3373 (2018)
33. Brézillon, C., Kroon, P.A., Faulds, C.B., Brett, G.M., Williamson, G.: Novel ferulic acid esterases are induced by growth of *Aspergillus niger* on sugar-beet pulp. Appl. Microbiol. Biotechnol. **45**(3), 371–376 (1996)
34. Doran, P.: Bioprocess Engineering Principles. Academic Press Limited, London (1995)
35. Hidayatullah, I.M., Arbianti, R., Utami, T.S., Suci, M., Sahlan, M., Wijanarko, A., Gozan, M., Hermansyah, H.: Techno-economic analysis of lipase enzyme production from agro-industry waste with solid state fermentation method. IOP Conf. Ser. **316**, 012064 (2018)
36. Harahap, A.F.P., Panjaitan, J.R.H., Curie, C.A., Ramadhan, M.Y.A., Srinophakun, P., Gozan, M.: Techno-economic Evaluation of Hand Sanitiser Production using Oil Palm Empty Fruit Bunch-Based Bioethanol by Simultaneous Saccharification and Fermentation (SSF) Process. Appl. Sci. **2020**(10), 5987 (2020)
37. Gubernur Riau. (2022). Surat Keputusan Gubernur Riau No. KPTS 1783/XII/2022 tentang Upah Minimum Kabupaten/ Kota Riau 2023. July 15, 2023. https://diskominfo.pelalawankab.go.id/asset/files/UPAH_MINIMUM_KABUPATEN_KOTA_RIAU_TAHUN_2023.pdf
38. PLN (2023). Peraturan Menteri Energi dan Sumber Daya Mineral Republik Indonesia No. 28 Tahun 2016. July 20, 2023. https://web.pln.co.id/pelanggan/tarif-tenaga-listrik
39. Statista. (2015). Cost of wastewater treatment to reduce pharmaceutical residues in 2015, by technology (in euros per cubic meter). Energy & Environment: Water & Wastewater.
40. Karimah, I., Suyuditomo, G., Harahap, A.F.P., Ramadhan, M.Y.A., Panjaitan, J.R.H., Sahlan, M., Hermansyah, H., Gozan, M.: Techno-economic analysis of furfural production with various pretreatment of oil palm empty fruit bunches using SuperPro Designer. IOP Conference Series: Earth and Environmental Science **749**(1), 012042 (2021)
41. Grand View Research. (2023). Furfural Market Size, Share & Trends Analysis Report By Process (Quaker Batch Process), By Raw Material (Corn Cob), By Application (Furfuryl Alcohol), By End-use, By Region, And Segment Forecasts, 2023 – 2030. Report ID: 978–1–68038–301–0. September 7, 2023. https://www.grandviewresearch.com/industry-analysis/furfural-market
42. Precedence Research (2023). Ferulic Acid Market (By Type: Synthesis, Natural; By Application: Cosmetic, Pharmaceutical Intermediates, Others; By Packaging: Interior Packaging, Exterior Packaging) - Global Industry Analysis, Size, Share, Growth, Trends, Regional Outlook, and Forecast 2023–2032. https://www.precedenceresearch.com/ferulic-acid-market/amp
43. Safaat, M., Wulan, P.P.D.K.: Technoeconomic Analysis of Integrated Bioethanol from Elephant Grass (Pennisetum purpureum) with Utilization of Its Residue and Lignin. Industria: Jurnal Teknologi dan Manajemen Agroindustri **11**(1), 64–80 (2022)
44. Fredsgaard, M., Hulkko, L.S.S., Chaturvedi, T., Thomsen, M.H.: Process simulation and techno-economic assessment of Salicornia

sp.-based jet fuel refinery through Hermetia illucens sugars-to-lipids conversion and HEFA route. Biomass Bioenergy **150**, 10 (2021)

45. Taiwo, A.E., Tom-James, A., Falowo, O.A., Okoji, A., Adeyi, O., Olalere, A.O., Eloka-Eboka, A.: Techno-economic analysis of cellulase production by Trichoderma Reesei in submerged fermentation processes using a process simulator. S. Afr. J. Chem. Eng. **42**, 98–105 (2022)

Waste and Biomass Valorization (2024) 15:5785–5804
https://doi.org/10.1007/s12649-023-02395-y

ORIGINAL PAPER

Coupled Production of Fatty Acid Alkyl Esters as Biodiesel and Fermentative Xylitol from Indian Palm (*Elaeis guineensis* Jacq.) Kernal Oil in a Biorefinery Loom

Jayacumar Sanjana[1] · S. P. Jeevan Kumar[2] · P. Naveen Kumar[2,4] · K. Ramachandrudu[3] · Samuel Jacob[1]

Received: 12 September 2023 / Accepted: 18 December 2023 / Published online: 25 January 2024

Abstract

Palm kernel oil (PKO) is a non-edible oil which is enriched with saturated fatty acids that can be used as a raw material for many industrial applications. Indian PKO (IPKO) was chosen in this study which has been explored sporadically in industries. IPKO was characterized and utilized for the synthesis of fatty acid alkyl esters through transesterification (solvolysis) using methanol and ethanol solvents coupled with alkali catalysts such as sodium hydroxide (NaOH) and potassium hydroxide (KOH). Upon comparison, methanol and NaOH resulted in the maximum biodiesel (esters) yield of 67.77% as compared to ethanol-based solvolysis. Compositional analysis of fatty acid methyl esters (FAMEs) through GC–MS elucidated the presence of long chain (C12:0 to C18:1) esters, which can be utilized as biodiesel. Therefore, IPKO FAME has been tested as diesel blend in engines without any modification, where, B5 (5% v/v) blend showed at-par fuel characteristics and engine efficiency as compared to non-blended diesel with minimal emissions. To induct a waste circular reprocessing startegy, crude glycerol resulted from transesterification of IPKO was supplemented to *Candida tropicalis* NCIM3118 for xylitol (a sweetener) synthesis. The results indicated that upon supplemention of IPKO crude glycerol as co-substrate, enhancement in xylitol production of about 0.93 $g_{xylitol}/g_{total\ organic\ carbon}$ as compared to only xylose as 'C' source (0.81 $g_{xylitol}/g_{total\ organic\ carbon}$) was observed with efficiency improvement in overall growth kinetic behavior. This study demonstrates the circular economy approach in which that the IPKO can be utilized for biodiesel production, while, the by-product (crude glycerol) generated could be deployed for xylitol production.

Jayacumar Sanjana, S. P. Jeevan Kumar and P. Naveen Kumar have equal first author contribution.

✉ Samuel Jacob
samueljb@srmist.edu.in

[1] Department of Biotechnology, School of Bioengineering, College of Engineering and Technology, Faculty of Engineering and Technology, SRM Institute of Science and Technology, SRM Nagar, Kattankulathur, 603203 Chengalpattu, Tamil Nadu, India

[2] ICAR-Directorate of Floricultural Research, Pune 411036, Maharashtra, India

[3] ICAR-Indian Institute of Oil Palm Research, Pedavegi, 534475 West Godavari, Andhra Pradesh, India

[4] ICAR-Indian Institute of Horticultural Research, Hesaraghatta, Bangalore 560089, Karnataka, India

Graphical Abstract

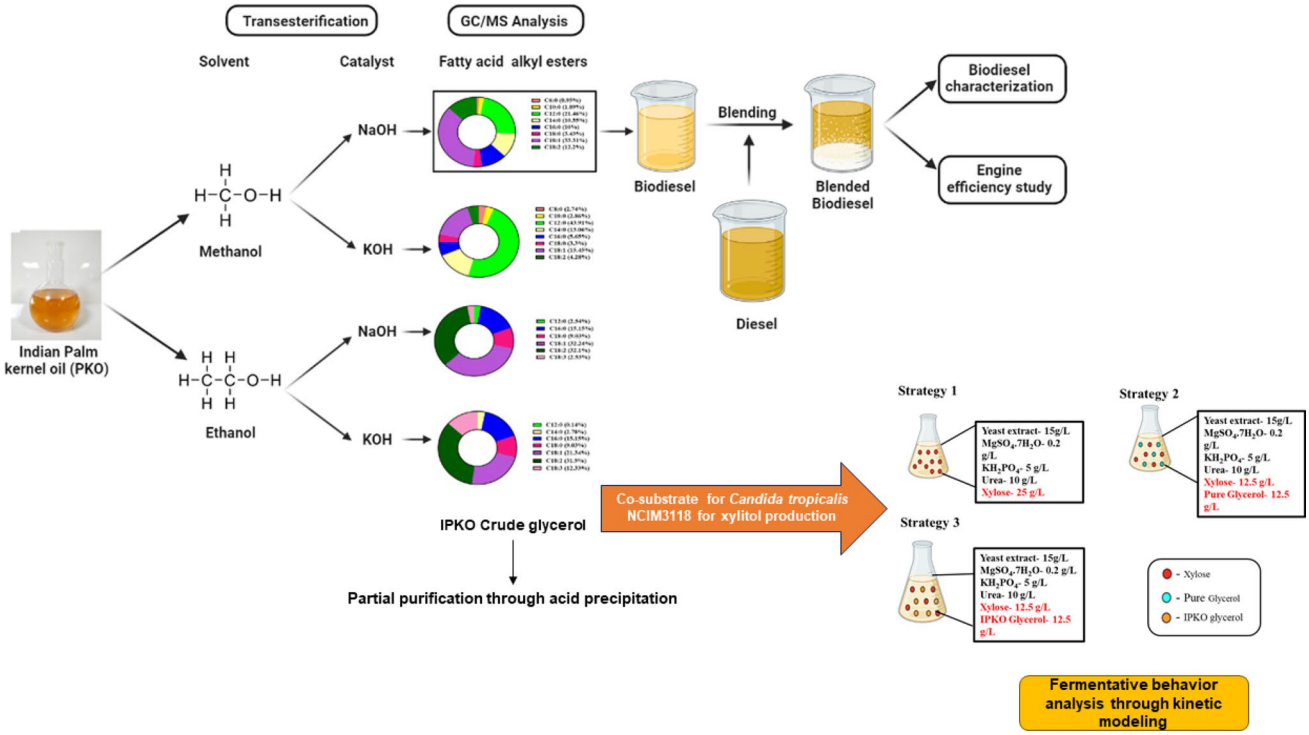

Keywords Biodiesel · Indian palm kernel oil · Solvolysis · Transesterification · Xylitol

Statement of Novelty

Indian palm kernel oil (IPKO) was chosen in this study which has been explored sporadically in industries. This is the first study to establish the bioprocessing aspects of this widely available bioresource for economical advantage of the oil processing units. The biodiesel obtained from the solvolysis of IPKO seems to be at par with the convetional fuel with low emission characteristics. Another important aspect of this study is by-product (glycerol) valorization to xylitol (a sugar alcohol) through microbial fermentation thereby establishing a circular biorefinery. This paves the way for sustainable utilization of IPKO as a potential industrial raw material that could solve the energy crisis as well as industrially important xylitol synthesis.

Introduction

Energy is a key indicator for the sustainable growth and development of a society. The indispensable role of energy in economic progress of a country through technological developments leads to social upliftment and improvement in the quality of life as being addressed through UN sustainable development goals (SDGs). To address the issues of increasing fuel demand, global climate change and decreasing conventional fuel resources, deployment of renewable energy resources as an alternative to fossil fuels are highly solicited. Given the ongoing fuel scarcity problems and worldwide rise in petroleum costs, huge investment in agro-wastes (biomass) based fuel is essential [1]. Amongst liquid biofuels, biodiesel finds a prominent position that has significant application in transportation and agricultural machinery. Biodiesel is a mixture of fatty acid alkyl esters (FAAEs) derived from animal fats or edible/non-edible plant oil through catalyst/enzyme-assisted solvolysis (methanol predominantly) otherwise termed as transesterification. It is a clean renewable fuel with less sulfur and aromatic content, eco-friendly, non-toxic, biodegradable and can be used to run any compression ignition engine without any modifications [2, 3]. FAAE is proportionally similar to the regular fossil fuel-based diesel in terms of its physico-chemical composition and functional properties [4]. Biodiesel can be produced from vegetable oils owing to its similar characteristics of higher flash points and cetane number with petroleum-based diesel [5]. Plants are an excellent renewable resource of natural oil/lipids serving the demand of

both edible and non-edible industrial applications. Though, there exist a cross-over in application of majorly available edible oils (soyabean, rapeseed and sunflower oil) for non-food purposes especially biodiesel, considering the food vs. fuel implications in developing countries (South East Asian Countries) exploitation of non-edible oils for green chemicals synthesis deemed to be a better alternative.

It is known that direct application of vegetable oil is not recommended for diesel engines due to high viscosity that leads to deposition of carbon, piston ring adhesion, and incomplete combustion [6]. However, after converting the triglycerides of oil into esters the viscosity is reduced that can be utilized as fuel based on its compliance of American society for testing and materials (ASTM) standards. The principle behind transesterification is solvolysis, more precisely the alcoholysis reaction where one alcohol displaces another alcohol from an ester present in fatty acid chain [7]. It is the process of conversion of triglycerides into diglycerides in the first step, followed by the diglycerides into monoglycerides in the second step, and finally the conversion of monoglycerides to glycerol in the third step, one ester molecule is produced from each glyceride at each stage of the reaction [8]. The industrial manufacturing of biodiesel must make use of oil seeds that are non-edible and animal fats [9]. Till date various plant oils have been utilized commercially to produce biodiesel which includes palm oil, castor oil, rapeseed oil and sunflower oil [10–14].

Among vegetable oils, palm is cultivated widely which accounts for a productivity of 4.4 MT per hectare annually with oil production of 69.30 MT securing first position [14, 15]. According to the United States Department of Agriculture (USDA) estimates, 75% of the global palm oil consumption in refined forms are used for edible purposes and food industries, while ~ 22% is for non-food purposes like cosmetics and marginal quantity is used for biodiesel. By-products such as palm stearin, palm fatty acid distillate and refined palm kernel oil are employed in some industrial application [14]. Palm oil is extracted from the fruit bunch after the removal of the kernel. Palm kernels discarded as waste makes up to 46–48% of palm fruit by weight and oil content in the kernel ranges between 45 and 60% which is rich in saturated triglycerides [16]. The industrial process of extraction of palm kernel oil (PKO) is shown in Fig. 1.

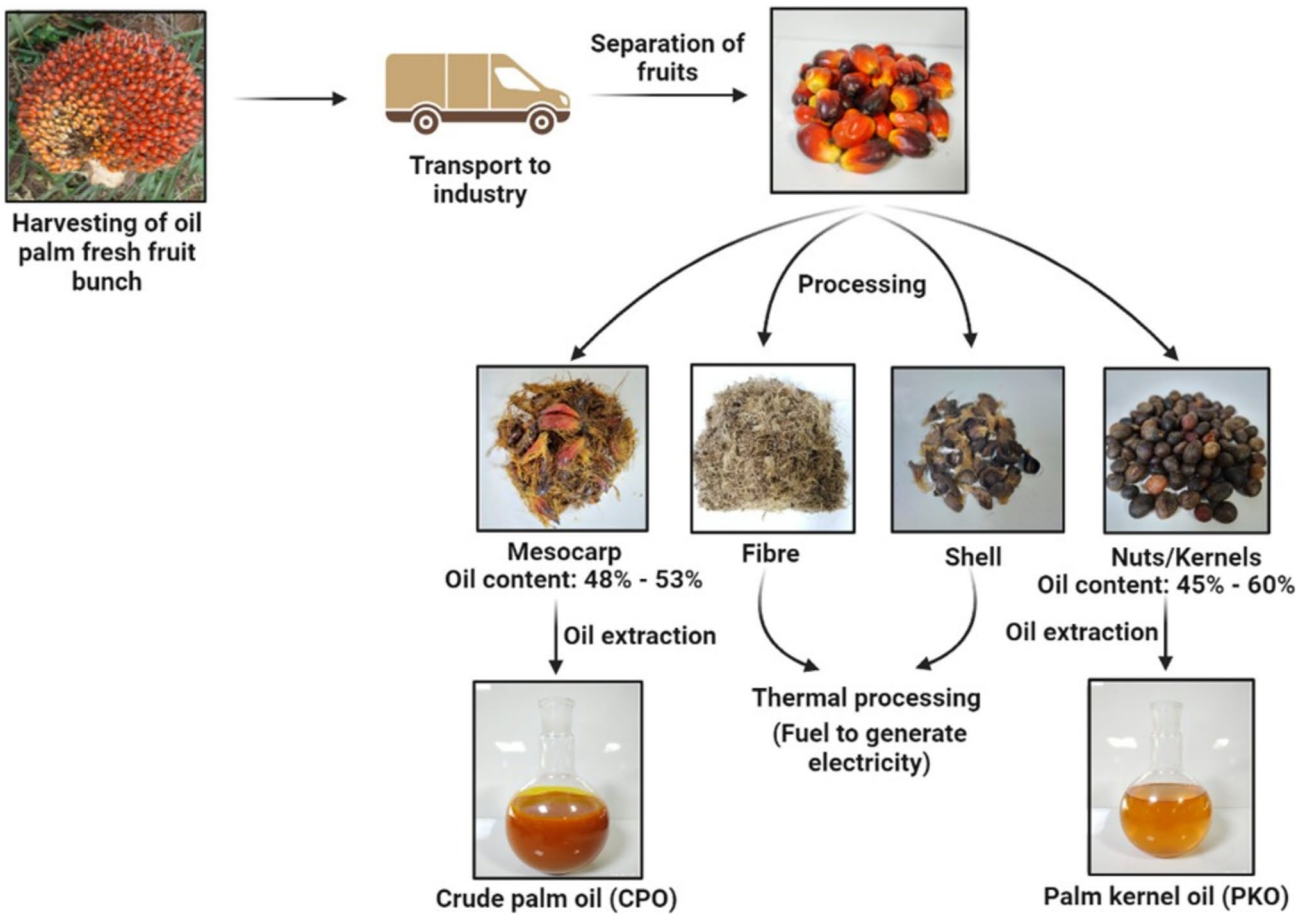

Fig. 1 Process flow of processing palm fruit processing and its oil derivatives

PKO from oil extraction industries is an important source for oleochemicals because of its rich source of short (C8–C10), medium chain (C12–C14) fatty acids that have been widely used in the industries [17]. Apart from conventional use, recent applications of PKO as fuel have triggered a great interest to explore owing to its lipid composition. Why et al. [18] demonstrated that the PKO at a ratio of 20% (v/v) coupled with bio-jet fuel, blended in Jet A-1 fuel showed promising efficiency. In another study, stabilization of PKO with methanol showed greater stability like tetrahydrofuran [15]. In the last five years the acreage of palm (*Elaeis guineensis* Jacq.) cultivation in India has been growing at a rate of 21% compound annual growth rate (CAGR). The oil palm development programme (OPDP) is being implemented by the relevant state governments with the help of horticulture and agriculture departments [19]. Though the major usage of Indian palm oil due to its versatile applications is in the food industry, PKO which does not meet the food-grade application is gaining importance in the fuel and industrially important chemicals production.

Ejeromedoghene [20] reported a study on PKO which was transesterified using methanol and acid catalyst (acetic acid) to produce biodiesel and characterized using ASTM protocols. Similarly, optimization study of PKO was performed using adaptive neuro-fuzzy inference system (ANFIS), artificial neural network (ANN) and response surface methodology (RSM) for improved biodiesel yield of 99.5% at oil/solvent ratio of 0.48 v/v, 0.86% (w/w) catalyst concentration and reaction time of 71.50 min [21]. To the best of the authors' knowledge, transesterification of Indian PKO (IPKO) for synthesis of FAAE is not found elsewhere. Moreover, valorization of crude glycerol for xylitol (a sugar alcohol) production has been envisaged through microbial fermentation as a means of circular economy.

Sugar alcohols are type of polyols obtained from monosaccharides (hexose and pentose) generally utilized as sweeteners and thickeners in the food industries to replace table sugar i.e., sucrose, mostly with other artificial sweeteners to compensate the poor sweetness. Because of its sweetness being similar to sucrose, xylitol is probably the most popular among sugar alcohols [22]. The global market demand of xylitol has been projected between 20000 to 40000 tons [23].

Currently, the industrial production of xylitol can be produced by hydrogenation of xylose (a pentose sugar) derived from plant-based xylan with nickel as catalyst under a temperature of 150 °C and 25 bars of pressure. As the process of xylose production and purification is cost intensive, consequently, it makes the xylitol more expensive [24, 25]. Some yeasts like *Candida, Rhodosporidium* and *Yarrowia* (*Yarrowia lipolytica*, *Candida guilliermondii*, *Candida zeylanoides*, *Candida tropicalis and Rhodosporidium toruloides*) have the ability to produce the xylitol with inexpensive carbon sources derived from lignocellulosic hydrolysates [26, 27]. Studies have reported that to enhance the xylitol production, co-substrates like glycerol, glucose, mannose were supplemented in the growth medium to modulate the metabolism of the producer organisms. Arruda and Felipe [28] studied the glycerol supplementation on xylitol production using xylose as substrate by *Candida guilliermondii* and reported a yield of 0.78 g/g and productivity was 1.13 g/L/h when media contains 53 g/L of xylose and 6.5 g/L of glycerol. Similarly, we have employed a fermentative strategy of replacing the 50% of xylose with the glycerol derived from IPKO transesterification and compared with the efficiency of the process with only xylose substrate and pure glycerol as co-substrate using *Candida tropicalis* NCIM3118 as a producer organism. The purpose of comparison between IPKO-derived and pure glycerol is to get an insight on the effect of impurities in IPKO glycerol on fermentation after transesterification.

IPKO is less explored as inexpensive feedstocks with significant triglycerides, hence, in this study, standardization of IPKO transesterification has been carried out for biodiesel production along with a microbial valorization of the by-product crude glycerol for xylitol production by fermentative means. This paves the way for sustainable utilization of IPKO as a potential industrial raw material that could solve the energy crisis as well as industrially important xylitol synthesis.

Materials and Methods

Physico-Chemical Characterization of IPKO

The IPKO extracted from an improved palm variety *Elaeis guineensis* Jacq. was procured from the Indian Council of Agricultural Research (ICAR)-Indian Institute of Oil Palm Research, Pedavegi, West Godavari District, Andhra Pradesh. The obtained IPKO was characterized as described in the subsequent sections. All the chemicals utilized for the study such as methanol (96%), ethanol (99%), sodium hydroxide (NaOH), potassium hydroxide (KOH), sulphuric acid (H_2SO_4, 96%), hydrochloric acid (HCl, 36%) are of analytical grade.

Determination of Density and Specific Gravity

An empty tube was weighed and the weight was noted as W1. About 5 mL of IPKO oil was measured and poured into the empty tube and weight was taken again and noted as W2. The density of the IPKO was calculated by using the Eq. 1. The specific gravity denotes the ratio between the density of the oil to density of the water as given in Eq. 2.

$$\text{Density(g/ml)} = \frac{\text{Mass of the oil (W2 - W1)(g)}}{\text{Volume of oil taken (mL)}} \quad (1)$$

$$\text{Specific gravity} = \frac{\text{Density of the oil (g/mL)}}{\text{Density of water (g/mL)}} \quad (2)$$

Estimation of Acid Value and Free Fatty Acid (FFA) Content

The acid value and FFA content of the IPKO was estimated using the standard method reported [29]. The acid value is a measure of the quantity of triacylglycerol that breaks down into FFAs. It also indicates that the amount of KOH required to neutralize the FFA present per gram of oil. Volumetric ratio of oil:ethanol (1:10) suspension was taken in a 100 mL conical flask and heated in a boiling water bath for 10 min. After cool down to room temperature, 2 to 3 drops of phenolphthalein indicator were added. The mixture was titrated against 0.1 N KOH till the pink color appeared (end point). The titre volume was noted and the acid value and FFA content were calculated using the Eqs. 3 and 4, respectively.

$$\text{Acid value}\left(\text{mg}\frac{\text{KOH}}{\text{g}}\right) = \frac{\text{Titre value} \times 5.6}{\text{Weight of the oil taken (g)}} \quad (3)$$

$$\text{Free fatty acid}\left(\text{mg}\frac{\text{KOH}}{\text{g}}\right) = \frac{\text{Acid value}}{2} \quad (4)$$

Estimation of Saponification Value and Ester Value

Saponification value indicates the quantity of KOH required to saponify one gram of the oil. When the saponification number is lower, the molecular weight of the triacylglycerol that is present in the oil tends to be higher [30]. To one gram of oil, 5 ml of ethanol was added followed by the addition of 25 mL of 0.5 N alcoholic KOH and heated for 10 min in a hot water bath. After cooling, 3 to 4 drops of phenolphthalein indicator were added. The mixture was titrated against 0.5 N HCl until the endpoint reaches colourless. The saponification value was calculated as given in Eq. 5.

$$\text{Saponification value}\left(\text{mg}\frac{\text{KOH}}{\text{g}}\right) = \frac{\text{Titre value} \times 28.05}{\text{Weight of the oil taken (g)}} \quad (5)$$

Ester value is obtained by the difference between saponification value and acid value (Eq. 6). Higher ester value results in a high number of esters and low molecular weight fatty acid content.

$$\text{Ester value}\left(\text{mg}\frac{\text{KOH}}{\text{g}}\right) = \text{Saponification value} - \text{Acid value} \quad (6)$$

Solvolysis of IPKO to Synthesize FAAE

For an efficient transesterification through solvolysis there is a prerequisite to reduce the FFA content in order to prevent soap formation [31]. Therefore, a two-step process that consists of esterification of the oil using an acid catalyst followed by transesterification of the esterified oil using an alkali catalyst was adapted as discussed in the subsequent sections.

Esterification for Reduction of Acid Value

The IPKO esterification process was performed as reported by Hayyan et al. [32] with the following conditions: oil to methanol molar ratio of 1:6 at 60 °C for 60 min with 1% (w/w) of sulphuric acid (catalyst). After the reaction, the suspension was transferred to a separating funnel to obtain a biphasic solution. The top layer that consists of esterified oil was carefully separated and utilized for transesterification. The acid value was determined in order to find the FFA level of esterified IPKO, which was found to be within the acceptable limit.

Transesterification

The efficiency of the transesterification reaction is dependent on the type of solvent used towards the chosen oil and the reaction operating conditions (time and temperature). In general, alcoholic solvents are more preferred for FAAE (biodiesel) synthesis due to its availability and ease in separation of glycerol from the ester mixtures. In this study, ethanol and methanol were employed as a solvent for transesterification IPKO. The reaction time (60 min) and temperature (60 °C) was fixed based on the previous report [33]. Addition of catalyst favors the forward reaction under the given conditions. Alkali catalysts (1% w/w) such as NaOH and KOH have been proven to enhance the FAAE yield and were employed to obtain maximum FAAE yield.

Following the completion of each process, the resultant mixture was put in a separating funnel in order to fractionate the FAAE (the upper layer) and the glycerol. Further, the yield of FAAE was calculated using the Eq. 7. The obtained FAAE was analyzed for fatty acid composition through Gas Chromatography-Mass spectrometer (GC–MS).

$$\text{Yield}(\%) = \frac{\text{Weight of the produced FAAE(g)}}{\text{Weight of the oil taken (g)}} \times 100 \quad (7)$$

The following denotation are used for convenience throughout the discussion.

- Fatty acid alkyl ester from Methanol-NaOH-Fatty Acid Methyl Ester (FAME) (Na)
- Fatty acid alkyl ester from Methanol-KOH-FAME (K)
- Fatty acid alkyl ester from Ethanol-NaOH-Fatty Acid Ethyl Ester FAEE (Na)
- Fatty acid alkyl ester from Ethanol-KOH-FAEE (K)

A radar plot was constructed using Microsoft Excel Office Suite 365 to signify the role of parameters such as type of solvent (methanol and ethanol) and catalysts (NaOH and KOH) to FAAE and glycerol yields.

Compositional Analysis of FAAE Derived from IPKO Through GC–MS

The analysis for fatty acid composition was carried out by GC–MS (Shimadzu, QP2010 Plus). Helium gas was used as the carrier gas at a flow rate of 1 ml/min. The initial temperature was kept at 70 °C for holding time of 2 min and final temperature was kept at 300 °C with holding time of 5 min at a ramp of 5 °C/min. The temperature of the injector was set to 280 °C and ion source temperature of 200 °C [34, 35].

Biodiesel Characterization for Fuel Application

Different blends of IPKO derived biodiesel and diesel fuel (BX where, X refers to percentage of volume of biodiesel (X = 5, 10, 20)) were prepared. Pure diesel is considered as a control. Fuel properties like density (Hydrometer), kinematic viscosity at 40 °C (Red wood viscometer), cloud point and pour point (Cleveland open-cup apparatus), flash point and fire point (EIE-PTLT-104NR4, EIE Instruments) cetane number (biodiesel analyzer software), calorific value (bomb calorimeter) were determined.

Engine Performance Testing

The blending of biodiesel with other fuels can result in a more homogeneous fuel mixture that can improve combustion efficiency and increase brake thermal efficiency (BTE). However, the blend ratio should be carefully selected to ensure optimal performance and to avoid adverse effects on engine performance and emissions. To test the engine performance with the fuel blends, a high-speed engine with eddy current dynamometer was used. The performance of the engine depends on inter-relationship between power developed, speed and the specific fuel consumption at each operating condition within a useful range of speed and load. The BTE and brake specific fuel consumption of the various blends of IPKO biodiesel at different loads were measured.

Partial Purification of Glycerol

For the purification of glycerol, the protocol reported by Miyuranga et al. [36] with slight modification was followed. The glycerol layer was obtained and upon gentle mixing the glycerol was acidified (pH 1) using phosphoric acid (H_3PO_4) on a hot plate until the formation of three different layers. The top layer consists of fatty acids, the middle layer of glycerol and the bottom layer of inorganic salts. The glycerol was carefully extracted and was neutralized using NaOH followed by evaporation at 100 °C. Further, the glycerol was purified using syringe filter (0.44 µm), where further inorganic salts were eliminated. The IPKO glycerol pH was adjusted to 4.5 inorder to add as a co-substrate for *Candida tropicalis* NCIM3118 growth. Fig. S5 (supplementary material) depicts the three-layer separation of the purified glycerol.

Characterization of Glycerol

Fourier-Transform Infrared Spectroscopy (FTIR)

The crude glycerol obtained after transesterification was analyzed with FTIR spectrophotometer (Shimadzu, IRTracer 100) and compared with the pure glycerol to detect any alterations in the functional groups. The scan spectrum range from 4000 to 400 cm^{-1} at a resolution of 4 cm^{-1} was employed for the analysis.

Gas Chromatography Mass Spectrometry (GC–MS)

To determine the composition of crude glycerol, GC–MS (Shimadzu, QP2010 Plus) was carried out. He (helium) gas was employed as the carrier gas at a rate of flow of 3 ml/min. The initial temperature was kept at 50 °C with holding time of 2 min and final temperature was kept at 300 °C for 5 min at a ramp rating of 5 °C/min. The temperature of the injector was set at 280 °C and ion source temperature of 200 °C [37].

Xylitol Production Through Fermentation

Inoculum Preparation for Fermentation

Candida tropicalis NCIM3118 was cultured in a 250 ml Erlenmeyer flask containing 100 ml of YEPX broth (yeast

extract—10 g/l, peptone—20 g/l, xylose—20 g/l) incubated at 32 °C in a rotary shaker set at 120 rpm. After incubation for 24 h, 5% (v/v) of the mother inoculum with optical density at 600 nm of about 1.0 was added to the fermentation medium.

Shake Flask Fermentation with Different Proportion of IPKO Glycerol and Xylose

Xylitol production was performed through shake flask fermentation in a 250 ml Erlenmeyer flask containing 100 ml of minimal salt media (MSM) which consist of yeast extract—15 g/l, $MgSO_4.7H_2O$—0.2 g/l, KH_2PO_4—5 g/l, Urea—10 g/l and xylose—25 g/l. The fermentation was carried at 32 ± 2 °C under constant agitation of 120 rpm for 7 days.

To enhance xylitol production, batch fermentation was carried out in three different strategies with varied initial level of carbon source.

- Strategy 1: Xylose (25 g/L)
- Strategy 2: 50% Xylose (12.5 g/l) and 50% pure glycerol (12.5 g/l)
- Strategy 3: 50% Xylose (12.5 g/l) and 50% IPKO glycerol (12.5 g/L)

Total Organic Carbon (TOC)

As the carbon source is provided as mixture of xylose and glycerol that have different chemical nature, in order to determine the substrate consumption, TOC reduction was used as a parameter that was measured at regular time intervals during the fermentation. Soil Organic Carbon Walkley Black Method, [38] method (titrimetric) was employed with slight modifications. To 0.5 ml of sample collected during fermentation (after removal of solids) 1 ml of 1N $K_2Cr_2O_7$ was added and swirled gently. To this 2 ml of concentrated H_2SO_4 was added and the solution was mixed vigorously and kept aside for 30 min. After incubation, 20 ml of distilled water was added to the solution. About 2 to 3 drops of ferroin indicator was added to the solution. The solution was titrated against 0.5N $FeSO_4$ until the colour changes from dark green to maroon red. The TOC content in the sample was calculated as given in Eq. 8.

$$\mathrm{TOC(g/L)} = \frac{\left(\text{Volume of } FeSO_4\text{(Blank)} - \text{Volume of } FeSO_4\text{(Sample)}\right) \times \text{Normality of } FeSO_4 \times 0.003 \times 1.33 \times 1000}{\text{Amount of sample (ml)taken}} \quad (8)$$

where, 1.33 is a correction factor and 0.003 is the carbon oxidized.

Cell Mass, Xylose, and Xylitol Estimation

About 4 ml of the culture was collected at every 24 h interval for 7 days and the growth of microorganism was estimated by measuring the absorbance at 600 nm followed cell biomass weight determination by centrifugation at 10000 rpm at 4 °C for 10 min. The pellet obtained was air-dried in a pre-weighed tube until it reaches a consistent weight and the concentration of the final cell biomass is represented as grams dry cell weight (DCW)/l. The obtained supernatant after centrifugation was stored for the further analysis. Xylitol was estimated using the protocol reported by Sánchez [39] to calculate the specific product yield coefficient ($Y_{P/S}$) as given in Eq. 9.

$$Y_{P/S} = \frac{\text{Final concentration of xylitol} - \text{Intial concentration of xylitol}}{\text{Intial concentration of TOC} - \text{final concentration of TOC}} \quad (9)$$

Kinetic Modeling

To examine the effects of different level of carbon sources used for cell growth and substrate consumption of *Candida tropicalis* NCIM3118 using hybrid-Logistic Monod kinetic model for substrate utilization; first-order and Luedeking-Piret equation for cell growth kinetics [40, 41]. These models can elucidate the near to real-time observations (global optima) by considering multi-level biochemical reactions and hetero-fermentations.

In order to solve the model equation a non-linear regression equation was fit with the experiment data to determine the kinetic parameters. The obtained data were solved using Solver toolkit (Levenberg–Marquardt algorithm) in MS Office Excel 2019 software to reduce the RMSE (residual sum of squares of errors). As reported by Xu [42], when Monod model which is based on limited substrate is incorporated with Logistic model based on limiting nutrients and growth inhibitors there might be a probability of understanding the physiology of cell when altered nutrient source

provided. In this study, *Candida tropicalis* NCIM3118 utilize the crude glycerol as growth medium and there might be presence of inorganic salts, fatty acids and etc. which could act as growth inhibitors. The kinetic parameter associated with the *C. tropicalis* growth (X_0, X_{max} and μ_{max}) were estimated using the Eq. 10.

$$X = \frac{X_o \times X_{max} e^{\mu_{max} t}}{X_{max} - X_o + X_o e^{\mu_{max} t}} \tag{10}$$

where, X (g/L)—concentration of cell biomass; X_0 and X_{max} (g/L)—Initial and maximum concentration of cell biomass; μ_{max} (h^{-1})—maximum specific growth rate and t (h)—fermentation time.

The kinetic parameters for the substrate utilization using Luedeking-Piret model (S_0, α and β) were estimated using as given in Eq. 11.

$$S = S_o - \left[\frac{n}{Y_{\frac{p}{s}} + k_e}\right]\frac{X_{max}}{\mu_{max}} \left[\left(\mu_{max} t + \ln\left(\frac{X_o}{X_t}\right)\right)\right] - \left[\frac{1}{Y_{x/s}} + \frac{m}{Y_{p/s}}\right](X_t - X_0) \tag{11}$$

With the kinetic parameters acquired through the model, the production of xylitol supplemented with crude glycerol was determined from Eqs. 12 and 13.

$$\alpha = \frac{1}{Y_{X/S}} + \frac{m}{Y_{P/S}} \tag{12}$$

$$\beta = \frac{n}{Y_{P/S}} + K_e \tag{13}$$

where, S_0—initial concentration of the substrate; $Y_{X/S}$ (gram of biomass produced/gram of TOC utilized)—yield coefficient for biomass; $Y_{P/S}$ (gram of xylitol produced/gram of TOC utilized)—yield coefficient for xylitol; K_e—maintenance coefficient; α—growth associated factor; β—non-growth associated factor; If α > β—growth associated factor; α < β—non-growth associated product.

If xylitol production by *C. tropicalis* NCIM3118 is a growth-associated product under aerobic condition then the product (xylitol) yield is proportional to the substrate (TOC) which can be expected to follow the first-order kinetics (Eq. 14).

$$M = M_o . e^{\pm kt} \tag{14}$$

where, M (g/L)—Variable of [Product, xylitol], [Substrate, TOC], [Biomass, DCW]; M_o (g/L)—initial concentrations of variables; k—Rate of change ((+) indicates production, (−) indicates consumption); t (h)—fermentation time.

Result and Discussion

Physico-Chemical Characterization of IPKO

The physico-chemical characterization (density, specific gravity, acid value, free fatty acid, saponification value and ester value) of IPKO were tabulated in Table 1. From the results, it has been observed that the density and specific gravity were found to be 0.843 g/mL and 0.85 respectively which is in accordance with the reported PKO characterization [35]. Estimation of FFA and the corresponding acid value is a paramount step before proceeding to transesterification. It has been reported that FFA > 1% leads to soap formation through saponification with alkali catalyst. In IPKO, the FFA was found to be 1.92 ± 0.23 mg equivalent KOH/g of oil which is higher than the critical limit (1%) that correlates with the saponification value of 247.61 ± 4.76 mg equivalent KOH/g of oil which is in line with the report on PKO [43]. Due to this reason, IPKO prerequisite the reduction of FFA through acid treatment thereby enhancing the ester value.

FAAE Yield from Solvolysis

Under the conditions of 60 °C for 90 min with a molar ratio of 1:6 (oil:methanol) and catalyst concentration (NaOH and KOH) of 1% (w/w), the FAME yield was observed to

Table 1 Comparison of physicochemical properties of IPKO with the PKO from other origin

Physicochemical properties	Indian PKO (This study)	Nigerian PKO[a]	Thailand PKO[b]
Density (g/ml)	0.843 ± n.d	–	0.908
Specific gravity	0.85 ± n.d	0.98	–
Acid value (mg equivalent KOH/g)	3.84 ± 0.46	22 ± 0.1	–
Free fatty acids (mg equivalent KOH/g)	1.92 ± 0.23	7.83	1.05
Saponification value (mg equivalent KOH/g)	247.61 ± 4.76	230	–
Ester value (mg equivalent KOH/g)	239.77 ± 4.67	–	–

[a]Betiku et al. [21]

[b]Jitputti et al. [35]

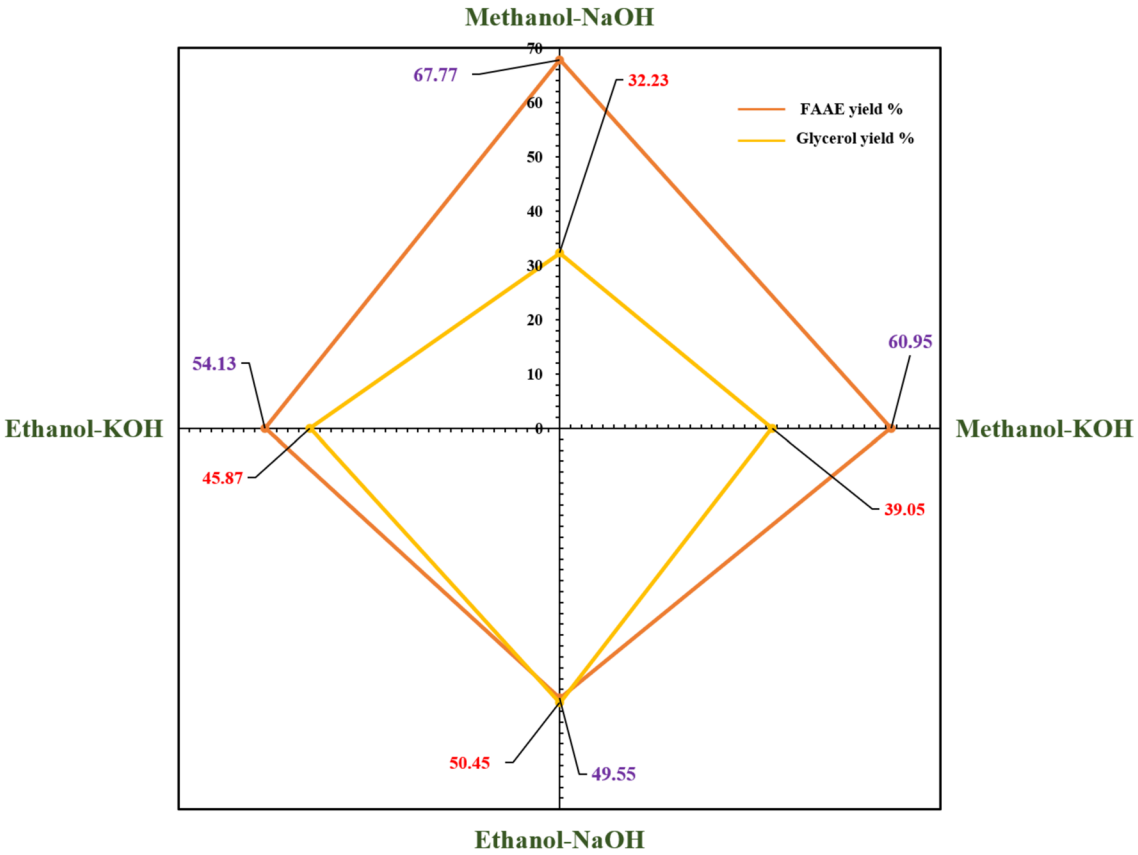

Fig. 2 Radar plot of FAAE and glycerol yield for IPKO using different solvents and catalysts

be 67.77% and 60.95% respectively (Fig. 2). It has been observed from the radar plot that the selection of solvent played a crucial role in transesterification to FAAE as compared to the catalyst. Methanol seems to be better for solvolysis of IPKO with both the catalyst NaOH and KOH when compared to ethanol. However, if glycerol is the product targetted than the FAAE, then ethanolysis acts as the better candidate. A study reported the biodiesel production from Nigerian PKO by transesterification with methanol in the presence of NaOH and KOH as catalyst have obtained FAME yield of 60–62% [44]. Under same condition and only the change of solvent from methanol to ethanol yielded FAEE of 49.55–54.13% (Fig. 2).

Silva et al. [45] have reported a similar study on soybean oil using ethanol and NaOH where ethyl esters yield of 49% was obtained. For biodiesel production though methanol and ethanol are frequently employed for transesterification, methanol is comparatively preferred due to its physical and chemical properties that compliments the alkali catalyst. Additionally, methanol content in the FAME employed as fuel blend reduces the temperature in the commercial chamber due to decline in latent heat of evaporation of methanol during vaporization. Upon comparing the efficiency of ester yield between NaOH and KOH through solvolysis, it has been observed that NaOH resulted in significant increase of FAME and FAEE. The reason for the varied reactivity between the catalyst is that the difference in density of electronegative exchangeable cations which undergoes Lewis and Brønsted reaction with the IPKO [46, 47].

Composition Analysis of FAAE Derived from IPKO

The knowledge on the fatty acid composition of the FAAE is of prime importance to know the amount of saturated and unsaturated fatty acid present. Röttig et al. [48] reported that the resultant FAAE from transesterification depends on the plant species and the role of process parameters set. It has been reported that common FAAEs from the vegetable oil are linolenic acid (C18:3), linoleic acid (C18:2), oleic acid (C18:1), stearic acid (C18:0) and palmitic acid (C16:0) in varied porportions which aligns with the composition as given in Fig. 3. Higher amount of saturated fatty acids in fuel improves the oxidative stability and combustion as compared to the unsaturated fatty acids [49]. GC–MS analysis was used to study the fatty acids composition of the synthesized FAAE and represented in Fig. 3 and the respective chromatograms were provided in Figs. S1, S2, S3, S4 (Supplementary information).

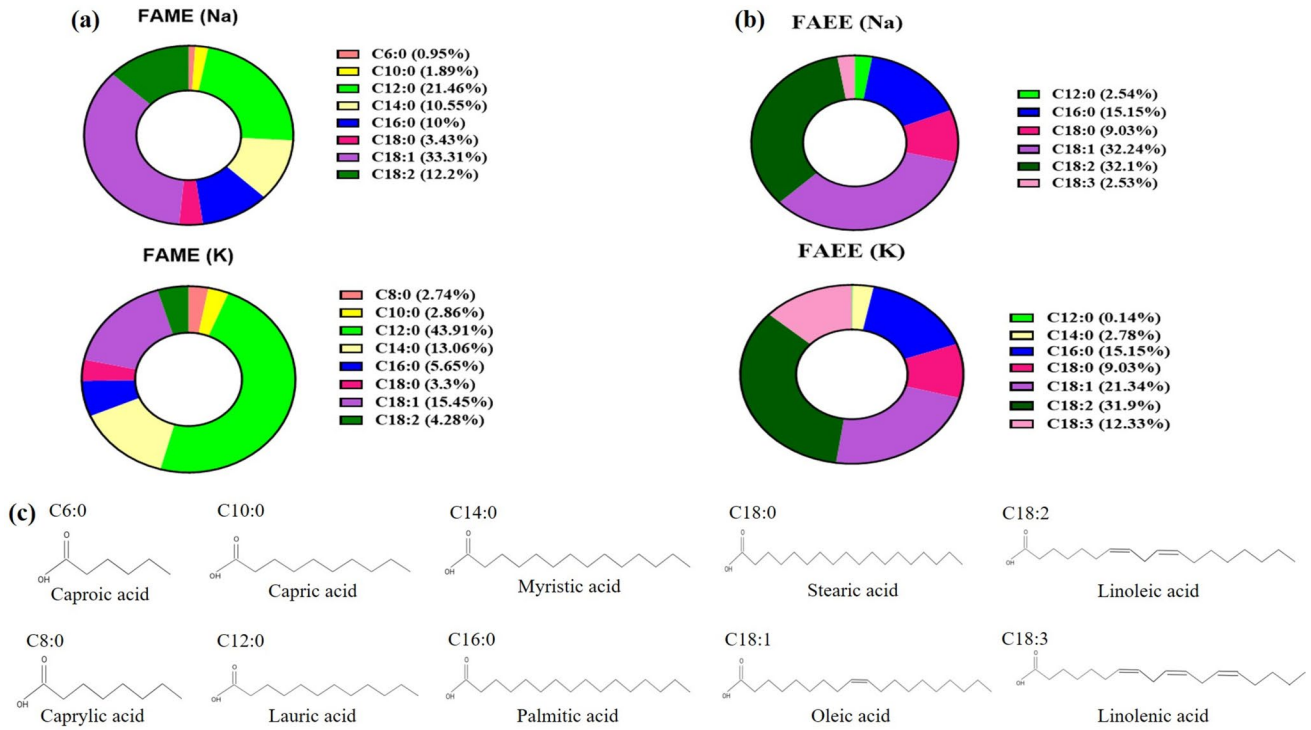

Fig. 3 Compositional analysis of alkyl esters based on GC–MS analysis **a** for FAME (Na) and FAME (K); **b** for FAEE (Na) and FAEE (K); **c** structures of fatty acids

FAME (Na) obtained contains lauric acid (21.46%), myristic acid (10.55%), palmitic acid (10%), oleic acid (33.31%) and linoleic acid (12.2%) in a significant amount. In parallel to a study by Allami et al. [33] reported similar composition of fatty acids. In FAME (K), lauric acid (43.91%), myristic acid (13.06%) and oleic acid (15.45%) are obtained at higher amounts which is in accordance to the report by Betiku et al. [43] as shown in (Fig. 3a). In Fig. 3b, as we can see palmitic acid (15.15%), stearic acid (9.03%), oleic acid (32.24%), linoleic acid (32.1%) were obtained in a significant amount for FAEE (Na) and the result is found to be in agreement with previous study reported by Anastopoulos et al. [7] with used frying oil. Palmitic acid (15.15%), stearic acid (9.03%), oleic acid (21.34%), linoleic acid (31.9%) and linolenic acid (12.33%) were found in higher amounts which is in-line with the observation made by Samuel et al. [50] using rubber seed oil. Nevertheless, the most frequent compounds detected are palmitic acid, stearic acid, oleic acid and linoleic acid where these acids are responsible for the formation of FAAE [51]. These acids are significantly used as emulsifiers and lubricants in cosmetic creams, soaps and tooth paste manufacturing [52]. Stearic acid is reported to be present in about 2465 cosmetic products and oleic acid is applied in 424 cosmetics formulations that are commercially available as listed by food and drug administration (FDA). Lauric acid, palmitic acid, myristic acid, stearic acid and oleic acid are regarded as safe for human consumption in the form of food additives (either directly or modified). Amongst these mentioned fatty acids, oleic and stearic acid are permitted to directly use in food application [53].

In view of fuel application as a blend (biodiesel) there is a pre-requisite to have higher composition of saturated and monounsaturated fatty acids in the obtained FAAE. On the other hand, the presence of polyunsaturated fatty acid might lead to higher viscous biodiesel that limits its fuel blend application. In our study, among the FAAE, FAME contains higher amount of saturated fatty acid and monounsaturated fatty acids of around 80–86% and FAEE as solvent 48–60% of saturated fatty acid and monounsaturated fatty acids were observed (Supplementary material Table S1). Therefore, methanol is considered as an effective solvent for transesterification of IPKO. The volumetric yield of saturated fatty acids and monounsaturated fatty acids resulted to about 55.51% for FAME (Na) and 53.07% of saturated fatty acid and monounsaturated fatty acids was obtained FAME (K) was used for transesterification of IPKO. In accordance with the above results, FAAEs transesterified using methanol and NaOH was used for further fuel studies.

In order to use FAAE as biodiesel or fuel blends certain characteristics such as degree of saturation, fatty acid

Table 2 Characterization of diesel-PKO biodiesel blends and diesel

Characteristics	Unit	Biodiesel	Diesel	B5	B10	B20	Standard range ASTM
Density	g/cm^3	856	841	844	849	851	680–970
Kinematic viscosity at 40 °C	mm^2/s	4.53	2.51	3.38	3.51	3.83	1.9–6.0
Flash point	°C	101	54	62	74	88	60–190
Fire point	°C	105	61	69	81	93	–
Cloud point	°C	4.1	1.0	1.8	2.4	3.0	–
Pour point	°C	2.7	0.2	0.9	1.6	2.1	− 15–6
Calorific value	MJ/kg	37.2	46.1	42.7	41.1	40.4	–

moiety, hydrocarbon chain length and its branching are to be considered [54]. The properties are dependent on the solvent used for transesterification of oil wherein the chain length (C1–C5) and the branching of alcohol moiety could significantly affect the cloud point and pour point as evident from this study [55]. Though higher chain esters (butyl and propyl) seems to have superior fuel properties, considering the cost and techno-economic feasibility low chain alcohols are employed in large scale [54]. Therefore, in our study methanol and ethanol only employed than other solvents. The results indicated that the ASTM standards of FAME blends with conventional diesel seems to be promising fuel alternatives as discussed in subsequent section.

IPKO FAME as a Potent Fuel Based on the Physcio-Chemical Properties

Density

The physical characterization of IPKO derived biodiesel blended with normal diesel at different ratios is mentioned in Table 2. The average density of the diesel and IPKO biodiesel blends were determined and the value of IPKO biodiesel was 856 g/cm^3 and for diesel it was 841 g/cm^3. The IPKO biodiesel density is found to be 1.8% higher than the diesel. All the blended samples have similar density to that of the diesel which could increase the atomization and reduce the viscosity.

Kinematic Viscosity

Kinematic viscosity is the measurement of resistance of a fluid to flow. Higher the viscosity lesser the flow of liquid. The kinematic viscosity at 40 °C for the IPKO biodiesel (4.53 mm^2/s) was higher than that of normal diesel (2.51 mm^2/s). The IPKO blended biodiesel was 25 to 35 percent higher than the diesel. However, the values fall within the standard range of ASTM indicating that these blended samples can be used in diesel engines. The viscosity is an important factor for biodiesel as it impacts the functioning of fuel injection machinery, especially at low temperatures [56]. Higher viscosity fuels may result in inefficient fuel combustion that results in the development of deposits that lead to greater motor oil dilution with fuel [57].

Flash and Fire Point

The flash point is the temperature at which a liquid sample produces enough vapor to cause an instantaneous flash of combustion when exposed to a typical source of ignition. Fire point is the temperature at which a particular fuel vapor will sustain to fire for at least five seconds after being ignited by an open flame. As observed from Table 2, the flash and the fire point of IPKO biodiesel is higher than that of diesel by 46.5% and 41.9% respectively. Lesser the flash point and fire point are a sign that the alcohol has not been eliminated from the biodiesel, according to research [58]. From a safety point of view, IPKO biodiesel is a better option when compared with the diesel and PKO blended biodiesel.

Cloud and Pour Point

The biodiesel cold flow temperatures are an important criterion for quality because fuel that has frozen can clog filters and lines, starving the motor for fuel. The cloud point is the temperature at which the quantity of wax in the fuel is adequate to solidify it, making it the lowest temperature at which the fuel can flow. The fuel pour point is the temperature at which it has accumulated many particles that it resembles a gel and can no longer flow [59]. Similar to other properties the cloud and the pour point is higher for the IPKO biodiesel than that of normal diesel. The cloud and the pour point of the IPKO biodiesel, diesel and IPKO blended biodiesel are determined and the values are mentioned in Table 2 and confine to ASTM standards. A biodiesel characterized by higher amounts of saturated fatty acids results in higher cloud and pour point which

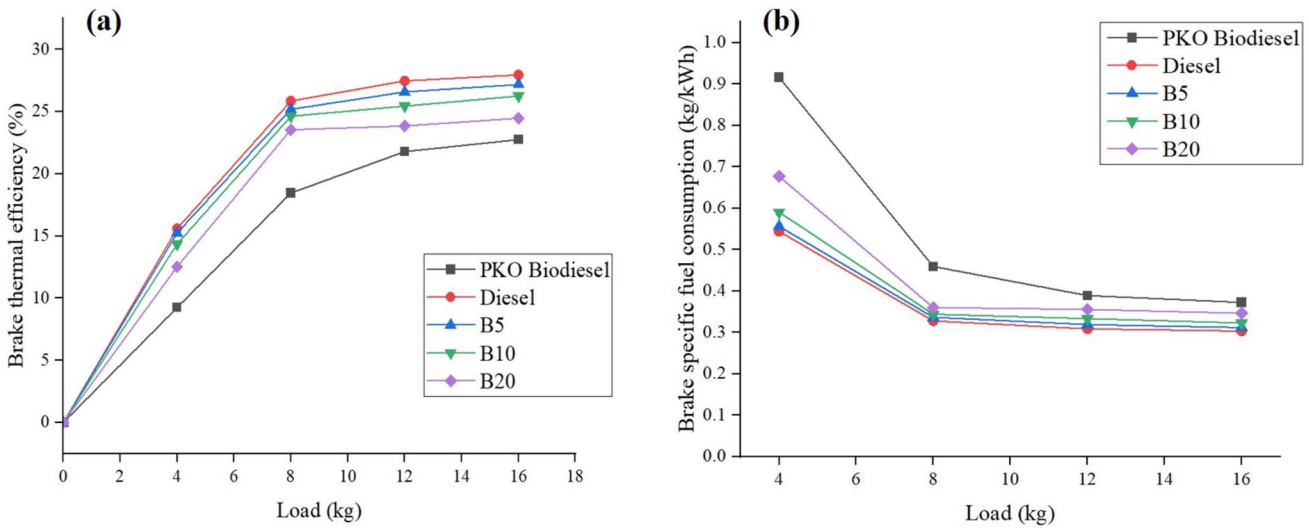

Fig. 4 **a** Brake thermal efficiency; **b** Brake specific fuel consumption of diesel and its blend with IPKO biodiesel at different engine loads

is not favorable for usage in countries which are low in temperature [60].

Calorific Value

The calorific value is a significant thermal property of fuels which implies the amount of heat energy generated during full combustion. The calorific value of IPKO biodiesel, diesel and PKO blended biodiesel is given in Table 2. The estimated calorific value of IPKO is 37.2 MJ/kg, whereas, for the normal diesel 46.1 MJ/kg. The calorific value of IPKO biodiesel is 19.31% less than the diesel which indicates that the amount of IPKO biodiesel usage should be higher to attain the same power as normal diesel.

Engine Performance Testing

Brake Thermal Efficiency (BTE)

Brake thermal efficiency of all tested samples is interpreted in Fig. 4a. BTE can be calculated using the brake power output and by the energy of the combustion fuel, which is one of the most significant variables in determining how quickly thermal energy is converted into useful work [61]. There was a gradual increase in BTE with respect to load. As shown in Fig. 4a, the maximum BTE was recorded for diesel and the lowest was recorded for the IPKO biodiesel. This is because of the higher viscosity (4.53 mm^2/s), lesser heating content [56]. The B5 fuel showed a similar BTE as that of the normal diesel.

Brake Specific Fuel Consumption (BSFC)

Brake specific fuel consumption is the mass rate of fuel consumption per unit brake power, which is proportionally reciprocal to BTE. The profiles of IPKO biodiesel, diesel and IPKO blended biodiesel BSFC at constant engine speed and at various load conditions is shown in the Fig. 4b. There is a decrease in BSFC with increase in load irrespective of the fuel types [62]. The IPKO biodiesel showed a higher BSFC when compared to pure diesel, this may be due to higher viscosity and low calorific value [63]. Higher kinematic viscosity favors fuel evaporation which results in lower fuel atomization thereby leading to poorer combustion and thermal efficiency. The oxygenated nature of the biodiesel causes negative impacts to the combustion process. Similar results were obtained by Karabektas [64] where, the BSFC of the biodiesel was higher than the pure diesel. However, the B5 fuel is almost close to the diesel sample.

Table 3 Characterization of IPKO glycerol and pure glycerol

Parameters	Standard values*	Pure glycerol	IPKO derived crude glycerol
pH	6.48–7.56	7.2	6.7
Ash content (%)	< 1.0	1.14 ± 0.07	2.41 ± 0.28
Volatile solids (%)	> 99	98.86 ± 0.07	97..59 ± 0.28
Moisture content (%)	–	0.03 ± 0.001	2.38 ± 0.045
Density (g/cm^3)	1.26	1.28 ± 0.05	1.19 ± 0.004
Colour	Clear	Clear	White

*British standard (BS) values

Further, to improve the efficiency of the biodiesel few additives are added which provide valuable benefits like reduction of oxidation stability, injector deposit formation, long-term storage corrosion and microbial contamination. Additives are a type of chemical compound that are added to various types of fuel, including diesel, biodiesel, gasoline, and aviation oil, with the goal of improving their performance and efficiency. By enhancing the properties of the fuel, additives can help to optimize engine performance and meet environmental emission control standards. When selecting additives for biodiesel fuel, factors such as fuel blending properties, economic feasibility, additive solubility, toxicity, fuel blend viscosity, flash point, and water solubility and partitioning must be taken into consideration [65]. Variety of additives such as metal-based, oxygenated additives, antioxidants, cold flow improver additives and cetane improvers, are profound to enhance various properties of biodiesel fuel [66].

Characterization of IPKO Glycerol

IPKO derived glycerol had a lower pH of 6.7, which is close to the pure glycerol of 7.2 (Table 3). This is because of the removal of alkali residues in the purification step. The density of the IPKO glycerol is found to be 1.19 ± 0.004 g/cm^3, which is slightly lower than the pure glycerol (1.28 g/cm^3). This is due the presence of some impurities like fatty acids, FAME and water. In the study of Hu et al. [37] the pH values of three different crude glycerol samples from three different soybean oil (based on region) varied from 6.9 to 10. In the same study, the density of crude glycerol was varied from 1.2 to 1.31 g/cm^3 which is similar to the IPKO glycerol obtained in this study (1.19 g/cm^3). The ash content and moisture content of IPKO glycerol was observed to be 2.41 ± 0.28% and 2.38 ± 0.045% respectively, which was higher than pure glycerol (1.14 ± 0.07% and 0.03 ± 0.003%)). The observation made was attributed to the aqueous nature of the by-product obtained post-transesterification.

Fourier-Transform Infrared Spectroscopy (FTIR)

The crude glycerol presence was confirmed using FTIR analysis (Supplementary material Fig. S5) through validation of functional groups related with glycerol. Large peak at 3371 cm^{-1} indicates the presence of –OH group and at sharp peaks at 2924 cm^{-1} and 2856 cm^{-1} represents the C–H stretching linked with the polyalcohol, mainly glycerol. Peak at 1456 cm^{-1} indicates C–O–H stretching related with polyalcohol. The presence of glycerol was confirmed by the peak observed at 1035 cm^{-1} which represents the C–O group. In crude glycerol sample, peak at 1741 cm^{-1} was observed which indicates the presence of impurities like soaps, fatty acids and salts and C=O bonds related to carboxylic acid or esters. The catalyst involved in the transesterification is present in the crude glycerol which was confirmed by the band observed at 1168 cm^{-1} that correspondes to COO– group [26].

Qualitative Analysis of Glycerol Through GC–MS

The crude glycerol obatined from biodiesel process can be possibly derivatized from the PKO. The impurities present in the crude glycerol was determined using GC–MS analysis (Supplementary material Fig. S6). At a retention time of 25.79 min the most prominent peak with an area percentage of 40.07% was found to be glycerol based on NIST library. Many fatty acids such as decanoic acid (2.88%), octanoic acid (6.71%), dodecanoic acid (9.69%), tetradecanoic acid (3.84%), hexadecenoic acid (6.64%), pentadecanoic acid (1.85%), butanedioic acid (0.89%), tetracasanoic acid (1.1%), octadecanoic acid (2.4%) were also present along with the glycerol which might influence the fermentative behaviour of the organism when supplemented as a co-substrate. In a study reported by Janajreh et al. [67], the waste cooking oil was transesterified and the crude glycerol obtained after transesterification was subjected to GC–MS analysis. Hexanoic acid (0.34%), octanoic acid (1.45%), decanoic acid (1.54%), dodecanoic acid (11.81%), doecanoic acid (0.43%), hexadecenoic acid (1.14%), hexadecoic acid (0.67%), heptadecanoic acid (0.41%), octadecanoic (0.63%) where detected in the crude glycerol with the glycerol area of 30.25% which is similar to the qualitative analysis of IPKO.

Production of Xylitol from Xylose as Substrate by *C. tropicalis* NCIM 3118 (Strategy 1)

The media containing xylose was used for the fermentation of *C. tropicalis* to produce xylitol. The maximum xylitol production was 6.75 ± 0.02 g/l after 7 days (Fig. 5a) with an initial xylose concentration of 25 g/l in the MSM media and the yield was found to be 0.52 $g_{xylitol}/g_{TOC}$ (Table 4). Delfín-Ruíz et al. [68] worked upon *C. tropicalis* wherein sugarcane bagasse hydrolysate was used as substrate which contained 27.95 g/l of xylose and obtained 5.5 g/l of xylitol with a yield of 0.39 g/g. Ko et al. [69] reported that *C. tropicalis* has resulted in the highest xylitol yield of 0.41 g xylitol/g xylose at 60 h which is similar to the outcome of this study. It has been reported that the initial concentration of xylose has a great impact towards its fermentation. If the initial concentration of xylose is too high then it leads to substrate inhibition of the xylitol synthesis. A study has been reported that gradual increase of xylose has resulted in improved xylitol production [70]. As observed in this study, the xylose is not completely utilized for the conversion of xylitol and the residual TOC was found to be 11.9 ± 0.2 g/l. The reason behind this observation might

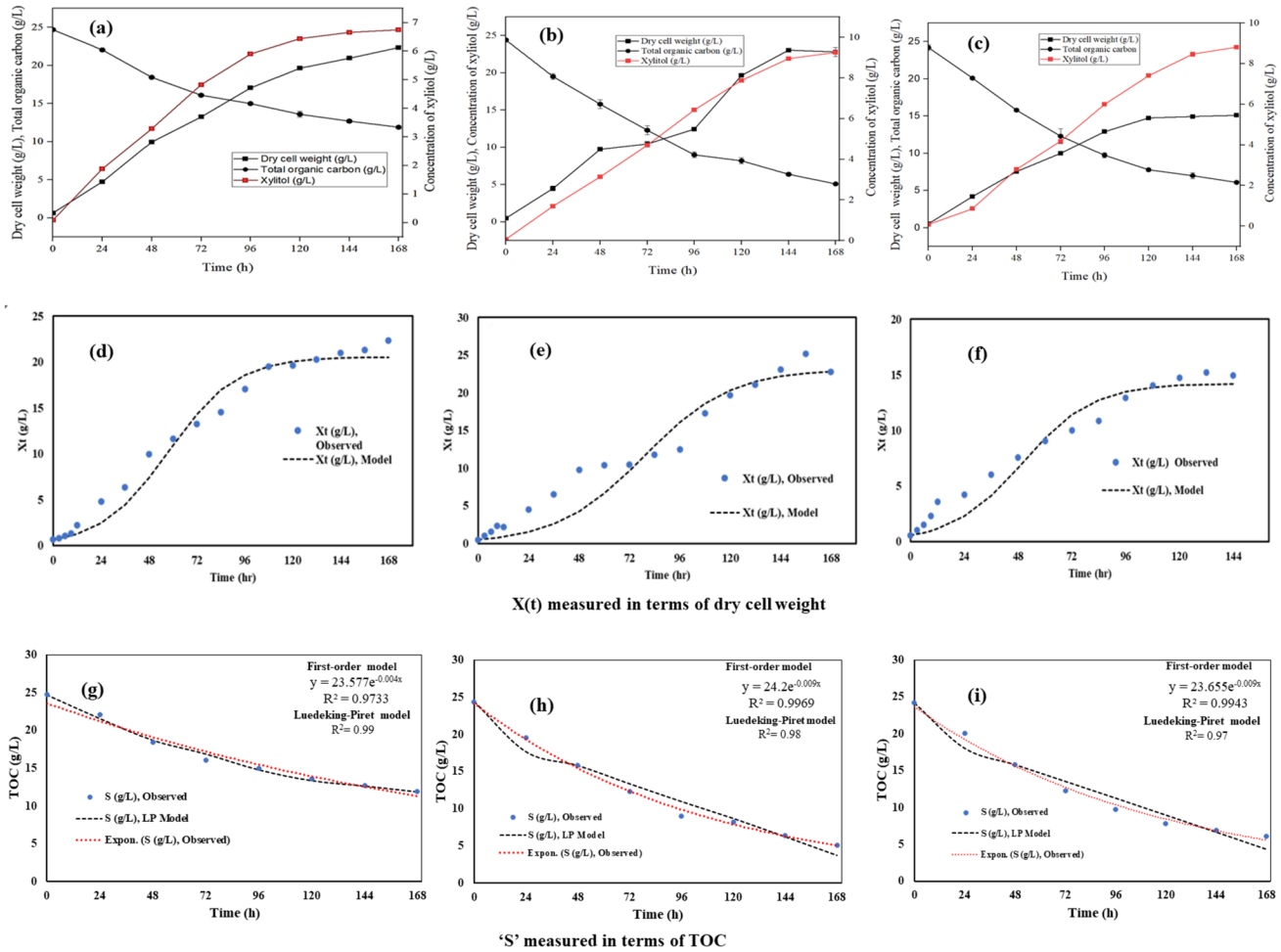

Fig. 5 Growth profile of *Candida tropicalis* NCIM3118 with **a** Xylose, **b** Xylose + Pure Glycerol, **c** Xylose + IPKO Glycerol, Hybrid-Monod kinetic profile **d** Xylose, **e** Xylose + Pure Glycerol; **f** Xylose + IPKO Glycerol and Substrate consumption pattern with Luedeking-Piret and First order kinetic profile **g** Xylose, **h** Xylose + Pure Glycerol; **i** Xylose + IPKO Glycerol

be the lack of coenzyme-Nicotinamide adenine dinucleotide phosphate (NADPH) for xylose reducatse that converts xylose to xylitol. Therefore, to have continuous xylitol production, an efficient xylose consumption can be increased by adding a co-substrate in the fermentation media which helps to regenerate NADPH [71]. The molecular mechanism of NAD + precursors homeostasis and regulation of NAD + metabolism are sporadically studied and still unclear which is due to the dynamic flexibility of precursors that a cell utilize to generate NAD + . However, it has been reported by Kato and Lin [72] that in eukaryotes like yeast the intracellular compartmentalization of significant metabolic reactions could lead to regulation of certain enzymatic functions by either acting as sink (sequestration) or tank (concentration) of specific metabolites which might be the plausible reason for the lack of coenzyme towards action of xylose reductase. Such interloping mechanism of interacting signaling pathways when co-substrate like glycerol supplemented along with xylose might establish metabolic flexibility that contribute to genomic stability and maintaining cell fitness as evident from the comparative kinetic parameters of strategy 1–3. These data indicate that xylitol production did not depend on cell growth, and that xylose metabolism could be tightly regulated by certain carbohydrates.

Effect of Pure and IPKO Glycerol as Co-substrate on *C. tropicalis* NCIM 3118 (Strategy 2 and 3)

Candida tropicalis, an oleaginous yeast which could adapt to fats, oils and fatty acids in the fermentation medium makes it unique organism to produce value-added chemicals [26]. Hence, a strategy of addition of glycerol as co-substrate was attempted. Also, there might be an influential factor for fermentation by the presence of impurities in glycerol post-transesterification, hence a comparison is drawn by addition

Table 4 The kinetic parameters acquired through modeling

Parameters	Xylose	Xylose/glycerol	Xylose/IPKO glycerol
Hybrid logistic-monod model			
μ_{max} (h^{-1})	0.059	0.048	0.064
X_0 (g/L)	0.8	1.05	1.0
X_{max} (g/L)	20.55	23.16	14.21
R^2	0.99	0.9	0.98
Luedeking-Piret model			
S_0 (g/L)	23.84	17.45	21.08
α	0.8002	0.4362	1.29
β	0.0113	0.005	0.012
$Y_{X/S}$ (g_{DCW}/g_{TOC})	1.48	4.23	0.77
	1.71 (observed)	1.98 (observed)	1.33 (observed)
$Y_{P/S}$ ($g_{xylitol}/g_{TOC}$)	0.81	0.71	1.42
	0.52 (observed)	0.48 (observed)	0.48 (observed)
k_e	0.0066	0.005	0.0118
R^2	1	0.98	0.98
First-order kinetics			
r_x (h^{-1})	0.025	0.025	0.03
r_s (h^{-1})	0.004	0.009	0.009
r_p (h^{-1})	0.039	0.034	0.034

of pure and IPKO derived glycerol into the fermentative medium. The maximum xylitol production in pure glycerol addition was 9.25 ± 0.02 g/l (Fig. 5b) while the set with IPKO glycerol as co-substrate resulted in 8.81 ± 0.07 g/l (Fig. 5c). The product yield was estimated to be 0.48 $g_{xylitol}/g_{TOC}$ for both pure glycerol and crude glycerol (Table 4). When a co-substrate such as glycerol is used, it regenerates NADPH to produce xylitol from substrate (xylose) by the enzyme xylitol reductase as reported by Ahmad et al. [73] when using *C. tropicalis* BSXDH-3 with 50 g/l of xylose and 20 g/l glycerol was supplemneted in the medium.

The rationale for the observation is when glycerol enters into cytoplasm it gets converted to dihydroxyacetone phosphate (DHAP) by glycerol metabolism. Under the glucose starvation condition the DHAP undergoes gluconeogenesis and gets converted to glucose-6-phosphate. This glucose-6-phosphate undergoes pentose phosphate pathway and produces excess amount of NADPH. The excess amount of NADPH will be utilized by xylose to get converted to xylitol and results in enhanced xylitol production. The crude glycerol derived from PKO transesterification can be utilized for enhanced production of xylitol. Zhang et al. [74] have utilized crude glycerol for vitamin K2 synthesis by *B. subtilis* Z-15 and denoted that crude glycerol could be used instead of pure glycerin for vitamin K2 production. The crude glycerol derived from PKO transesterification can be utilized for enhanced production of xylitol.

Kinetic Modeling of Fermentative Strategies

Kinetic models especially in bioprocessing sector aid in the formulation of upstream and downstream process by considering the complex biochemistry of cells. Through mathematical analysis, it can be used to understand, precisely predict, and appraise the effects of different components of a fermentation process [75]. Further, models are formulated to describe the kinetics of microbial growth, substrate consumption, and product synthesis which play a fundamental role in process optimization and control by providing a basis for process design, control and scale-up [76]. Many industrially important products have been commercialized by making use of these models to increase the yield and productivity also minimize the formation of unwanted by-products thereby resulting the high quality product [75].

In this study, three different models have been employed to estimate the kinetic constants which would provide a clear understanding on the fermentative behavior of the organism when glycerol is supplemented as co-substrate. The kinetic analysis of *C. tropicalis* was done using hybrid Logistic-Monod model to understand the biomass production pattern as it plays role in xylitol synthesis with altered 'C' source (Fig. 5d–f), Luedeking-Piret model and first-order kinetics were employed for the substrate consumption behavior, rate of uptake and the product yield (Fig. 5g–i). These models were found to fit well with the experimental values with a significant regression coefficient (R^2) > 0.95 and the obtained kinetic constants were tabulated in Table 4. The prediction of the kinetic modeling for X_0 and X_{max} of *C.*

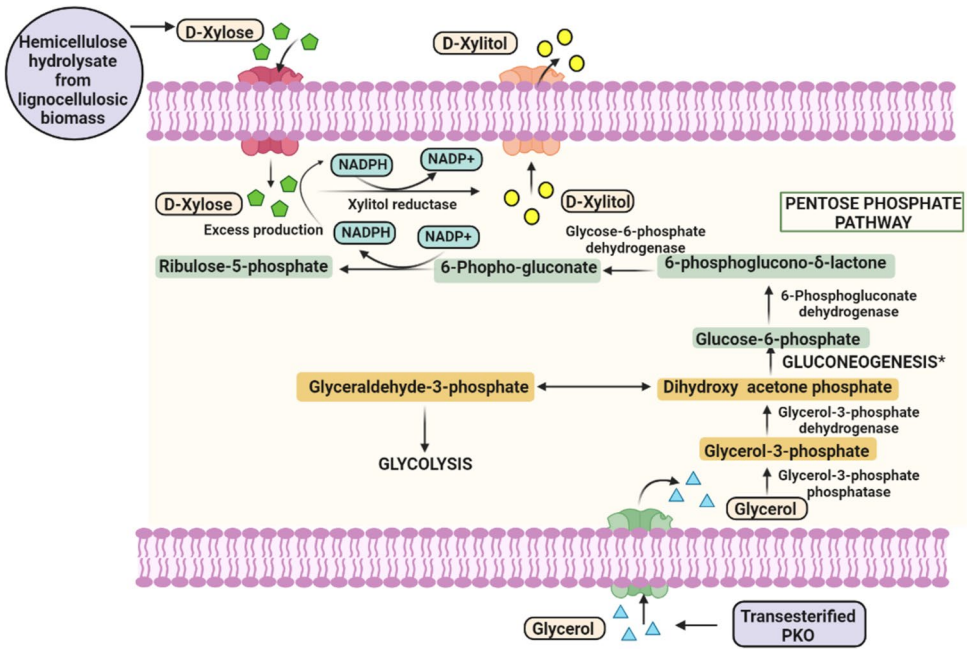

Fig. 6 Probable mechanism of enhanced xylitol production through co-utilization of D-xylose and glycerol by *Candida tropicalis* NCIM3118

tropicalis until the growth phase was observed to be constant with the experiment data as shown in Fig. 6a–c. The maximum specific growth rate (μ_{max}) was found to be higher when IPKO glycerol was used as co-substrate (0.064 h^{-1}) followed by 0.059 h^{-1} and 0.048 h^{-1} for xylose as substrate and pure glycerol as co-substrate respectively. Zhang et al. [71] reported a similar study where the maximum specific growth rate was observed to be 0.35 h^{-1}.

From Table 4, it was observed that the maximum cell biomass (23.16 g/l) produced was higher when xylose and pure glycerol (strategy 2) was used as the substrate followed by 20.55 g/l and 14.21 g/l when xylose (strategy 1) as substrate and IPKO glycerol as co-substrate (strategy 3) respectively. The decrease of biomass concentration in IPKO glycerol might be due to the limitations posed by the inhibitors. Considering the product yield coefficient (Yp/s), though there is a significant difference in the predicated yield coefficient between varied substrates (Strategy 3 > Strategy 1 > Strategy 2) while comparing the experimental yield coefficient, glycerol (pure and IPKO) supplemented media showed 0.48 g/g which is near comparable to the only xylose medium (0.52 g/g). Prabhu et al. [77] reported a yield of about 53.2 g of xylitol/l when pure glycerol and xylose was provided as a 'C' source for *Yarrowia lipolytica* with a bioconversion yield of 0.97 g/g. Similar results were obtained when pure glycerol was substituted with crude glycerol from the biodiesel industry (titer: 50.5 g/l; yield: 0.92 g/g). Glycerol offers an advantage of higher degree of reducation than carbohydrates (sugars) thus capable of bio-manufacturing of ethanol, propionate, succinate and xylitol with higher yields than those obtained by using sugars. In addition, glycerol serves as a cheap and abundant resource for microbial fermentation thereby increasing the techno-economic viability of the overall process. The comparative analysis of the xylose and glycerol supplementation for xylitol production by *Candida tropicalis* NCIM3118 corroborates with the observation made by Prabhu et al. [77].

The kinetic modeling prediction of *C. tropicalis* growth phase was observed to be consistent with the experimental data (Fig. 5d–f). When pure glycerol was given as co-substrate, *C. tropicalis* was able to utilize maximum substrate which corresponds to the $Y_{X/S}$ of 4.23 which was higher when compared to other substrates. The model prediction shows that the consumption of substrate by *C. tropicalis* depend on the growth based on the $\alpha > \beta$ from Luedeking-Piret Model predications (Fig. 5 g–i). Zhang et al. [74] reported that non-purified crude glycerol and pure glycerol exerted the similar effect on vitamin K2 production by *B. subtilis* Z-15 that corrobrated the results obtained in this study. Additionally, it is further demonstrated the feasibility of solvolysis-derived glycerol as a suitable alternative to pure glycerol in microbial fermentation thereby proving a cost effective stretegy. The high cost involved in the purification of crude glycerol that contains salts, solvents and other impurities makes it economically unviable, consequently resulting in a drastic reduction in the price of crude glycerol, which prompts to consider it as an industrial waste without much value. This created a scope for a new pollution source from oil processing units, thereby making the biodiesel production industries a cost intensive with low economic benefits. Application biotechnology to utilize crude glycerol as a fementative substrate to bio-manufacture high-value products posses a feasible startegy.

The rate of substrate consumption, biomass and product production was given by first-order kinetics. The rate of biomass (r_x) produced is almost equal for all the conditions ranging from 0.025 to 0.03 h^{-1} that shows the robustness of the producer organism to modulate the metabolism when varied substrates are administered. The rate of substrate utilization (r_s) was higher when pure glycerol and IPKO glycerol (0.009 h^{-1}) was given as co-substrate when xylose alone was given as substrate. The rate of product production (r_p) was about 0.034 h^{-1} when glycerol and IPKO glycerol was given as co-substrate and for xylose containing medium about 0.039 h^{-1} was observed. The mechanism behind the enhanced xylitol production is that, the regeneration of NADPH by glycerol for the conversion of xylose to xylitol using an enzyme called xylitol reductase (Fig. 6). In the context of waste route for sustainable lipid production, the source of xylose can be obtained from the hemicellulosic (xylan) fraction that serve as a cheap courbon source along with IPKO derived glycerol as a co-substrate. This production model becomes a complete biorefinery with waste valorization for sustinable production of microbial oleochemicals.

Conclusion

Utilization of non-conventional agrowaste-based feedstocks as a resource for high value products is deemed to befit for the techno-economic feasibility and viable option for biorefineries. This study for the first time demonstrated the simultaneous valorization of IPKO and transesterfication-derived glycerol to biodiesel and xylitol respectively. It also explored the FAME from IPKO as superior fuel alternative for diesel engines without any modification with limited emission characteristics. Further, the effect of different solvent on alkyl ester synthesis and hetergeneous catalysis of the IPKO could further widen the scope of its application in industries. The formulated strategy through this study could pave a way for sustainable valorization of IPKO as an effective bioresource for biodiesel as well as fermentative production of xylitol instead of cost incurring chemical route.

Supplementary Information The online version contains supplementary material available at https://doi.org/10.1007/s12649-023-02395-y.

Acknowledgements The authors would like to acknowledge the Department of Biotechnology, School of Bioengineering, SRM Institute of Science and Technology (SRMIST) for the financial support provided for research and dissertation work as well as the infrastructure to carry out the research work. We acknowledge Nanotechnology Research Centre (NRC), College of Engineering and Technology, Faculty of Engineering and Technology SRMIST, Kattankulathur for providing analytical support for the studies. Authors would like to acknowledge the ICAR-Directorate of Floricultural Research, Pune-411036, Maharashtra, India and ICAR-Indian Institute of Oil Palm Research, Pedavegi, West Godavari District, Andhra Pradesh for the provision of Indian palm kernel oil for the study.

Author Contributions SJ and SPJK are responsible for design of the experiment, evaluation of results and manuscript; JS executed the experiments in the laboratory, compiled, analyzed and interpreted the results and drafted the manuscript. PNK and KR imparted agronomical aspects of the palm kernel oil for biovalorization work.

Funding No external funding/grants are associated with this work. The work is done with infrastructural support from the Department of Biotechnology, School of Bioengineering, SRM Institute of Science and Technology, Kattankulathur, Tamil Nadu, India.

Data Availability Specific experimental design and figures to support the observation during the experiments shall be provided based on the request made for it.

Code Availability Not applicable.

Declarations

Competing interests This article is an original research work designed and executed by the authors. There is no conflict of interest associated with this scientific work.

Ethical Approval Not Applicable.

Informed Consent The authors have consented to participate in the research work carried and publish the technical outcome of the same.

Consent for Publication All the authors mutually agree to publish this scientific work carried out by them to this journal.

Research Involving in Animal Participants No animals used in this study.

References

1. Yusuff, A.S., Gbadamosi, A.O., Atray, N.: Development of a zeolite supported CaO derived from chicken eggshell as active base catalyst for used cooking oil biodiesel production. Renew. Energy **197**, 1151–1162 (2022). https://doi.org/10.1016/j.renene.2022.08.032
2. Ajala, O.E., Aberuagba, F., Odetoye, T.E., Ajala, A.M.: Biodiesel: sustainable energy replacement to petroleum-based diesel fuel—a review. ChemBioEng Rev. **2**, 145–156 (2015). https://doi.org/10.1002/cben.201400024
3. Kareem, S.O., Falokun, E.I., Balogun, S.A., Akinloye, O.A., Omeike, S.O.: Enzymatic biodiesel production from palm oil and palm kernel oil using free lipase. Egypt. J. Pet. **26**, 635–642 (2017). https://doi.org/10.1016/j.ejpe.2016.09.002
4. Tongroon, M., Suebwong, A., Kananont, M., Aunchaisri, J., Chollacoop, N.: High quality jatropha biodiesel (H-FAME) and its application in a common rail diesel engine. Renew. Energy **113**, 660–668 (2017). https://doi.org/10.1016/j.renene.2017.06.006
5. Fukuda, H., Kondo, A., Noda, H.: Biodiesel fuel production by transesterification of oils. J. Biosci. Bioeng. **92**, 405–416 (2001). https://doi.org/10.1016/S1389-1723(01)80288-7
6. Ferella, F., Mazziotti Di Celso, G., De Michelis, I., Stanisci, V., Vegliò, F.: Optimization of the transesterification reaction in

biodiesel production. Fuel **89**, 36–42 (2010). https://doi.org/10.1016/j.fuel.2009.01.025
7. Anastopoulos, G., Zannikou, Y., Stournas, S., Kalligeros, S.: Transesterification of vegetable oils with ethanol and characterization of the key fuel properties of ethyl esters. Energies **2**, 362–376 (2009). https://doi.org/10.3390/en20200362
8. Encinar, J.M., González, J.F., Rodríguez-Reinares, A.: Ethanolysis of used frying oil. Biodiesel preparation and characterization. Fuel Process. Technol. **88**, 513–522 (2007). https://doi.org/10.1016/j.fuproc.2007.01.002
9. Koh, M.Y., Ghazi, T.I.M.: A review of biodiesel production from *Jatropha curcas* L. oil. Renew. Sustain. Energy Rev. **15**, 2240–2251 (2011). https://doi.org/10.1016/j.rser.2011.02.013
10. Al-Widyan, M.I., Al-Shyoukh, A.O.: Experimental evaluation of the transesterification of waste palm oil into biodiesel. Bioresour. Technol. **85**, 253–256 (2002). https://doi.org/10.1016/S0960-8524(02)00135-9
11. Antolin, G., et al.: Optimisation of biodiesel production by sunflower oil transesterification. Bioresour. Technol. **83**, 111–114 (2002). https://doi.org/10.1016/S0960-8524(01)00200-0
12. Azcan, N., Danisman, A.: Microwave assisted transesterification of rapeseed oil. Fuel **87**, 1781–1788 (2008). https://doi.org/10.1016/j.fuel.2007.12.004
13. Keera, S.T., El Sabagh, S.M., Taman, A.R.: Castor oil biodiesel production and optimization. Egypt. J. Pet. **27**, 979–984 (2018). https://doi.org/10.1016/j.ejpe.2018.02.007
14. Rupilius, W., Ahmad, S.: Palm oil and palm kernel oil as raw materials for basic oleochemicals and biodiesel. Eur. J. Lipid Sci. Technol. **109**, 433–439 (2007). https://doi.org/10.1002/ejlt.200600291
15. Jin, C., Liu, X., Sun, T., Ampah, J.D., Geng, Z., Ji, J., Wang, G., Liu, H.: Preparation and performance improvement of methanol and palm oil/palm kernel oil blended fuel. Fuel Process. Technol. **223**, 106996 (2021). https://doi.org/10.1016/j.fuproc.2021.106996
16. Nik Norulaini, N.A., Md Zaidul, I.S., Anuar, O., Omar, A.K.M.: Supercritical enhancement for separation of lauric acid and oleic acid in palm kernel oil (PKO). Sep. Purif. Technol. **35**, 55–60 (2004). https://doi.org/10.1016/S1383-5866(03)00130-8
17. Ahmed, S.: State of the Art and Future of Palm Oleochemistry in the World. Fedepalma, Colombia (2007)
18. Why, E.S.K., Ong, H.C., Lee, H.V., Chen, W.H., Asikin-Mijan, N., Varman, M.: Conversion of bio-jet fuel from palm kernel oil and its blending effect with jet A-1 fuel. Energy Convers. Manag. **243**, 114311 (2021). https://doi.org/10.1016/j.enconman.2021.114311
19. Mathur, R.K., Manorama, K., Kalyanababu, B., Ravichandran, G., Ramachandrudu, K., Prasad, M.V.: Innovations to make india self-reliant in edible oil production: the story of oil palm. In: Innovations in Agriculture for a Self-Reliant India. CRC Press, London (2021)
20. Ejeromedoghene, O.: Acid-catalyzed transesterification of Palm Kernel Oil (PKO) to biodiesel. Mater. Today Proc. **47**, 1580–1583 (2021). https://doi.org/10.1016/j.matpr.2021.04.042
21. Betiku, E., Odude, V.O., Ishola, N.B., Bamimore, A., Osunleke, A.S., Okeleye, A.A.: Predictive capability evaluation of RSM, ANFIS and ANN: a case of reduction of high free fatty acid of palm kernel oil via esterification process. Energy Convers. Manag. **124**, 219–230 (2016). https://doi.org/10.1016/j.enconman.2016.07.030
22. Maguire, A., Rugg-Gunn, A.J.: Xylitol and caries prevention—is it a magic bullet? Br. Dent. J. **194**, 429–436 (2003). https://doi.org/10.1038/sj.bdj.4810022
23. Chen, X., Jiang, Z.H., Chen, S., Qin, W.: Microbial and bioconversion production of D-xylitol and its detection and application. Int. J. Biol. Sci. (2010). https://doi.org/10.7150/ijbs.6.834
24. Dasgupta, D., Bandhu, S., Adhikari, D.K., Ghosh, D.: Challenges and prospects of xylitol production with whole cell bio-catalysis: a review. Microbiol. Res. **197**, 9–21 (2017). https://doi.org/10.1016/j.micres.2016.12.012
25. Umai, D., Kayalvizhi, R., Kumar, V., Jacob, S.: Xylitol: bioproduction and applications—a review. Front. Sustain. **3**, 826190 (2022). https://doi.org/10.3389/frsus.2022.826190
26. Mitrea, L., Ranga, F., Fetea, F., Dulf, F.V., Rusu, A., Trif, M., Vodnar, D.C.: Biodiesel-derived glycerol obtained from renewable biomass—a suitable substrate for the growth of *Candida zeylanoides* yeast strain ATCC 20367. Microorganisms. **7**, 265 (2019). https://doi.org/10.3390/microorganisms7080265
27. Umai, R.D., Jacob, S., Kumar, V.: Deep eutectic solvent pretreatment of water hyacinth for improved holocellulosic saccharification and fermentative co-production of xylitol and lipids using rhodosporidium toruloides NCIM 3547. Fermentation. **8**, 591 (2022). https://doi.org/10.3390/fermentation8110591
28. Arruda, P.V., Felipe, M.G.A.: Role of glycerol addition on xylose-to-xylitol bioconversion by *Candida guilliermondii*. Curr. Microbiol. **58**, 274–278 (2009). https://doi.org/10.1007/s00284-008-9321-7
29. Paquot, C.: Standard Methods for the Analysis of Oils, Fats and Derivatives. Elsevier, Pergamon (1979)
30. Petrauskaite, V., De Greyt, W., Kellens, M., Huyghebaert, A.: Physical and chemical properties of *trans* -free fats produced by chemical interesterification of vegetable oil blends. J. Am. Oil Chem. Soc. **75**, 489–493 (1998). https://doi.org/10.1007/s11746-998-0252-z
31. Hashemzehi, M., Saghatoleslami, N., Nayebzadeh, H.: A study on the structure and catalytic performance of Zn Cu1−Al2O4 catalysts synthesized by the solution combustion method for the esterification reaction. Comptes Rendus Chim. **19**, 955–962 (2016). https://doi.org/10.1016/j.crci.2016.05.006
32. Hayyan, A., Alam, Md.Z., Mirghani, M.E.S., Kabbashi, N.A., Hakimi, N.I.N.M., Siran, Y.M., Tahiruddin, S.: Sludge palm oil as a renewable raw material for biodiesel production by two-step processes. Bioresour. Technol. **101**, 7804–7811 (2010). https://doi.org/10.1016/j.biortech.2010.05.045
33. Allami, H.A., Tabasizadeh, M., Rohani, A., Farzad, A., Nayebzadeh, H.: Precise evaluation the effect of microwave irradiation on the properties of palm kernel oil biodiesel used in a diesel engine. J. Clean. Prod. **241**, 117777 (2019). https://doi.org/10.1016/j.jclepro.2019.117777
34. Egbuna, S.O., Nwachukwu, U.J., Agu, C.M., Asadu, C.O., Okolo, B.: Production of biolubricant samples from palm kernel oil using different chemical modification approaches. Eng. Rep. (2021). https://doi.org/10.1002/eng2.12422
35. Jitputti, J., Kitiyanan, B., Rangsunvigit, P., Bunyakiat, K., Attanatho, L., Jenvanitpanjakul, P.: Transesterification of crude palm kernel oil and crude coconut oil by different solid catalysts. Chem. Eng. J. **116**, 61–66 (2006). https://doi.org/10.1016/j.cej.2005.09.025
36. Miyuranga, K.A.V., Arachchige, U.S.P.R., Jayasinghe, R.A., Samarakoon, G.: Purification of residual glycerol from biodiesel production as a value-added raw material for glycerolysis of free fatty acids in waste cooking oil. Energies **15**, 8856 (2022). https://doi.org/10.3390/en15238856
37. Hu, S., Luo, X., Wan, C., Li, Y.: Characterization of crude glycerol from biodiesel plants. J. Agric. Food Chem. **60**, 5915–5921 (2012). https://doi.org/10.1021/jf3008629
38. Soil Organic Carbon Walkley Black Method. Food and Agriculture Organization of the United Nations (2019)
39. Sánchez, J.: Colorimetric assay of alditols in complex biological samples. J. Agric. Food Chem. **46**, 157–160 (1998). https://doi.org/10.1021/jf970619t
40. Alankar, S.S.L., Sajesh, N., Rastogi, S., Sakhuja, S., Rajeswari, G., Kumar, V., Chandel, A.K., Jacob, S.: Bioprocessing of fermentable sugars derived from water hyacinth into microbial lipids

and single cell proteins by oleaginous yeast *Rhodosporidium toruloides* NCIM 3547. Biomass Convers. Biorefinery. (2021). https://doi.org/10.1007/s13399-021-02007-6
41. Rajeswari, G., Jacob, S.: Saccharolysis of laccase delignified *Aloe vera* leaf rind and fermentation through free and immobilized yeast for ethanol production. J. Food Process Eng (2021). https://doi.org/10.1111/jfpe.13514
42. Xu, P.: Analytical solution for a hybrid Logistic-Monod cell growth model in batch and continuous stirred tank reactor culture. Biotechnol. Bioeng. **117**, 873–878 (2020). https://doi.org/10.1002/bit.27230
43. Betiku, E., Osunleke, A.S., Odude, V.O., Bamimore, A., Oladipo, B., Okeleye, A.A., Ishola, N.B.: Performance evaluation of adaptive neuro-fuzzy inference system, artificial neural network and response surface methodology in modeling biodiesel synthesis from palm kernel oil by transesterification. Biofuels **12**, 339–354 (2021). https://doi.org/10.1080/17597269.2018.1472980
44. Ishola, F., Adelekan, D., Mamudu, A., Abodunrin, T., Aworinde, A., Olatunji, O., Akinlabi, S.: Biodiesel production from palm olein: a sustainable bioresource for Nigeria. Heliyon. **6**, e03725 (2020). https://doi.org/10.1016/j.heliyon.2020.e03725
45. Silva, G.F., Camargo, F.L., Ferreira, A.L.O.: Application of response surface methodology for optimization of biodiesel production by transesterification of soybean oil with ethanol. Fuel Process. Technol. **92**, 407–413 (2011). https://doi.org/10.1016/j.fuproc.2010.10.002
46. Pappu, V.K.S., Kanyi, V., Santhanakrishnan, A., Lira, C.T., Miller, D.J.: Butyric acid esterification kinetics over Amberlyst solid acid catalysts: the effect of alcohol carbon chain length. Bioresour. Technol. **130**, 793–797 (2013). https://doi.org/10.1016/j.biortech.2012.12.087
47. Sani, Y.M., Daud, W.M.A.W., Abdul Aziz, A.R.: Activity of solid acid catalysts for biodiesel production: a critical review. Appl. Catal. Gen. **470**, 140–161 (2014). https://doi.org/10.1016/j.apcata.2013.10.052
48. Röttig, A., Wenning, L., Bröker, D., Steinbüchel, A.: Fatty acid alkyl esters: perspectives for production of alternative biofuels. Appl. Microbiol. Biotechnol. **85**, 1713–1733 (2010). https://doi.org/10.1007/s00253-009-2383-z
49. Knothe, G., Krahl, J., Gerpen, J.V.: The Biodiesel Handbook. AOCS Press, Urbana (2010)
50. Samuel, O.D., Okwu, M.O., Amosun, S.T., Verma, T.N., Afolalu, S.A.: Production of fatty acid ethyl esters from rubber seed oil in hydrodynamic cavitation reactor: study of reaction parameters and some fuel properties. Ind. Crops Prod. **141**, 111658 (2019). https://doi.org/10.1016/j.indcrop.2019.111658
51. Murugesan, A., Subramaniam, D., Avinash, A., Nedunchezhian, N.: Quantitative and qualitative analysis of biodiesel—an in-depth study. Int. J. Ambient Energy **36**, 19–30 (2015). https://doi.org/10.1080/01430750.2013.820146
52. Aly, A.A., Maraei, R.W., Ali, H.G.M.: Fatty acids profile and chemical composition of Egyptian *Moringa oleifera* seed oils. J. Am. Oil Chem. Soc. **93**, 397–404 (2016). https://doi.org/10.1007/s11746-015-2781-6
53. Yuan, M.H., Chen, Y.H., Chen, J.H., Luo, Y.M.: Dependence of cold filter plugging point on saturated fatty acid profile of biodiesel blends derived from different feedstocks. Fuel **195**, 59–68 (2017). https://doi.org/10.1016/j.fuel.2017.01.054
54. Knothe, G.: Dependence of biodiesel fuel properties on the structure of fatty acid alkyl esters. Fuel Process. Technol. **86**, 1059–1070 (2005). https://doi.org/10.1016/j.fuproc.2004.11.002
55. Foglia, T.A., Nelson, L.A., Dunn, R.O., Marmer, W.N.: Low-temperature properties of alkyl esters of tallow and grease. J. Am. Oil Chem. Soc. **74**, 951–955 (1997). https://doi.org/10.1007/s11746-997-0010-7
56. Ramírez-Verduzco, L.F., García-Flores, B.E., Rodríguez-Rodríguez, J.E., del Rayo Jaramillo-Jacob, A.: Prediction of the density and viscosity in biodiesel blends at various temperatures. Fuel **90**, 1751–1761 (2011). https://doi.org/10.1016/j.fuel.2010.12.032
57. Hoang, A.T., Pham, V.V.: Impact of jatropha oil on engine performance, emission characteristics, deposit formation, and lubricating oil degradation. Combust. Sci. Technol. **191**, 504–519 (2019). https://doi.org/10.1080/00102202.2018.1504292
58. Boog, J.H.F., Silveira, E.L.C., de Caland, L.B., Tubino, M.: Determining the residual alcohol in biodiesel through its flash point. Fuel **90**, 905–907 (2011). https://doi.org/10.1016/j.fuel.2010.10.020
59. Dwivedi, G., Sharma, M.P.: Investigation and improvement in cold flow properties of pongamia biodiesel. Waste Biomass Valorization. **6**, 73–79 (2015). https://doi.org/10.1007/s12649-014-9330-7
60. Bhale, P.V., Deshpande, N.V., Thombre, S.B.: Improving the low temperature properties of biodiesel fuel. Renew. Energy **34**, 794–800 (2009). https://doi.org/10.1016/j.renene.2008.04.037
61. Erdoğan, S., Balki, M.K., Aydın, S., Sayın, C.: Performance, emission and combustion characteristic assessment of biodiesels derived from beef bone marrow in a diesel generator. Energy **207**, 118300 (2020). https://doi.org/10.1016/j.energy.2020.118300
62. Gharehghani, A., Asiaei, S., Khalife, E., Najafi, B., Tabatabaei, M.: Simultaneous reduction of CO and NOx emissions as well as fuel consumption by using water and nano particles in diesel-biodiesel blend. J. Clean. Prod. **210**, 1164–1170 (2019). https://doi.org/10.1016/j.jclepro.2018.10.338
63. Tompkins, B.T., Song, H., Bittle, J.A., Jacobs, T.J.: Efficiency considerations for the use of blended biofuel in diesel engines. Appl. Energy **98**, 209–218 (2012). https://doi.org/10.1016/j.apenergy.2012.03.025
64. Karabektas, M.: The effects of turbocharger on the performance and exhaust emissions of a diesel engine fuelled with biodiesel. Renew. Energy **34**, 989–993 (2009). https://doi.org/10.1016/j.renene.2008.08.010
65. Rashedul, H.K., Masjuki, H.H., Kalam, M.A., Ashraful, A.M., Ashrafur Rahman, S.M., Shahir, S.A.: The effect of additives on properties, performance and emission of biodiesel fuelled compression ignition engine. Energy Convers. Manag. **88**, 348–364 (2014). https://doi.org/10.1016/j.enconman.2014.08.034
66. Nagappan, M., Devaraj, A., Babu, M.J., Vibhav Saxena, N., Prakash, O., Kumar, P., Sharma, A.: Impact of additives on Combustion, performance and exhaust emission of biodiesel fueled direct injection diesel engine. Mater. Today Proc. **62**, 2326–2331 (2022). https://doi.org/10.1016/j.matpr.2022.04.114
67. Janajreh, I., ElSamad, T., AlJaberi, A., Diouri, M.: Transesterification of waste cooking oil: kinetic study and reactive flow analysis. Energy Procedia. **75**, 547–553 (2015). https://doi.org/10.1016/j.egypro.2015.07.451
68. Delfín-Ruíz, M.E., Aguilar-Uscanga, M.G., Gómez-Rodríguez, J.: Xylitol Production by *Candida tropicalis* IEC5-ITV using sugarcane bagasse acid pretreated. Sugar Tech. **25**, 1231–1240 (2023). https://doi.org/10.1007/s12355-023-01256-1
69. Ko, B.S., Rhee, C.H., Kim, J.H.: Enhancement of xylitol productivity and yield using a xylitol dehydrogenase gene-disrupted mutant of *Candida tropicalis* under fully aerobic conditions. Biotechnol. Lett. **28**, 1159–1162 (2006). https://doi.org/10.1007/s10529-006-9068-9
70. Xu, L., Liu, L., Li, S., Zheng, W., Cui, Y., Liu, R., Sun, W.: Xylitol production by *Candida tropicalis* 31949 from sugarcane bagasse hydrolysate. Sugar Tech. **21**, 341–347 (2019). https://doi.org/10.1007/s12355-018-0650-y

71. Zhang, C., Zong, H., Zhuge, B., Lu, X., Fang, H., Zhuge, J.: Production of xylitol from d-xylose by overexpression of xylose reductase in osmotolerant yeast *Candida glycerinogenes* WL2002-5. Appl. Biochem. Biotechnol. **176**, 1511–1527 (2015). https://doi.org/10.1007/s12010-015-1661-8
72. Kato, M., Lin, S.J.: Regulation of NAD+ metabolism, signaling and compartmentalization in the yeast *Saccharomyces cerevisiae*. DNA Repair **23**, 49–58 (2014). https://doi.org/10.1016/j.dnarep.2014.07.009
73. Ahmad, I., Shim, W.Y., Jeon, W.Y., Yoon, B.H., Kim, J.H.: Enhancement of xylitol production in *Candida tropicalis* by co-expression of two genes involved in pentose phosphate pathway. Bioprocess Biosyst. Eng. **35**, 199–204 (2012). https://doi.org/10.1007/s00449-011-0641-9
74. Zhang, C., Wu, D., Ren, H.: Economical production of vitamin K2 using crude glycerol from the by-product of biodiesel. Sci. Rep. **10**, 5959 (2020). https://doi.org/10.1038/s41598-020-62737-x
75. Dodić, J.M., Vučurović, D.G., Dodić, S.N., Grahovac, J.A., Popov, S.D., Nedeljković, N.M.: Kinetic modelling of batch ethanol production from sugar beet raw juice. Appl. Energy **99**, 192–197 (2012). https://doi.org/10.1016/j.apenergy.2012.05.016
76. Ordoñez, M.C., Raftery, J.P., Jaladi, T., Chen, X., Kao, K., Karim, M.N.: Modelling of batch kinetics of aerobic carotenoid production using *Saccharomyces cerevisiae*. Biochem. Eng. J. **114**, 226–236 (2016). https://doi.org/10.1016/j.bej.2016.07.004
77. Prabhu, A.A., Thomas, D.J., Ledesma-Amaro, R., Leeke, G.A., Medina, A., Verheecke-Vaessen, C., Coulon, F., Agrawal, D., Kumar, V.: Biovalorisation of crude glycerol and xylose into xylitol by oleaginous yeast *Yarrowia lipolytica*. Microb. Cell Factories **19**, 121 (2020). https://doi.org/10.1186/s12934-020-01378-1